NEURONAL MECHANISMS FOR THE MAINTENANCE OF CONSISTENT BEHAVIOR IN THE STOMATOGASTRIC GANGLION OF CANCER BOREALIS

A Dissertation
Presented to
The Academic Faculty

by

Amber Elise Hudson

In Partial Fulfillment
of the Requirements for the Degree
Doctor of Philosophy in
Bioengineering

Wallace H. Coulter Department of Biomedical Engineering
Georgia Institute of Technology
May 2013

NEURONAL MECHANISMS FOR THE MAINTENANCE OF CONSISTENT BEHAVIOR IN THE STOMATOGASTRIC GANGLION OF CANCER BOREALIS

Approved by:

Dr. Astrid A. Prinz, Advisor
Department of Biology
Emory University

Dr. Robert J. Butera
Department of Biomedical Engineering
Georgia Institute of Technology

Dr. Deborah J. Baro
Department of Biology
Georgia State University

Dr. Ronald L. Calabrese
Department of Biology
Emory University

Dr. Ravi V. Bellamkonda
Department of Biomedical Engineering
Georgia Institute of Technology

Date Approved: March 29, 2013

To my first teachers, Cheryl, Michael, and John,
and all those that came after

ACKNOWLEDGEMENTS

I have been very fortunate during my time in Atlanta to have met, collaborated with, and/or befriended a large number of phenomenal people. So much so, sitting down to write an acknowledgements section is in some ways more daunting than writing the thesis itself! So let me begin by saying a general thank you to the Bioengineering communities at Georgia Tech and Emory, and to the social groups that have grown up around them. Y'all know how to work hard and play hard, and I've done my best to keep up. I'm not going to try to list everyone here, so please know that your efforts have not gone unnoticed!

That said, there are a number of people that I feel deserve a specific mention. First and foremost, I would like to thank my advisor, Astrid Prinz. Astrid has provided me with an exceptional amount of intellectual freedom and professional space, while still being available to me as a mentor and a "bullshit detector". Her honesty and expertise were invaluable at all stages of my graduate career, and I feel exceptionally lucky to have had a mentor that was always in my corner. Astrid, thank you and I can't wait to see the exciting work that will be coming from your lab in the future.

I'd also like to thank the members of my thesis committee. Dr. Deborah Baro, (sorry, I mean, Deb!), I cannot thank you enough for our extended conversations while I was troubleshooting my immunohistochemistry experiments. Thank you for all of your generosity with reagents, technical tips, and kind words. Dr. Ravi Bellamkonda, thank you for contributing your expertise, lab supplies, and in some cases, even students, to the

CSPG project. Dr. Robert Butera and Dr. Ronald Calabrese, thank you both for your feedback and advice as I was trying to plan experiments and the basis for my thesis work.

To the members of the Prinz lab, past and present, thank you for all of your feedback, support, and baked goods! I couldn't imagine a better group of people to work with. Tomasz Smolinski, thank you for the delicious coffee, silly conversations, and all of your excellent advice, constructive feedback, and shared code. The lab hasn't been the same since you left! Andrei Olifer, thank you for helping me get through some particularly thorny math problems. Cengiz Gunay (and Anca Doloc-Mihu!), thanks for always challenging me to see things from a different perspective (or pun-spective?). You are both hil-ar-ious ☺ Fred Sieling, thanks for reminding me never to take anything too seriously, and for introducing me to Nick (sorry if maybe you didn't see as much of him thereafter – whoops!). Thanks also for getting me started in the Prinz lab, with a well-crafted rotation project and some excellent starter code. Santiago Archila, I've learned a tremendous amount from you. It seems like everything from dissection techniques to social-professional finesse, you know what's up. Thanks for sharing your wisdom and your time, and being so damn humble (and kind) while you're at it. Wafa Soofi, you're a running, cooking and science-ing inspiration! That you chose to expand on techniques from my PloS paper was a compliment of the highest order. Thanks for being so generous with your time, and always being ready with constructive feedback. Ryan Hooper, the wine cooler rig wouldn't have come together without your help and the groundwork you set down for the lab. Thanks for your time, patience, and your delicious cinnamon rolls! Lin Zhuang, Claire Tang, and Rebecca Butterfield, thanks for navigating the mentor-mentee relationship as I've learned how to teach. My work has benefitted from your

contributions! To everyone in the Prinz lab – I wish you lots of luck with all of your future endeavors, but I'd venture to guess that you won't need too much of it. I count myself lucky to have worked with such talented individuals.

To the 2nd and 4th floor Rollins biology communities – you all rock. In particular the Calabrese lab has been especially generous with tools, reagents and advice – Damon Lamb, Anca Doloc-Mihu, and Angela Wenning, thank you for your time! To the Cummings lab, thank you for letting me crash the party, and for teaching me the ins and outs of Western blots. Jean-Philippe Gourdine – sharing your time, not to mention your lab bench, for such a period was over and above. Thank you!

To my classmates in the BME/BIOE programs, thank you for being such a fantastic group to work with and learn from. In particular, I need to give a big ol' thanks to Clare Gollnick, who inspired me to take a risk on my Aim 2 project, and has basically held my hand throughout the process. I appreciate your science idealism, and I'll admit that I took the "you're really on the same page" comment as a fantastic compliment. Also, half of this science wouldn't have happened without the stress relief I've found in my new running habit!! Thank you (and Sarah Forte, my favorite snow-day running buddy)! Also, Michelle Kuykendal, thank you for introducing me to the wonders of FEP membranes. My cultures were happier, and therefore I was happier, after this thoughtful suggestion (and donation!).

To my family and friends – you know who you are – thank you for knowing all the right times to lend an ear, or talk mine off. Your support and enthusiasm for my work has been an incredible source of motivation, and the "distractions" are always much appreciated. I could write another hundred pages on how lucky I am to have you all in my

life. But briefly, I'd like to thank my parents – Cheryl Manriquez, Michael Cuddihy and John Foote – for providing so many good opportunities for learning, and for always telling me I could do anything I set my mind to. In particular, I want to thank my dad, John, and my grandparents, Margaret and Gordon Gudmestad, for funding my undergraduate education. I quite literally would not be where I am today without your support, financial and otherwise.

And finally, my dear, Nick Willett. I'll save (most of, let's be honest here) the mushy stuff for the altar, but let me just say that I would not have chosen to cross this finish line without your support. Your cool head and unwavering belief in my abilities has gotten me through more than a couple rough spots, and I couldn't be more grateful. Thank you for inspiring me to be a better person and a better scientist. I love you and I can't wait to see what our next adventure will bring us.

TABLE OF CONTENTS

LIST OF TABLES

LIST OF FIGURES

LIST OF SYMBOLS AND ABBREVIATIONS

χ^2	chi-squared statistic, test of independence
ρ	rho statistic, Spearman's rank correlation test
1D	1 Dimensional
2D	2 Dimensional
3D	3 Dimensional
ANOVA	Analysis of Variances
BSA	Bovine Serum Albumin
chABC	Chondroitinase ABC
CoG	Commissural Ganglia
CS	Chondroitin Sulfate
CSPG	Chondroitin Sulfate Proteoglycan
DNA	Deoxyribonucleic Acid
DNchABC	Denatured Chondroitinase ABC
ECM	Extracellular Matrix
GAG	Glycosaminoglycan
GM	Gastric Mill
I_A / g_A	A-type transient K^+ current / conductance
I_h / g_H	Hyperpolarization-activated mixed ion current / conductance
I_{Na} / g_{Na}	Fast Na^+ current / conductance
I_{CaT} / g_{CaT}	Fast transient Ca^{2+} current / conductance
I_{CaS} / g_{CaS}	Slow transient Ca^{2+} current / conductance
I_{KCa} / g_{KCa}	Calcium-dependent K^+ current / conductance

I_{Kd} / g_{Kd}	Delayed-rectifier K^+ current / conductance
I_{leak} / g_{leak}	Voltage-independent leak current / conductance
LP	Lateral Pyloric Neuron
lvn	Lateral Ventricular Nerve
mRNA	Messenger Ribonucleic Acid
OG	Esophageal Ganglion
PBS	Phosphate Buffered Saline
pdn	Pyloric Dilator Nerve
PD	Pyloric Dilator Neuron
PNN	Perineuronal Net
PY	Pyloric Neuron
RT	Room Temperature
STG	Stomatogastric Ganglion
stn	Stomatogastric Nerve
STNS	Stomatogastric Nervous System
TBS	Tris Buffered Saline
TTBS	Tris Buffered Saline with Tween20

SUMMARY

Each neuron needs to maintain a careful balance between the changes implicit in experience, and the demands of stability required by its function. This balance tips depending on the neuronal system, but in any role, disease or neural disorders can develop when the regulatory mechanisms involved in neuronal stability fail. The objective of this thesis was to characterize mechanisms underlying neuronal stability and activity maintenance, in the hopes that further understanding of these processes might someday lead to novel interventions.

The pyloric circuit of decapod crustaceans controls the rhythmic muscle contractions of the stomach, and has long been recognized as an excellent model system in which to study neuronal network stability. Recent experimental evidence has shown that each neuronal cell type of this circuit exhibits a unique set of positive linear correlations between ionic membrane conductances, which suggests that coordinated expression of ion channels plays a role in constraining neuronal electrical activity. In Aim 1, we hypothesized a causal relationship between expressed conductance correlations and features of cellular identity, namely electrical activity type. We partitioned an existing database of conductance-based model neurons based on various measures of intrinsic activity to approximate distinctions between biological cell types. We then tested individual conductance pairs for linear dependence to identify correlations. Similar to experimental results, each activity type investigated had a unique combination of correlated conductances. Furthermore, we found that populations of models that conform to a specific conductance correlation have a higher likelihood of exhibiting a particular

feature of electrical activity. We conclude that regulating conductance ratios can support proper electrical activity of a wide range of cell types, particularly when the identity of the cell is well-defined by one or two features of its activity.

The phenomenon of pyloric network recovery after removal of top-down neuromodulatory input – a process termed decentralization – is seen as a classic model of homeostatic change after injury. After decentralization, the pyloric central pattern generator briefly loses its characteristic rhythmic activity, but the same activity profile is recovered 3-5 days later via poorly understood homeostatic changes. This re-emergence of the pyloric rhythm occurs without the full pre-decentralization set of fixed conductance ratios. If conductance ratios stabilize pyloric activity before decentralization as we have shown in Aim 1, then other mechanisms must account for the return of the pyloric rhythm after network recovery**.** Based on vertebrate studies demonstrating a role for the extracellular matrix (ECM) in activity regulation, our Aim 2 hypothesis is that the ECM participates in activity maintenance in the stomatogastric nervous system. We used the enzyme chondroitinase ABC (chABC) to degrade extracellular chondroitin sulfate (CS) in the stomatogastric ganglion while in organ culture. Our results are the first to demonstrate the presence of CS in the crustacean nervous system via immunochemistry. Furthermore, our results are the first to show that CS has a role in neuronal activity maintenance in crustaceans. We show that while ongoing activity is not disrupted by chABC treatment, recovery of pyloric activity after decentralization was significantly delayed without intact extracellular CS. Our results suggest that CS may be involved in initiating or directing activity maintenance needed in times of neuronal stress.

CHAPTER 1

INTRODUCTION

Lay Introduction

What is a thought? How do we learn? How does a physical object give rise to subjective experience? These are some of the big unanswered questions in neuroscience. Like most big questions, they become easier to answer when you break each up into many smaller and more tractable questions.

Since the mid-19th century — with the arrival of Ramon y Cajal and the neuron doctrine — modern neuroscience has come a long way toward answering these questions. We now know that thoughts and actions are dependent on the organs of our nervous system: the brain, spinal cord and peripheral nerves. These organs are made up of many smaller units known as cells, and these cells communicate with each other using a variety of chemical and electrical signals transmitted via small physical connection points called synapses. The pattern of these communications encodes information, allowing information storage (memory), computation (thoughts), and communication with other bodily systems such as muscle (actions). Changes in these patterns, due to interaction with the outside world via sensory systems, give rise to learning. Within this system, it is vitally important that each cell remains *functional* — it must keep its communications, or what we call activity, within a range that other cells can use and understand.

Functional neural activity requires a careful balance between plasticity and stability at the cellular level. Plasticity, defined loosely as change in cellular or synaptic properties that then results in a change in activity, is required for learning. On the other hand, mechanisms regulating the stability of these properties are needed; else any changes made during learning will not be preserved. Both forces can result in disease or

disorder when taken to extremes or applied in the wrong context. Balance and regulation are key.

Plasticity and its role in learning often has the limelight in neuroscience, but as the other side of the coin, stability is just as important. Particularly interesting are regulatory mechanisms that appear homeostatic – those that bring some identified aspect of the cellular system back to a baseline, or ideal value, after a perturbation. If we knew the details of these mechanisms, we might be able to intervene when something goes wrong. Disorders such as epilepsy or problems with learning, memory, attention and focus might be helped by a greater understanding of the mechanisms underlying neuronal stability.

When interested in any biological problem, it's often best to find the simplest case (or model) of that problem that is available to you. As we are interested in the balance between plasticity and stability, often the best place to start are the extremes – a system in which there is a lot of plasticity or none at all. In these cases, we can begin to understand the ways in which cellular systems regulate change without the possible complication of two opposing forces working at the same time and cancelling each other (strangely, this seemingly inefficient control structure is common in biology). There are many neuronal networks whose function demands almost absolute stability: some familiar examples might be the systems that control breathing, heartbeat, and smooth muscle movements. These networks don't tend to "learn" over time – they are constant throughout life. These kinds of neural networks are ideal candidates for study due to their repetitive and reliable output. By studying their response to various kinds of stress or injury, we can monitor the change in output (or lack thereof) and deduce the mechanisms involved in maintaining consistent behavior over time. In short, because these systems have very little plasticity, they are our simplest possible system.

To further simplify the study of neuronal stability, it is best to find a small, well-characterized neural circuit in which outside influences can be controlled or completely

removed. Mammalian neural systems provide a challenge in this regard; most are extremely large with high inter-connectivity to the nervous system as a whole. The average invertebrate neural circuit, on the other hand, is substantially simpler than any mammalian system, with far fewer cells and connections. A well-known example of this is the stomatogastric ganglion (STG) of decapod crustaceans, such as lobsters and crabs. The STG is comprised of approximately 30 cells, which together control the rhythmic movement of the animal's foregut musculature. This model system has everything we need to study the basics of neuronal stability – it is small, easily isolated, all of the cells and connections are known, and it has consistent rhythmic output throughout life.

This dissertation describes two studies using the STG as a model system that are designed to add to our knowledge of the cellular mechanisms underlying stable neural activity. First, I used a mathematical model of STG neurons to show that some previously controversial experimental results are in fact evidence for a new molecular mechanism controlling stability. Then, by using a model of injury in which the first mechanism fails, I showed evidence for another new, previously unknown mechanism working in parallel to the first – or in this case, as a backup plan in case of injury or disease.

Technical Overview

Parts of the following introduction have been published in the journal Physiology in 2010 (Hudson et al., 2010).

Homeostasis and Activity Maintenance

Homeostatic regulation of neuronal activity is integral to neural function. Without successful mechanisms to constrain the process of plasticity and counter the entropic effects of high molecular turnover, every neuron would drift toward silence or death via excitotoxicity. When these mechanisms falter there is the risk of loss of function, such as after neuronal injury, or the development of neural disorders, such as the runaway excitation involved in epilepsy. The study of mechanisms involved in homeostatic

regulation is not only central to understanding brain function, it may also provide therapeutic targets for treatment of brain injury and disease.

The Stomatogastric Nervous System

The stomatogastric ganglion (STG) of decapod crustaceans, such as lobsters and crabs, is an ideal system to study the regulation and maintenance of stable ongoing neuronal activity. The STG is comprised of approximately 30 neurons that control the rhythmic movement of the animal's foregut musculature (Figure 1.1A,B).

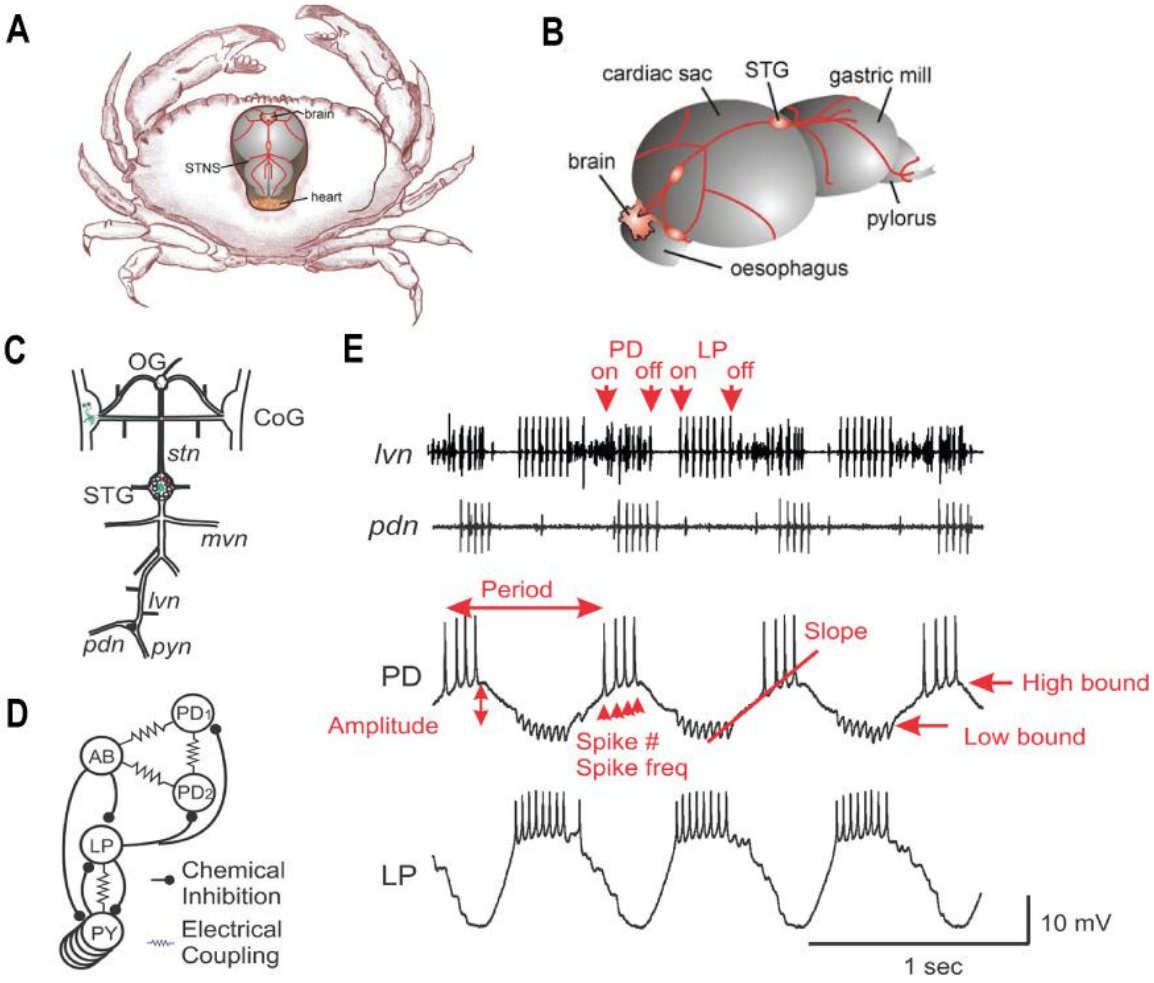

Figure 1.1: The stomatogastric nervous system and the pyloric network. (A) Dorsal view of the crab Cancer pagurus with parts of its dorsal carapace removed. The heart, the STNS and the brain are visible. (B) Antero-lateral view of the foregut, including esophagus, cardiac sac and gastric mill, as well as pylorus. The STNS is located dorsally on the foregut and innervates all of its compartments (A,B) panels and caption adapted from (Stein, 2009) (C) Schematic diagram of the STNS. The paired CoGs and OG contain modulatory projection neurons (colored cells) that send axons to the STG through the stomatogastric nerve (*stn*).Most pyloric neurons are motorneurons that project their axons via individual nerves [pyloric dilator nerve (*pdn*), pyloric constrictor nerve (*pyn*) shown] to their target muscles via the lateral ventricular nerve (*lvn*) or through the medial ventricular nerve (*mvn*) (D) Schematic diagram of the core of the pyloric network. The AB and both PD neurons are all strongly electrically coupled to each other. LP receives inhibition from AB and inhibits both PD neurons, while it also reciprocally inhibits the PY neurons. (E) The triphasic pyloric rhythm was recorded simultaneously from the *lvn* and *pdn* and intracellularly from one of the two PD neurons and the LP neuron. The arrows above the *lvn* recording highlight the onset (on) and termination (off) of the PD and LP neuron bursts. Red lines and arrows point out other neuronal activity attributes discussed in this thesis. IPSPs in PD are elicited by the action potentials of the LP neuron. (C-E) panels and caption adapted with permission from (Zhao and Golowasch, 2012)

These neurons have robust, stereotyped activity and connectivity patterns that are invariant both between animals of each species and over the life of each animal. Many of these neurons are readily identifiable, meaning that individual neurons can be identified as serving a unique and necessary function in every animal (Selverston et al., 1976). When a neural circuit contains identifiable cells, targeted perturbations can be made directly to universally known circuit components. In this way, inferences can be made about the structure of the circuit and the mechanisms behind generating a particular stereotyped behavior. Identifiable cells also allow long-term observations regarding adaptation to a changing environment or response to sensory input that might not otherwise be possible. In addition, the consistent identification of individual cells allows for especially fruitful comparison of data among labs working on the same system. For these reasons, the circuits of the STG have been highly studied over the last 50 years, with a particular focus on circuit analysis and activity maintenance.

There are two general motor patterns that are controlled by the neurons in the STG: the grinding of the gastric teeth to break down large food particles in the stomach, known as the gastric mill, and the dilation and constriction of the pylorus to filter and push food through to the digestive gland or midgut (Harris-Warrick et al., 1992). The first neurons in the STG to be consistently identified were the motor neurons that drive these patterns. Motor neuron function in the STG was conclusively determined by using electrophysiology to confirm the anatomical muscle innervation patterns that had previously been elucidated with methylene blue staining (Maynard and Dando, 1974). Extracellular wire pin electrodes were placed on motor nerves near the point of muscle innervation while sharp glass microelectrodes were used to impale cell bodies in the STG (Selverston et al., 1976). In this way, intracellular neuronal activity could be correlated with the extracellular nerve activity driving particular muscles, and motor neuron connectivity to stomach musculature could be determined. Simultaneous intracellular recordings in multiple cell bodies were used to identify the connectivity and character of

the few interneurons in the STG, as well as the electrical and chemical synaptic connections between motor neurons (Mulloney and Selverston, 1974; Selverston and Mulloney, 1974). Furthermore, a combination of pharmacology to inspect neuronal response to applied synaptic channel agonists, electron microscopy to distinguish vesicle features at synaptic terminals, and biochemistry to identify the presence of enzymes in neurons that help produce certain neurotransmitters, allowed for the identification of the different neurotransmitters released by STG neurons (Marder, 1974, 1976; King, 1976a, 1976b; Marder and Paupardintritsch, 1978; Hooper and Marder, 1987). During this early period of crustacean STG study, identifiable STG neurons were defined as the cells that were functionally identical in different animals of the same species (Selverston and Mulloney, 1974). Thus a functional description became the basis for the established naming system for the neurons in the STG, and by this definition, it was often the case that multiple neurons were given the same name if they were electrically connected and carried axons to the same muscle, making them functionally indistinguishable.

The identified neurons in the STG are typically functionally segregated based on what motor pattern each particular neuron is found to participate in. In the research that follows, we have focused on the pyloric circuit which contains six neuron types: the anterior burster neuron (AB), the two pyloric dilator neurons (PD), the ventricular dilator neuron (VD), the inferior cardiac neuron (IC), the lateral pyloric neuron (LP), and the three to eight pyloric neurons (PY) (Figure 1.1D). The variability in PY neuron number depends on the species of decapod crustacean and can even vary between animals of the same species (Bucher et al., 2007). The pyloric circuit can be separated into 3 functionally distinct nodes whose inhibitory neurons fire in successive bursts to give rise to a characteristic triphasic pyloric firing pattern with a cycle period of 1-2 seconds (Figure 1.1D,E).

The AB/PD node, which consists of the AB neuron that is electrically coupled to the two PD neurons, is considered the circuit pacemaker; when neuromodulatory inputs

from the adjacent commissural ganglia (CoG) and esophageal ganglion (OG) are intact (Figure 1.1C), AB oscillates strongly and drives the two PD neurons to fire bursts of action potentials in synchrony through gap junctions (Harris-Warrick et al., 1992). The LP, IC and VD neurons, which begin bursting immediately after the AB/PD node falls silent, comprise the next node in the circuit. The final node includes the PY neurons, which burst after the LP neuron falls silent. The AB/PD pacemaker node sends fast glutamatergic and slow cholinergic inhibitory inputs to each of these cells to drive the staggered periodic bursting in those two circuit nodes. The neurons of the pyloric circuit are referred to as conditional bursters because if the nerve that carries the various neuromodulatory inputs (Figure 1.1C) to the STG is blocked or cut, a technique known as decentralization, the triphasic rhythm is quickly abolished with each cell in the circuit falling silent or spiking tonically (Thoby-Brisson and Simmers, 1998). The LP and PY neurons of the pyloric network are also known as rebound bursters because they are not pacemaking neurons with the intrinsic oscillatory behavior of the AB/PD neurons; they instead fire bursts of action potentials when they are released from inhibition.

Cellular Parameter Variability

Ion channels that ultimately control the unique electrical properties of any cell can be created, modulated, replaced, or destroyed as a result of many converging molecular pathways or events (reviewed in (Schulz et al., 2008)). Consequently, slight differences in the intracellular milieu from one cell to another can mean the difference between a silent or bursting cell. As molecular techniques become more advanced, it is increasingly clear that there are a variety of notable biochemical differences underlying the cell-type specific electrophysiological properties of cells in the STG. These differences can be loosely divided into two categories: those that are intrinsic to the cell and those that depend on extrinsic input.

There is considerable variability in intrinsic properties between the cell types of the STG. For example, it has been observed that the kinetics of some ionic membrane

conductances are subtly different from one cell type to another, which suggests slight differences in the probability of the ion channels mediating the conductance to open or close as a function of the membrane potential (Golowasch and Marder, 1992; Baro et al., 1997). Recent research points to a combination of alternative splicing of the ion channel genes and various post-translational modifications as underlying these differences. Though there is still much work to be done to link specific splice variants to expressed activity, evidence for alternative splicing in the STG is widespread (Baro et al., 1994, 1997, 2001; Kim et al., 1997, 1998; Ouyang et al., 2007). The most intensely studied case of alternative splicing in the STG is the shal gene, which has at least 14 possible isoforms (Baro et al., 1997, 2001). The shal gene codes for the ion channel mediating a transient K^+ conductance (g_A), and this conductance has graded kinetics between cell types (Figure 1.2B).

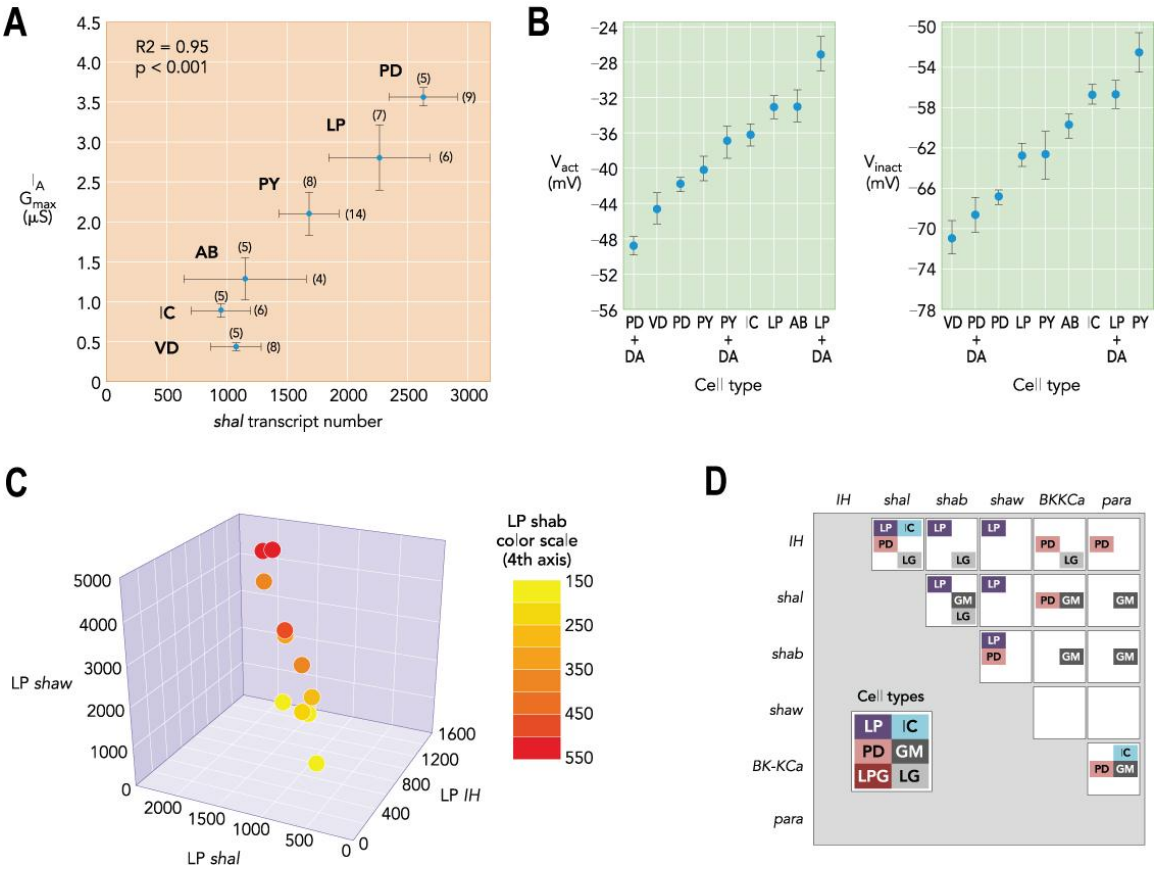

Figure 1.2: STG neurons exhibit cell-type specific constraints despite conductance variability. (A) conductance variability exists within and between cell types. This figure shows the maximal conductance of the A-current (I_A) for each cell type as a function of shal gene expression. The numbers in parentheses represent the number of cells used to measure either the G_{max} or the number of shal transcripts. (B) neuromodulators can affect cell- type-specific characteristics that may lead to differences in maximal conductances between different cell types. Shown are the voltages at which I_A activates and inactivates for each cell type, with and without the addition of exogenous dopamine (DA). (C) STG neurons show linear correlations of ion channel expression. Shown is a unique four-way correlation between ion channel mRNA transcript numbers measured in the LP neuron. (D) pairwise correlations of ion channel mRNA also exist among STG neurons. Axis labels correspond to six different ion channel mRNAs present in STG neurons. Colored labels depict existence of significant pairwise linear correlation for the corresponding mRNA pair. Figure and caption used with permission from (Hudson et al., 2010) with component panel (A) from (Baro et al., 1997), (B) from (Baro et al., 2001) and panels (C) and (D) adapted from (Schulz et al., 2007).

However, it has been shown that many of the identified isoforms of this gene have few distinguishable electrical properties, and therefore, they cannot be solely responsible for the large diversity of g_A. Other mechanisms, such as post-translational modifications or

cell-specific auxiliary proteins (Zhang et al., 2003), must be involved and this is an interesting area for further research.

There is also considerable variability in intrinsic properties within each cell type. When comparing identified cells between different animals of the same species, the maximal expression of each conductance (G_{max}) is highly variable (Golowasch et al., 2002; Schulz et al., 2006, 2007) (Figure 1.2A). As mentioned, the G_{max} of each class of ion channel directly influences the electrical phenotype of a cell, so determining how a cell type with variable conductances can have dependable activity is an interesting question. Recently, several type-specific constraints on this variability have been discovered. For example, though crab populations of PD and LP cells both have large (2 and 3 fold, respectively) ranges of shal mRNA expression, these ranges do not overlap (Schulz et al., 2006). In fact, each cell type studied has been found to have a unique pattern of ion channel mRNA expression, with often distinct ranges of expression (Baro et al., 1997; Schulz et al., 2007). Furthermore, the expressed conductance values for an individual cell are not as random as these large ranges might suggest. It has recently been shown that members of several STG cell types conform to fixed ratios between two or more conductances (MacLean et al., 2003, 2005a; Khorkova and Golowasch, 2007; Schulz et al., 2007; Goaillard et al., 2009) (Figure 2C,D). Every cell type studied shows a unique combination of conductance relationships; both the conductances involved and the exact ratio of each conductance pair vary between cell types. These conductance ratios provide a likely mechanism for maintaining cell type-specific electrical activity in the face of conductance variability (Tobin et al., 2009; Hudson et al., 2010), although the functional benefits of these ratios may depend on the characteristics of activity which are maintained by each cell type (Taylor et al., 2009).

Another neuronal property that can help distinguish different neuron types is responsiveness to external input, such as neuromodulation. Neuromodulation generally refers to a diffuse chemical signal, sent from one area of the nervous system to another.

This signal can be mediated by axonal projections into the region of interest or neuromodulators may be released into the blood stream and circulated throughout the animal as hormones. The STG is an ideal system for studying the effects of neuromodulation due to its physical separation from all modulatory influences, such as the neurons of its neighboring ganglia (reviewed in (Marder and Bucher, 2007; Stein, 2009)). This physical isolation has allowed the detailed comparison of cellular behavior with and without neuromodulation, or with a subset of the large number of neuromodulators usually present in the STG. When all neuromodulators are removed from the ganglion, each cell type responds differently, but the overall result is the temporary loss of network activity. Over time the activity is restored via cell-type specific changes in conductance levels (Haedo and Golowasch, 2006) which in some cases may mean the loss of the conductance ratios discussed earlier (Khorkova and Golowasch, 2007) (Figure 1.3).

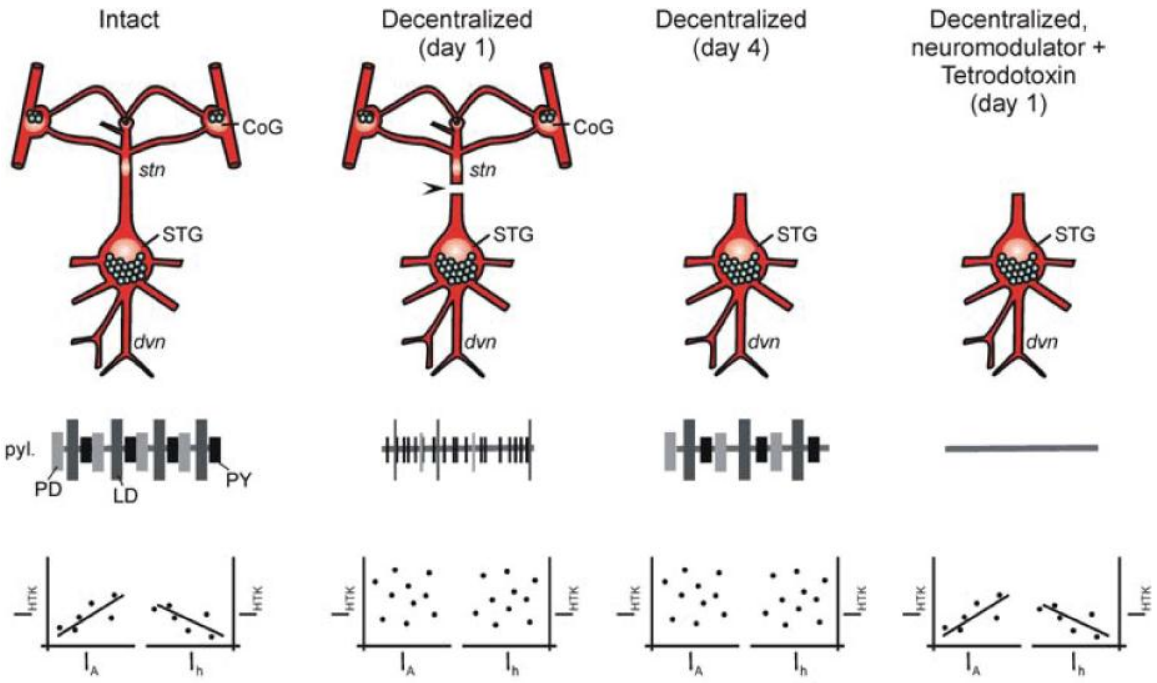

Figure 1.3: Decentralization of the pyloric network results in temporary loss of activity and permanent loss of some conductance correlations. With intact neuromodulatory input from the CoG projection neurons (left), the pyloric CPG generates a rapid triphasic pattern (pyl.). In the PD neurons, the maximum conductance levels of I_{HTK} and I_A and I_{HTK} and I_h are correlated when measured across many animals (below). When the stomatogastric nerve (*stn*) is transected (decentralization; second from left), the pyloric rhythm stops and most pyloric neurons generate tonic activity. The correlation of I_{HTK} and I_A and I_{HTK} and I_h is lost. After 4 days (third from left), the pyloric rhythm has recovered, but current correlations have not. In contrast, when decentralization occurs and proctolin is applied to substitute the absent neuromodulator input (right), current correlation is maintained even when circuit activity is completely suppressed by Tetrodotoxin. Figure and caption, which was adapted from (Khorkova and Golowasch, 2007), is used with permission from (Stein, 2009).

This raises the question, if activity is restored without the hypothesized stabilizing effects of conductance ratios, what mechanisms are driving this return of stable activity?

The Extracellular Matrix (ECM)

The ECM is often described as determining the structural properties of a tissue, and providing a physical substrate for cell attachment. However, there is growing evidence that this is only a partial description of ECM function, particularly for neuronal ECM. In mammalian systems, neuronal ECM has been shown to participate in a great

variety of neuronal processes, such as structural plasticity (Galtrey and Fawcett, 2007; Kwok et al., 2011), synaptic receptor membrane diffusion (Frischknecht et al., 2009), LTP/LTD (Wlodarczyk et al., 2011) and intrinsic excitability (Snow et al., 1994; Dityatev et al., 2007). The ECM has also been suggested to stabilize neuronal activity (Dityatev and Fellin, 2008; Dityatev et al., 2010) and defects in this function have been implicated in epileptogenesis (Dityatev, 2010). In support of this idea, specialized membrane-bound ECM structures called perineuronal nets (PNNs) are commonly found around cell types with high firing rates (Celio and Blumcke, 1994; Morris and Henderson, 2000; Galtrey and Fawcett, 2007), which may need additional homeostatic mechanisms to promote stability or protection from oxidative stress (Egea et al., 2010; Martin-de-Saavedra et al., 2011). Furthermore, PNN component secretion and turnover in the extracellular space is activity dependent (Lander et al., 1997; Dityatev et al., 2007), providing a mechanism by which changes in activity output can feedback onto regulatory mechanisms – the hallmark of a homeostatic process. Taken together, the data suggest a role for the ECM in homeostasis that warrants further investigation (Dityatev et al., 2010).

One of the major components of mammalian PNNs is a class of molecules called chondroitin sulfate proteoglycans (CSPGs) (Galtrey and Fawcett, 2007). The structure of CSPGs is fairly simple: a core protein with attached chondroitin sulfate side chains. However, this family of proteoglycans is incredibly diverse. The identity of the core protein, the number of CS side chains and the type of sulfation pattern can vary widely and will determine the function of the molecule (Figure 1.4).

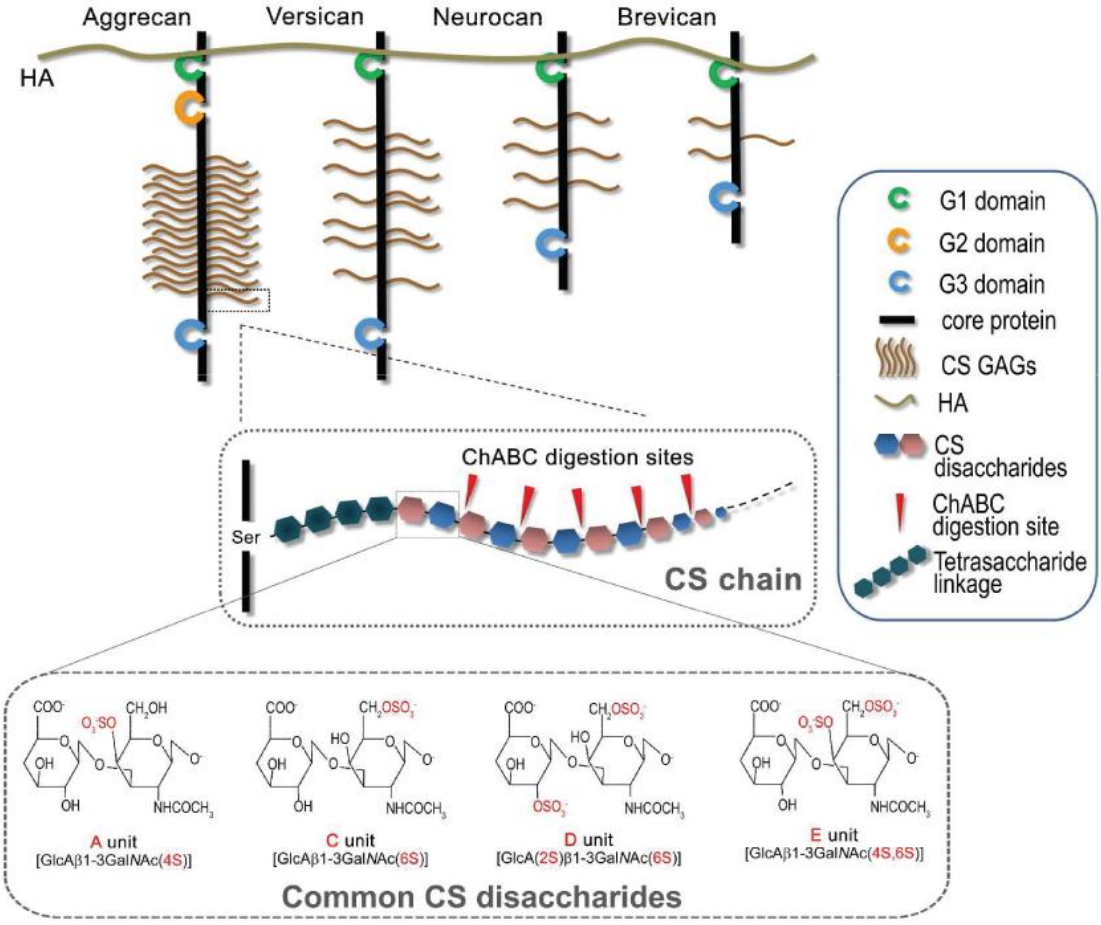

Figure 1.4: A schematic diagram showing the variable structures of CSPGs. Aggrecan, versican, neurocan and brevican are the members of a well-studied group of mammalian CSPGs called lecticans. All lecticans contain a N-terminal G1 domain which consists of an Ig repeat and two link modules, a middle GAG attachment region and a C-terminal G3 domain which consists of two EGF-like repeats, a C-type lectin like domain and a complement regulatory protein like module. Aggrecan contains an additional G2 domain of which the function is not clear. While the G1 domain is important for hyaluronan (HA) binding, the C-type lectin domain in the G3 domain is responsible for binding to glycoprotein Tn-R. The length of the middle GAG attachment domain is highly variable among lecticans and it determines the final sizes of the core proteins. The middle box shows the attachment of a CS-GAG chain to the serine residue on a core protein, via a tetrasaccharide linkage. CS is a linear polymer of GlcA and GalNAc subunits. ChABC digests the CS chain into its basic disaccharide units, hence removing the GAG chain from the core protein. The disaccharide subunit of CS can be modified with different sulphations. CS-A and -C contain either a single C-4 sulphation or a C-6 sulphation on the GalNAc, CS-D contains a C-2 sulphation on the GlcA and a C-6 sulphation on the GalNAc, and CS-E contains both C-4 and C-6 on the GalNAc simultaneously. Figure and caption adapted from (Kwok et al., 2011) with permission of John Wiley & Sons, Inc.

The component CSPGs present in PNNs are cell-type specific (Lander et al., 1997), suggesting that the function of CSPGs differs slightly from one cell type to the next. Furthermore, many of the cellular effects attributable to PNNs have been studied by removing, or introducing, CSPGs (Snow et al., 1994; Morris and Henderson, 2000; Crespo et al., 2007; Dityatev et al., 2007; Galtrey and Fawcett, 2007; Balmer et al., 2009; Gogolla et al., 2009; Martin-de-Saavedra et al., 2011). CSPGs are therefore a good choice for studying the role of the ECM in homeostasis.

Invertebrate CSPGs

It has recently been shown that chondroitin sulfate is a significant component of the ECM throughout the kingdom Animalia (Medeiros et al., 2000). The structure of CS and sulfation patterns appear to be conserved between most vertebrate and invertebrate species (Sugahara and Yamada, 2000; Selleck, 2001; Fongmoon et al., 2007). There has been less study of the functional roles of chondroitin sulfate in invertebrates, particularly their effects on neuronal function. Fongmoon et al recently demonstrated that invertebrate CS functions similarly to mammalian neuronal CS, by introducing a novel king crab CS to cultured mouse hippocampal neurons (Fongmoon et al., 2007). They showed that invertebrate CS significantly increased neurite outgrowth, similar to the effects of mammalian CS. Though this is evidence that invertebrate CS has at least some structural and functional similarity to mammalian CS, no studies have been done to determine if invertebrate neurons also respond to CS in a similar way.

Specific Aims

Experimental evidence shows surprising variability in the molecular makeup of identified cells between animals. How then is the same electrical activity achieved with a variety of maximal conductance combinations? Recent experimental evidence has shown that some identified cells conform to type-specific fixed ratios between two or more conductances, and these conductance ratios have been suggested to stabilize neuronal

activity (MacLean et al., 2005a; Khorkova and Golowasch, 2007; Schulz et al., 2007; Tobin et al., 2009; Temporal et al., 2012). However, a subset of these ratios are lost when the pyloric circuit is isolated from top-down control via neuromodulatory input, a process termed decentralization (Khorkova and Golowasch, 2007; Temporal et al., 2012). After decentralization, the pyloric central pattern generator briefly loses its characteristic rhythmic activity, but the same activity profile returns 3-5 days later via poorly understood homeostatic changes. This re-emergence of the pyloric rhythm somehow occurs without the full pre-decentralization set of fixed conductance ratios. If conductance ratios stabilize pyloric activity before decentralization, then other mechanisms must account for the return of the pyloric rhythm after network recovery**.** Vertebrate studies demonstrating a role for the extracellular matrix in activity regulation suggest that this may be a fruitful area of study in the stomatogastric nervous system, as well.

Specific Aim 1: **Are conductance ratios functionally tied to cellular activity maintenance?** Our results show that implementation of fixed conductance ratios will constrain single or multiple features of electrical activity in a neuronal population, depending on the conductance ratios chosen. A database of generic STG conductance-based model neurons was used to demonstrate that fixed conductance ratios shape neural activity. These model neurons were partitioned in two ways: first to groups with similar activity, then to groups that conform to fixed conductance ratios. The cause-and-effect relationship between conductance ratios and conserved features of activity was quantified in both cases.

Specific Aim 2: **Is the extracellular matrix functionally tied to cellular activity maintenance?** Our results show that the extracellular environment plays a key role in the recovery of stereotyped activity after decentralization of the STG. The enzyme chondroitinase ABC (chABC) was used to degrade extracellular chondroitin sulfate (CS) in the stomatogastric ganglion while in organ culture. Activity of the pyloric circuit was

monitored before and after decentralization. We show that without intact extracellular CS, long-term maintenance of pyloric activity was disrupted.

CHAPTER 2

CONDUCTANCE RATIOS AND CELLULAR IDENTITY

This chapter was published in full in PLoS Computational Biology in 2010 (Hudson and Prinz, 2010).

Introduction

In well studied neuronal networks, it is often observed that each neuron has a specific role in the function of the circuit. In some cases, this role is unique and vital, and the health of the animal depends on a robust cellular identity. One example of this occurs in the pyloric circuit of the crustacean stomatogastric ganglion (STG). This well-studied system must produce robust rhythmic activity for successful digestion (Harris-Warrick et al., 1992), and does so through the dependable cellular properties of its component neurons. These neurons are identified by their reliable network activity, morphology, and connectivity (Harris-Warrick et al., 1992). This reliability is surprising, because identified cells can have different sets of ion channel maximal conductances in different animals of a population, despite generating the same predictable electrical activity (Prinz et al., 2004; Schulz et al., 2006). Furthermore, these ion channels are constantly replaced or modified due to synaptic input, sensory feedback, and neuromodulatory action (Marder and Prinz, 2002; Marder and Thirumalai, 2002). In light of these sources of variability, how stomatogastric cells produce consistent, stable output is an open question.

Recent experimental evidence suggests that coordinated expression and regulation of ion channels may play a role in constraining cellular electrical properties. The first such relationship found in the lobster STG was a positive co-regulation between the transient K^+ current (I_A) and the hyperpolarization-activated mixed ion current (I_h) (MacLean et al., 2003, 2005a). The investigators discovered that cellular injection of mRNA coding for the ion channel underlying I_A caused an endogenous increase in the

opposing I_h current, without changing the electrical activity of the cell. The same conductance pair was shown to be correlated in a population of identified neurons in the crab STG, and this correlation was found to be independent of the effects of neuromodulators (Khorkova and Golowasch, 2007). The latter study compared correlations of current density in the pyloric dilator (PD) neuron before and after removal of top-down neuromodulatory input, and found two additional K^+ conductance correlations that were neuromodulator-dependent. A variety of positive linear correlations in ion channel mRNA copy numbers have been found in other identified STG cell types, as well (Schulz et al., 2007). Each cell type appears to express a unique set of ion-channel correlation types and linear relationship slopes. In some cell types, correlations have been seen to involve three or four channel types. Similar relationships, involving conductances (Linsdell and Moody, 1994; Vahasoyrinki et al., 2006; Peng and Wu, 2007), or ion-channel kinetics (McAnelly and Zakon, 2000), have been found in other model systems at the single cell (co-regulation) and population (correlation) levels. Combined, the data suggest a means for constraining cellular activity despite the often several-fold conductance variability seen in these cell types.

To date, all experimentally demonstrated conductance correlations within a wild type population of identified neurons have had a positive slope; no negative correlations have been found. This finding raises several questions about the mechanisms underlying the conductance correlations and their relation to maintenance or definition of activity type. At this time, the mechanisms are unknown, though there are several possibilities. Two membrane channel genes may be concurrently regulated by a single transcription factor in a cell-type specific manner (Colvis et al., 2005). Alternatively, a cleaved section of one ion channel can act as the transcription factor (or repressor) for another (Gomez-Ospina et al., 2006). A unidirectional mechanism of this type may explain why the I_A-I_H co-regulation is not reciprocal in STG neurons (Zhang et al., 2003). In addition, correlations may be controlled by coordinated post-transcriptional or -translational

modification of one or more channel gene products (Baro et al., 2001; Ouyang et al., 2007). Though there is evidence for activity-independent co-regulation (MacLean et al., 2005a; Khorkova and Golowasch, 2007), changes in activity are needed for co-regulation to be expressed during *Xenopus laevis* development (Linsdell and Moody, 1994). This raises the possibility that activity-dependent regulatory cascades may also be involved in conductance co-regulation in some cases (Bito et al., 1997; Fields et al., 2005). A number of conductance correlations are also neuromodulator dependent (Khorkova and Golowasch, 2007). There is a possibility that any of the above mechanisms are influenced by the presence of neuromodulator, and that correlation differences between cell types are due to differences in neuromodulator sensitivity (Hooper and Marder, 1987; Johnson et al., 2003).

In addition to questions about the underlying mechanisms, questions remain regarding the cellular effects of linear conductance correlations. The effects on activity are likely different for each conductance pair; however, recent modeling studies have shed light on general trends in the structure of the conductance space with regard to activity type. Goldman et al. undertook a study of the pair-wise conductance space of stomatogastric neurons and neuron models, and demonstrated quasi-linear grouping of broadly categorized activity types (Goldman et al., 2001a). Similar results have been obtained with a high-dimensional visualization technique of a model neuron database, wherein all conductance parameters are considered (Taylor et al., 2006). Hand-tuned models have also been a useful tool for demonstration of conductance correlation effects on activity. In one stomatogastric neuron model, a linear relationship between I_A and I_H maintains a specific number of spikes per burst (MacLean et al., 2005a). Further theoretical studies demonstrated that correlated changes in these conductances can adjust neuronal input-output gain, while maintaining other features of activity (Burdakov, 2005). Parameter changes in a leech heartbeat neuron model with narrowly constrained burst period and spike frequency demonstrated a correlation in the spike-mediated

synaptic conductance and the inactivation time constant of the transient calcium current I_{CaS} (Olypher and Calabrese, 2007). A tempting conclusion to draw from these results would be that as more features of activity are constrained, more correlations may be required to maintain proper activity. This may not be true, as has been suggested previously (Olypher and Calabrese, 2007). Taylor et al. recently published a detailed model of the lateral pyloric (LP) neuron constrained to reproduce 9 experimentally measured activity characteristics, but found no strong linear correlations between conductance parameters (Taylor et al., 2009).

Here, we expand on previous work by investigating the general relationship between the presence of conductance correlations and the manifest features of activity type. We hypothesize that conductance correlations do contribute to the robustness of critical features of electrical activity. To test this, we use a database of generic STG conductance-based model neurons (Prinz et al., 2003). These model neurons were first partitioned into groups based on ranges of a single characteristic of the electrical activity, or combinations of biologically-inspired activity characteristics. The conductance space for each group was examined and individual conductance pairs were tested for linear dependence. The conductance correlations found were further evaluated for their effect on activity type by building correlation-based populations of models. Our results show that while regulating conductance ratios can support the maintenance of a single cellular activity characteristic, the effects of correlations are less clear when multiple characteristics are required to specify activity type.

Methods

Model Database

A model neuron database was used to investigate the relationship between conductance correlations and intrinsic activity type. This database has been previously described (Prinz et al., 2003). Briefly, a single-compartment conductance-based model

was used. Seven of the eight conductance types used in this model were derived from experiments on unidentified stomatogastric cells in culture (Turrigiano et al., 1995). They include: a fast Na^+ (g_{Na}), fast transient Ca^{2+} (g_{CaT}), slow transient Ca^{2+} (g_{CaS}), fast transient K^+ (g_A), Ca^{2+}-dependent K^+ (g_{KCa}), delayed-rectifier K^+ (g_{Kd}), and a voltage-independent leak conductance (g_{leak}). The hyperpolarization-activated mixed-ion inward conductance (g_H) was modeled after that found in guinea pig lateral geniculate relay neurons (Huguenard and McCormick, 1992). Each maximal conductance parameter was independently varied over 6 equidistant values, ranging from zero to a physiologically relevant maximum. By simulating the model neurons corresponding to all 6^8= 1,679,616 possible combinations of these parameters, a large variety of intrinsic electrical activity patterns were created. This systematic variation of parameters created an eight-dimensional grid of simulated parameter sets within the conductance space of the model. A single model neuron, with its particular intrinsic activity type, inhabits one grid point in this eight-dimensional space.

The currents used to generate this model were not based on any one STG cell type. To approximate distinctions between cell types, which are identified in part by activity, the database was partitioned based on intrinsic activity type of each model neuron. The first level of categorization divided the model neurons into five subsections: silent, periodic spiking, periodic bursting, irregular (non-periodic) spiking or irregular bursting (Figure 2.1).

A

All models
1.7 million total

	Spiking models		Silent	Bursting models		
Group	Periodic	Irregular		Periodic	Irregular	1-spike
% of database	17.5	0.5	17.1	42.2	3.3	19.2
# of correlations	0	7	1	0	4	0

	Spike rate (Hz)				Duty cycle					
Group	<10	10-25	25-50	50-75	>75	< .05	.05-.1	.1-.2	.2-.4	.4-.6	> .6
%	4.8	0.3	3.8	6.2	2.5	23.4	7.7	6.5	4.1	0.6	0.1
#	3	4	6	7	2	3	5	6	4	6	2

B

	Average slope of rise phase of slow wave (mV/ms)				Central slope of rise phase of slow wave (mV/ms)					
Group	<.049	.049-.059	.059-.072	>.072	< 0	0-.04	.04-.06	.06-.08	.08-.1	> .1
%	18.3	3.3	4.6	16.1	0.03	19.7	5.5	6.2	7.1	3.7
#	2	4	5	4	2	3	5	4	5	11

Figure 2.1: Levels of database segmentation based on single activity characteristics. (A) The first tier of this hierarchy includes all models in the database. These models are then divided into groups based on activity type. The second tier includes the groups periodic spiking, irregular spiking, silent, periodic bursting, irregular bursting, and one-spike bursting models. For each group, the number of models (shown in percent of database) and the number of correlations found within that group is shown. The groups "periodic spiking" and "periodic bursting" are further subdivided in the third tier. The spiking models are partitioned by spike frequency in Hz, and the bursting models are partitioned by duty cycle. (B) In addition to duty cycle, periodic bursting neurons were also partitioned based on the slope of the rising phase of their slow wave activity. Three measurement techniques and segmentation schemes were used, two are shown here. See methods.

Silent models exhibited no membrane voltage maxima. Periodic spiking models had inter-maximum intervals that were consistent within 1% of their mean. Periodic bursting activity was detected and defined as follows. First, the peaks and troughs of the membrane potential were subjected to a spike detection threshold. Any peak greater than -30 mV was defined as a spike, and all others were ignored as sub-threshold activity.

Next, the inter-burst interval was defined as any inter-spike interval that deviated from the length of the greatest inter-spike interval by less than 30%. These definitions are different from previous burst classification metrics (Prinz et al., 2003) to avoid minor classification errors associated with alternating burst features. The second level of categorization further partitioned the periodic spiking and bursting models. The large group of periodic bursting neurons was either partitioned based on the duty cycle, defined as the fraction of the burst period taken up by the burst duration, or by the average slope between the inter-burst minimum and the start of the next burst, hereafter referred to as the rising phase of the slow wave (see Figure 2.2C).

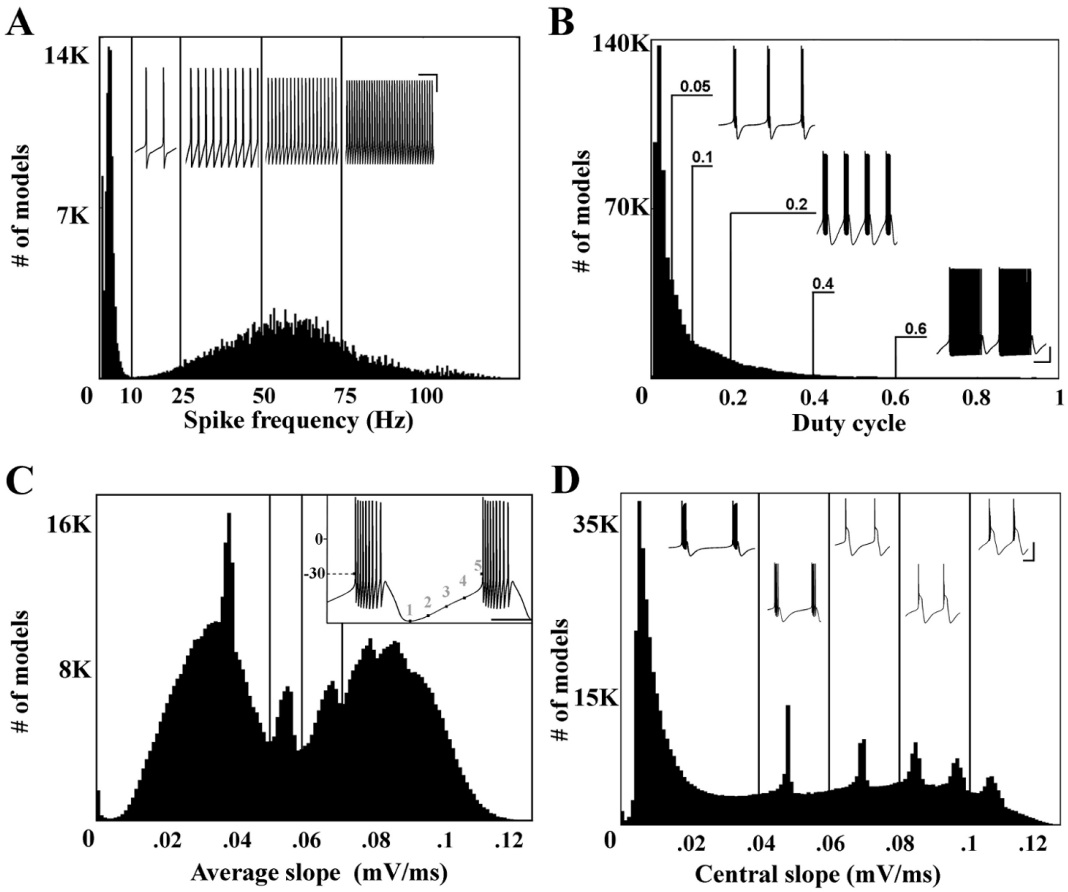

Figure 2.2: Histograms of main features used for partitioning the database. (A) Periodic intrinsically spiking model neurons sorted by spike frequency. Thin vertical lines indicate group boundaries used for sorting activity type. Voltage traces are for models at the lower bound of each group. Bin size is 0.5 Hz. Scale bars for voltage traces are 20 mV (vertical) and 100 msec (horizontal). (B) Periodic intrinsically bursting model neurons sorted by duty cycle. Labeled lines indicate group boundaries and the duty cycle of adjacent voltage traces. Bin size is 0.01. Scale bars for voltage traces are 20 mV and 500 msec. (C) Periodic bursting models were also sorted by the average slope of the rising phase of their slow wave activity. Inset shows the method of calculation of this slope. Average slope was calculated between points 1 and 4 (see inset), to avoid any artifact generated by the sharp incline of the first spike in the burst. Bin size 0.001 mV/ms. Scale bar for inset is 200 msec. (D) Periodic bursting models were finally sorted by the central slope of the rise phase of the slow wave. Central slope was calculated by taking the average slope between points 2 and 4 seen on the inset in part C. Bin size 0.001 mV/ms. Scale bars for voltage traces are 40 mV and 200 msec. (C-D) Thin vertical lines indicate group boundaries used for sorting activity type.

Briefly, the slope was calculated by first locating the inter-burst minimum (point 1 on the inset of Figure 2.2C). Then, the next crossing of the spike detection threshold (-30 mV) was recorded (point 5). The distance between the two points was divided into four equal

sections (demarcated by points 2-4). Average slope was calculated between points 1 and 4, omitting the portion between points 4 and 5 to avoid any artifact generated by the sharp incline of the first spike in the burst. Initial slope (average slope between points 1 and 2) and central slope (average slope between points 2 and 4) were also investigated. These characteristics were chosen because both duty cycle and the average slope of the rise phase are thought to be regulated within a narrow range in biological cells (Bucher et al., 2005; MacLean et al., 2005a). Periodic spiking neurons were similarly partitioned by spike frequency. Group size and boundaries were chosen based on population distributions shown in Figure 2.2. Clustering of low spike frequency and high spike frequency models were seen respectively (Figure 2.2A) and the first group boundaries for spiking models were chosen based on this delineation. In the absence of clear subpopulations arising from model clustering – such as for the high frequency spiking models – an effort was made to achieve optimal resolution within the conductance space by avoiding large differences in group size. Clustering of the bursting models was also seen, and subpopulations based on features of the rising phase of the slow wave were similarly chosen (Figure 2.2C,D). For activity metrics without clear subpopulations, shifting the arbitrarily chosen population boundaries shown in Figure 2.2 did not drastically change the correlations found. Additional metrics were used to partition the periodic spiking and bursting models, such as spike height and the number of spikes per burst, respectively. However, these metrics resulted in a lower overall success rate for finding correlations and were therefore not reported here.

The segmentation scheme described above investigates the relationship between correlations and single activity characteristics. We also looked for correlations in model populations based on multiple activity characteristics. To do this, we constructed model populations based on subsets of the pacemaker activity criteria previously described, including characteristics of the "slow wave" voltage oscillation underlying bursts in STG pacemaker neurons (Prinz et al., 2003). Briefly, the slow wave is the membrane potential

of a bursting model after spikes have been subtracted. The peak of the slow wave was approximated by the last maximum in a burst, and the slow wave amplitude is then the difference between this maximum and the between-burst minimum. The ranges of activity characteristics used are based on experimental data from the spontaneously bursting pacemaker kernel of the STG, which consists of one anterior burster (AB) neuron electrically coupled to two PD neurons. The complete dataset, including the descriptive statistics used to classify models, is available online as a supplemental file (http://www.ploscompbiol.org , datasets S1 and S2 under supporting information for (Hudson and Prinz, 2010)).

Conductance Plots

After model neurons were sorted based on intrinsic activity, conductance plots were generated for each activity subsection (Figure 2.1). As shown in Figure 2.3, these plots graph the value of one conductance parameter versus another, for a particular activity subsection.

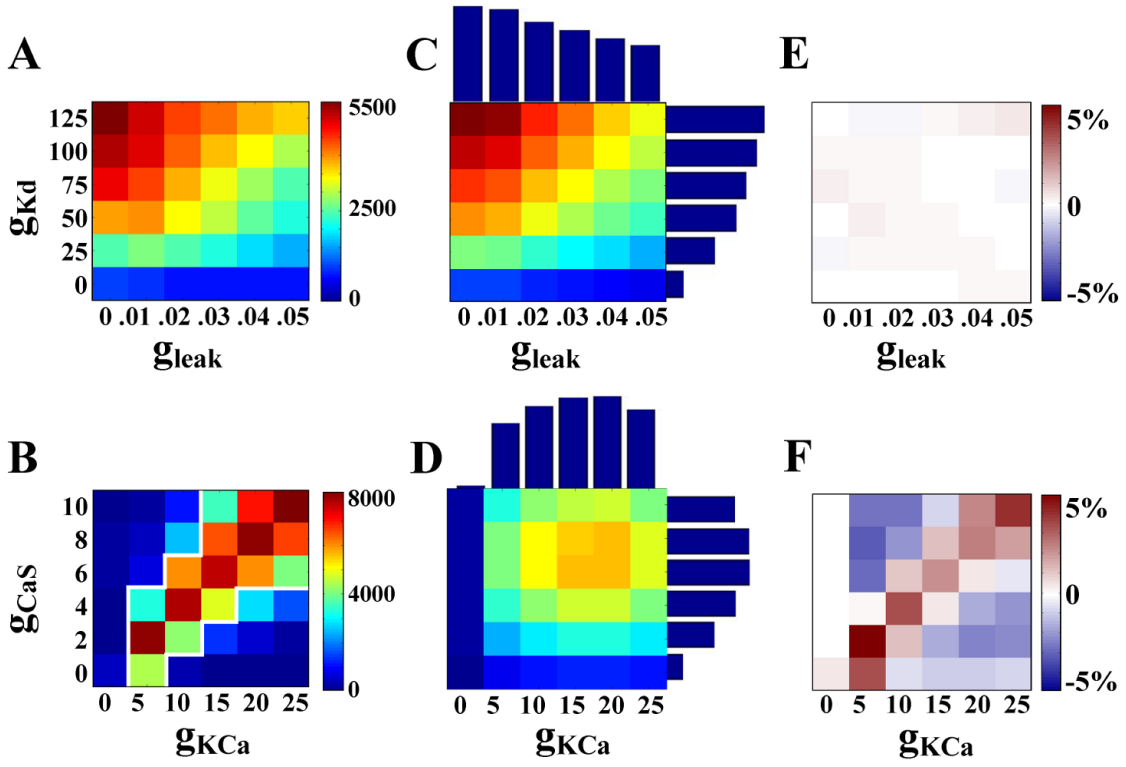

Figure 2.3: Ramp-type conductance relationships can be fully explained by the independence assumption, whereas linear correlations cannot. (A) The activity type "periodic bursters with duty cycle 0.1-0.2" tends toward high values of g_{Kd} and low values of g_{leak} (χ^2=253, ρ=0.006). Colors represent the number of models on each grid point. All maximal conductance units are mS/cm^2. For each plot, no assumptions are made about the values of the other six conductances. (B) The same activity type shows a linear relationship between the CaS and KCa conductances (χ^2=72,330, ρ=0.627). The white outline encases correlation boundaries as used for creating a correlation-based population, see methods. (C,D) Data generated under the independence assumption. 1-D histograms protrude from the axis of the conductance they represent. The resulting independence matrix was generated by multiplying the two 1-D histograms, then scaling by total number of models in this activity group (see Methods). Color scale is the same in A and C and in B and D, respectively. (E,F) Difference matrix. The independence matrix (C,D) was subtracted from the actual data (A,B). Colors in (E,F) represent percent difference between independence matrix and actual data at each grid point.

Each model in the activity subsection falls on one grid point on this plot, positioned by the maximal conductance parameters it was assigned for the pair in question. The other 6 conductance parameters were not constrained when plotting.

Analysis of Conductance Relationships

The grid structure used to generate simulation points for this database creates a conductance space wherein all conductance values are initially equally represented. After segmentation of the database, this is no longer the case and each activity type has a unique distribution of each conductance parameter. Bursting models, for example, have a higher average value of g_{KCa} than spiking models. These non-standard one-dimensional (1D) conductance distributions violate the assumptions of parametric tests and significance testing. Instead, we used two non-parametric tests with simple cutoff values to define correlations. For each activity subsection: if the value of one conductance was determined to be dependent on the value of another (by a chi-squared test of independence $\chi^2>500$), and this dependence was confirmed to have a linear trend (by a Spearman's rank correlation $|\rho|>0.2$), the relationship was considered a correlation. Note that, in the absence of significance testing, these definitions are not dependent on the number of observations (models in each population). This was chosen purposefully because, due to the sparse sampling of the conductance space, populations with very few models may not contain enough information to reliably identify correlations. Cutoff values independent of the number of observations ensures that those correlations reported are strong in all cases.

In addition to the described statistics, a simple visual check for a linear dependence was performed as follows. Assuming independence between conductances, it is possible to generate the expected two-dimensional (2D) conductance distribution for a particular activity type by multiplying normalized single-conductance histograms for that activity type (hereafter referred to as an independence matrix). By looking at the deviations in the actual data from this independent assumption, a linear dependence or lack thereof is more clearly visible than when looking at the correlation plots alone (Figure 2.3E,F). We chose to use this simple, graphical representation of dependence as a visual check to distinguish correlations from conductance relationships that can be

explained by independently varying parameters. Specifically, the independence matrix was created by multiplying two conductance histograms for a particular activity type (units in % of models of that activity type). Then, this independence plot was subtracted from the actual data (units in % of models of that activity type). Note that the resulting plot of percent difference (hereafter referred to as a difference matrix, shown in Figure 2.3E,F) is distinct from, but complementary to, the chi-squared test of independence.

Correlation-based Populations

Defined correlations were used to generate populations of model neurons that fit within those correlation boundaries. The shape of each correlation was defined by setting a threshold of 3% (models/all models in the activity type, the latter hereafter referred to as $type_i$) per grid point of the correlation plot raw data (see the white outline in Figure 2.3B for an example). The entire database, regardless of activity type, was scanned for models that fell within the boundaries of one defined correlation or a combination of correlations. We call the resulting "correlation-based" population cb_i.

If a correlation is successful in restricting activity to a particular type, it is expected that a large number of models in the correlation-based population would be of that type. Specifically, we would expect that there would be a greater percentage of $type_i$ models in cb_i when compared to the original database. We therefore calculated a statistic we termed success percentage (%Success), by dividing the number of models in cb_i that are of $type_i$ by the total number of models in cb_i ($\%Success_{Correlation\text{-}based}$). The percent of $type_i$ models in the original database ($\%Success_{Original}$) was also calculated (see percentages shown in Figure 2.1). The two were compared as follows:

$$f_{\text{Success}} \equiv \frac{\%Success_{Correlation-based}}{\%Success_{Original}} = \frac{N\left(cb_i \bigcap type_i\right) \Big/ N\left(cb_i\right)}{N\left(O \bigcap type_i\right) \Big/ N\left(O\right)}$$

where O represents the original database, N denotes a function returning the number of models in the parameter population, and O∏type$_i$ should be read as "the intersection of the original database and the set of models of type$_i$". The success factor ($f_{Success}$) is therefore a multiplicative factor by which implementing a correlation increases or decreases the likelihood of a particular activity type. An increase in % success for the correlation-based population versus the original database ($f_{Success} > 1$) indicates a correlation that is useful in supporting a desired activity type.

As a control, $f_{Success}$ was also calculated for a randomly distributed conductance plot applied to a random conductance pair. For the case of multiple correlations, the control case employed the same number of randomly generated conductance plots as there are defined correlations for that activity type. As further verification of our methods, we also applied an ideal linear correlation shape to randomly selected conductance pairs and activity types, and found no unexpected increases in $f_{Success}$ (data not shown).

Results

Conductance Relationship Types

A model neuron database partitioned by activity type was screened for pair-wise conductance relationships, to elucidate the possible functional role of linear conductance relationships seen in experiments (MacLean et al., 2005a; Khorkova and Golowasch, 2007; Schulz et al., 2007). However, linear dependence was not the only relationship type seen in this database. A wide variety of nonlinear relationship types were also seen (for examples, the correlation plots of activity type "spiking models 50-75 Hz" are used, Figure 2.4).

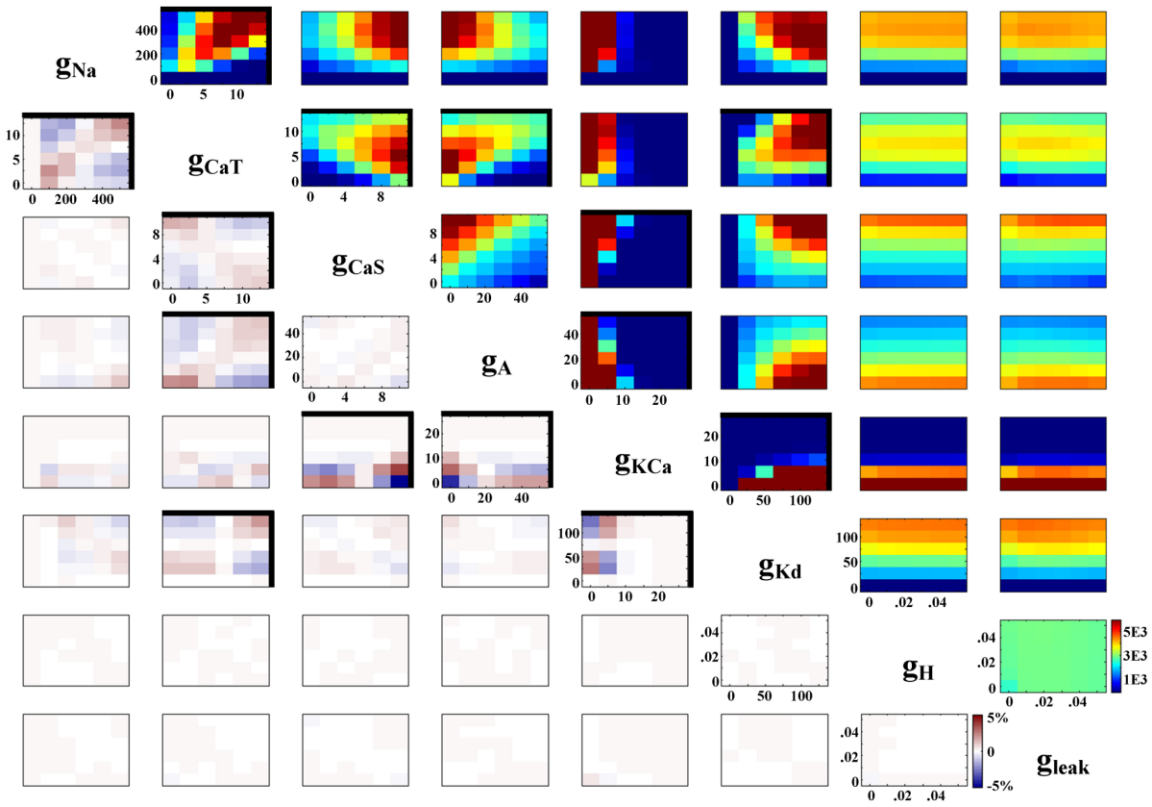

Figure 2.4: All possible pair-wise conductance combinations for the group of spiking models with frequency between 50 and 75 Hz (upper right). Color scheme represents the number of models. The lower left half of the plot contains the difference matrices for this activity type. The blue/red color scheme represents percent difference between data and the independence assumption (see Methods). For all plots, a bold border indicates a linear dependence according to our criteria (χ^2>500 and |ρ|>0.2).

Many conductance pairs were clearly independent of one another; examples include completely flat distributions (g_H and g_{leak}, Figure 2.4) or correlation plots with a striped appearance (g_{Na} and g_H, Figure 2.4). In these cases, one or both of the conductances involved has a flat 1D distribution, and therefore the activity type in question does not require a particular value or range of values of that conductance. Another type of relationship commonly seen was the "ramp" type. These conductance plots had a high concentration of models in one corner, few models in the opposite corner, and a gradient in between. Intuitively, this would suggest dependence. On the contrary, many of these apparent relationships could be explained by independent variation of conductances. For

example, the g_{CaS} and g_A conductance plot shown in Figure 2.4 is one example of a ramp type relationship where the corresponding chi-squared statistic was low, and the percent-difference plot between actual data and the independence assumption (difference matrix) shows no interesting trend. Indeed, this relationship appears to be fully explained by independent variation of parameters, as many of the ramp-type relationships we saw were (Figure 2.3A,C). Finally, both positive (g_{Na} and g_{CaT}, Figure 2.4) and negative (g_{CaT} and g_{CaS}, Figure 2.4) linear correlations were seen and will be described in detail.

Efficacy of Linear Dependence Statistics

The statistical criteria used to define correlations were chosen with the goal of distinguishing those conductance pairs linearly dependent on one another. To verify the statistics, each plot and its corresponding difference matrix were checked for visual confirmation of a linear trend (Figure 2.4). In a small number of cases (16/174) we found that a plot would fit the statistical criteria for linear dependence but linearity was not evident. This was most often an edge effect; for instance, a relationship wherein one or both conductances were zero for a majority of the models (Figure 2.5).

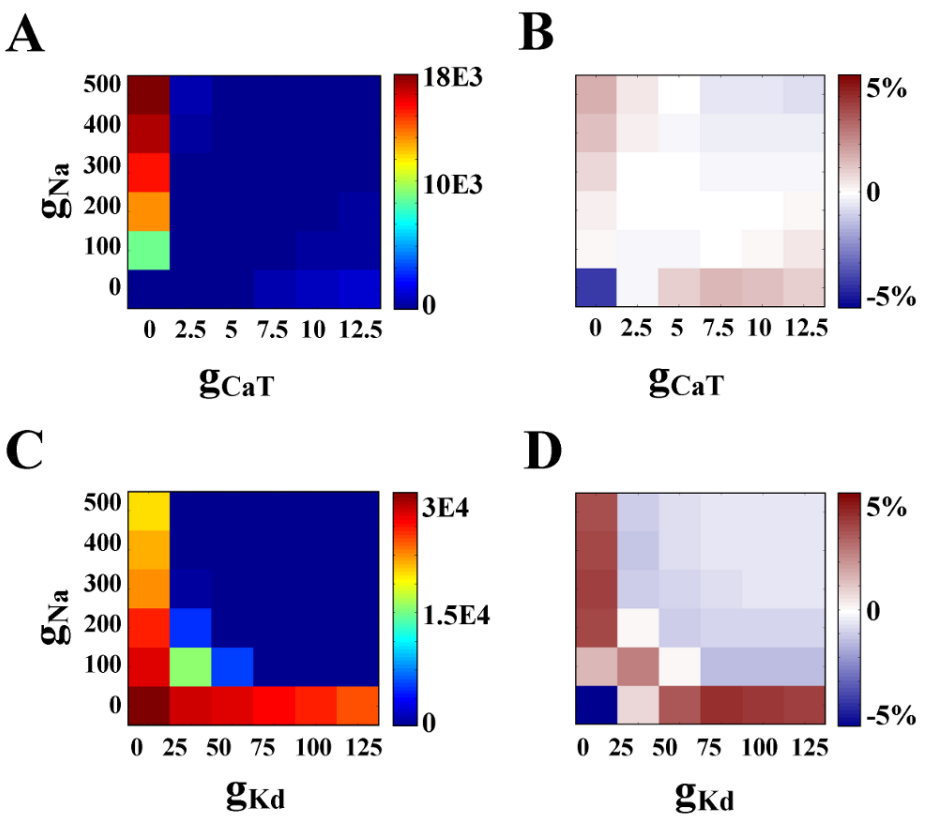

Figure 2.5: Eleven conductance relationships met the cutoff criteria for correlation, but did not have a convincing linear trend upon visual inspection. These false-positives were not included in the correlation totals. (A) Example of plot which met criteria for correlation, but not linearity. From group "spikers < 10 Hz". (B) Difference plot for relationship in A. (C) Another example. From group "one-spike bursters". (D) Difference plot for relationship in C.

Notably, most false positives were due to low average values of g_{KCa} or g_{CaT} or both, and were found in activity types such as silent and fast spiking models. False-positives, though they met the statistical criteria, were not considered correlations (see Table A.2). Statistical criteria were chosen based on minimization of false-positive results. Excluding those cases discussed above, our statistical criteria identified 174 pair-wise linear correlations out of a possible 1316 conductance pair combinations in 47 model sub-populations (see Figure 2.6B and Table A.1).

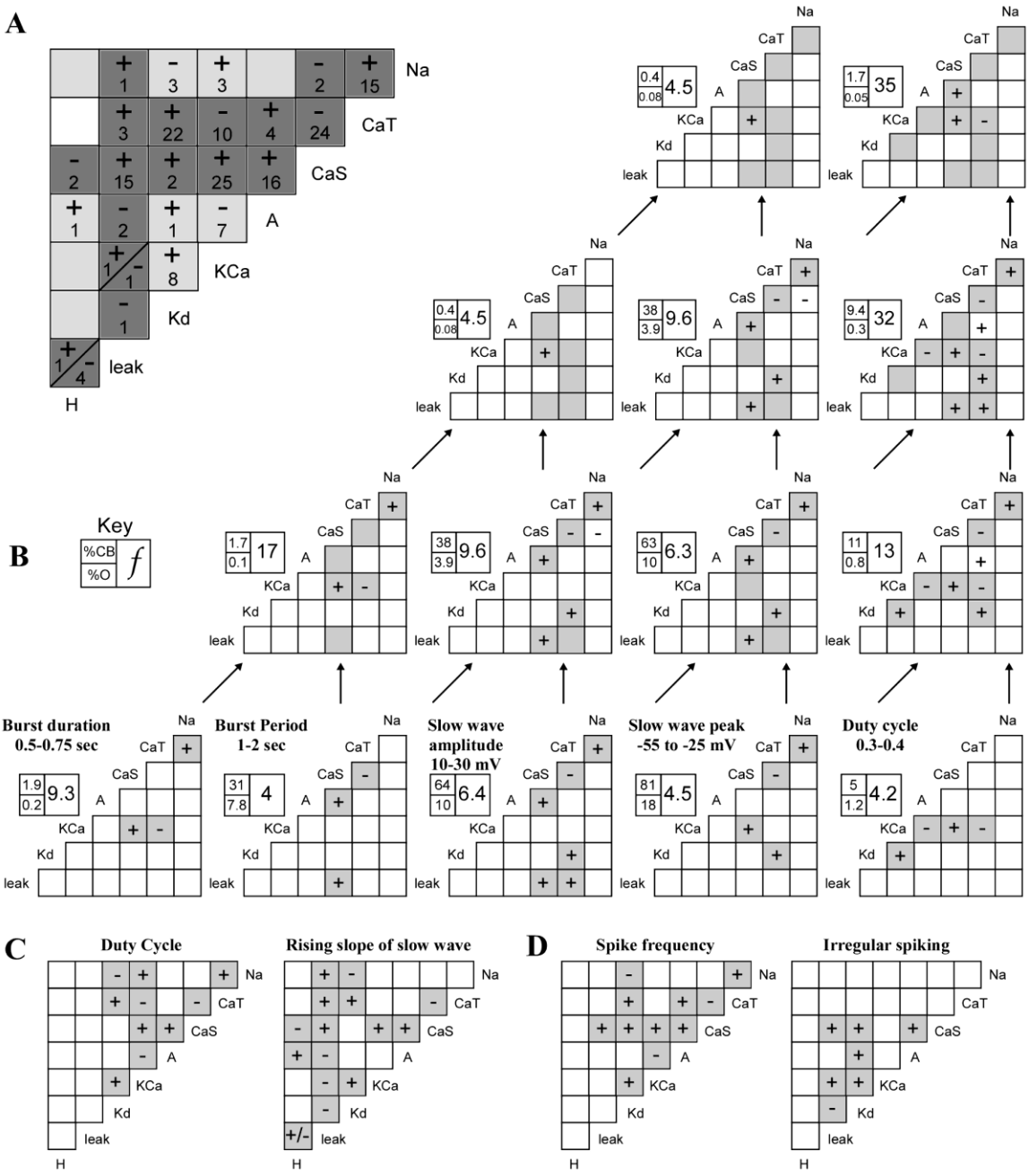

Figure 2.6: Each activity type utilizes a unique combination of conductance correlations. For all plots, a plus sign (+) indicates that a linear relationship with a positive slope was found for this conductance pair. Likewise, a minus sign (-) indicates a linear relationship with a negative slope. (A) Summary of entire database. If a correlation was seen, in any activity subsection investigated, it is included here. Conductance pairs shown in dark grey are those that have not yet been observed experimentally, whereas those highlighted with light grey have been found in experiments on STG neurons [8,9]. Two negative relationships reported here (g_{Na} vs. g_{Kd} and g_A vs. g_{KCa}) were found to be positive relationships when investigated experimentally by Schulz et al [9]. However, there is also agreement with experimental results, such as a positive correlation (g_A vs. g_H) found by Khorkova and Golowasch [8]. Numbers indicate how many activity types showed a particular conductance correlation. (B) Example of how restricting multiple aspects of activity type may influence the appearance of correlations. The bottom row shows correlations for populations based solely on one of the previously published pacemaker criteria [28]. Arrows indicate populations based on combinations of these criteria. Shading here is used only to show that a correlation was present in a "parent" population; if a plus or minus sign is absent then no correlation was observed. %CB is %Success for a correlation-based population, %O is %Success for the original database, and f is the ratio of the two, or $f_{Success}$. See Methods. (C) Periodic bursting models were either segmented by duty cycle, or the slope of the rising phase of the slow wave. The correlations of all activity subsections created for each schema are summarized here. Shading is used for contrast only. (D) All correlation types seen in any of the spike frequency defined activity types and all correlation types seen in the irregular spiking group.

We did not tally the relationships that appeared linear but did not meet the cutoff criteria (apparent false-negatives) because they tended to occur only in activity subsections with relatively low numbers of models. A property of the chi-squared test of independence, that relationships with more data points will more easily reach a cutoff value, was intentionally used to compensate for the sparse sampling of the conductance space. One example of an apparent false negative is shown in Figure 2.7.

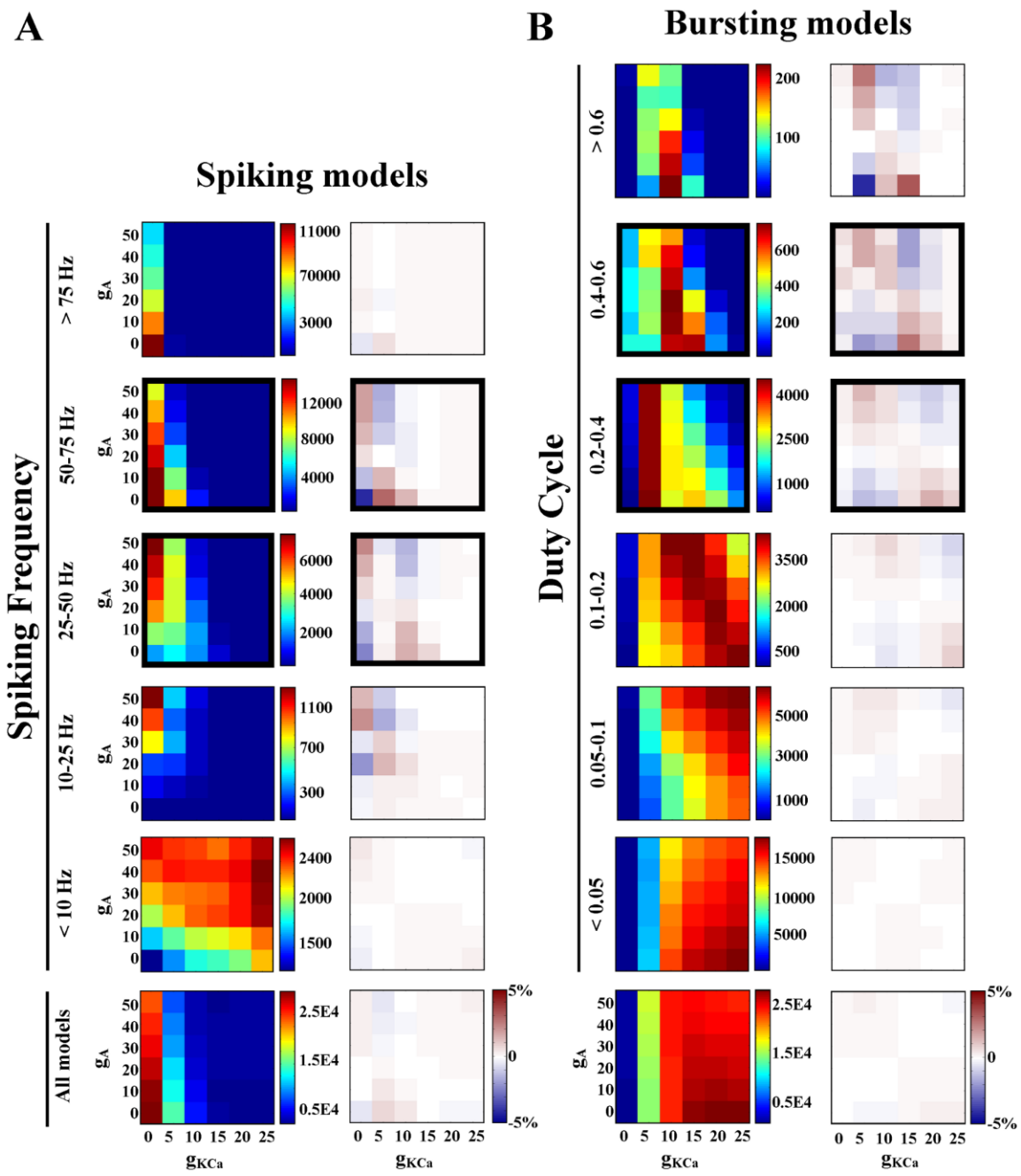

Figure 2.7: Values of g_A and g_{KCa} are correlated for spiking models with a frequency between 25 and 75 Hz and bursting models with duty cycle between 0.2 and 0.6 . Spiking models are represented by the leftmost two columns (A), and bursting models are shown to the right (B). Frequency or duty cycle range is specified to the left of each pair of plots, excluding the bottom row which represents all spiking or bursting models. Bold black borders indicate a correlation (χ^2>500 and |ρ|>0.2). The g_A and g_{KCa} relationship in bursting models with duty cycle >0.6 (top right) was considered a false negative result (χ^2=262, ρ=-0.33).

The activity type "bursting models with a duty cycle greater than 0.6" appears to have a linear dependence between g_A and g_{KCa}; however, the chi-squared statistic is less than 500 for this plot. A possible solution to avoid excluding this apparent correlation would be to use a chi-squared statistic that is scaled by the total number of models in the population, because this group contains only 1776 models compared to an average of 100,000 (Table S1). However, that approach would exclude other, possibly more reliable, relationships. For example, a scaled cutoff would exclude the g_A and g_{KCa} correlation from the activity type "bursting models with a duty cycle between 0.2 and 0.4" which appears very similar to the 'false negative' discussed above (Figure 2.7). We chose to use the raw statistic (unscaled) because we found this result counter-intuitive. A relationship found in a population with a large number of models should be more reliable than an equivalent relationship found in a population with very few models, especially on a sparse grid. This is not to say that relationships fitting our statistical criteria were not apparent in populations with low numbers of models. On the contrary, we found several correlations in this and other populations with relatively few models (Table S1).

Model Populations Based on Activity Characteristics

When model populations were defined by a single activity characteristic, a correlation was more likely to appear in a group with a narrow range of that characteristic (Figure 2.1). For example, the group "all periodic spikers" had no correlations; however, when this group was segmented by spike frequency every subsection had at least one correlation. Similarly, the group "all periodic bursters" demonstrated no correlations, whereas all of its subsections partitioned by duty cycle did. Although the categories without correlations each included over 200,000 model neurons (see Figure 2.1 and Table A.1), this phenomenon was not linked to the size of the activity subsection. For example, the group "bursters with duty cycle < 0.05" contains a large number of models (392,398) and has three correlations. It is reasonable then to assume that correlations arise by virtue

of the narrowly defined activity type of a group rather than simply the number of models in a group.

Very few conductance pairs were seen to demonstrate a positive correlation in one activity type and a negative correlation in others (Figure 2.6A). Thirteen conductance pairs exhibited only positive correlations, eight conductance pairs exhibited only negative correlations, and two conductance pairs had both relationship types. We found no correlations for the remaining five possible conductance pairs. As shown in Figure 2.7, the relationship between g_A and g_{KCa} is one example of a negative correlation. This conductance pair was negatively correlated for spiking models with a frequency of 25-75 Hz (subsections 25-50 Hz and 50-75 Hz) and bursting models with a duty cycle between 0.2 and 0.6 (subsections 0.2-0.4, and 0.4-0.6) (Figure 2.7). Interestingly, though all of the correlations for the g_A /g_{KCa} pair are negative, they appear to have a slightly different slope in each case. This is only one example of slope differences seen between activity types for a single conductance pair, though there are also cases of correlations with the same slope in several activity groups. In the latter case, correlations in different activity groups generally inhabit different areas of the conductance space (Figure 2.8).

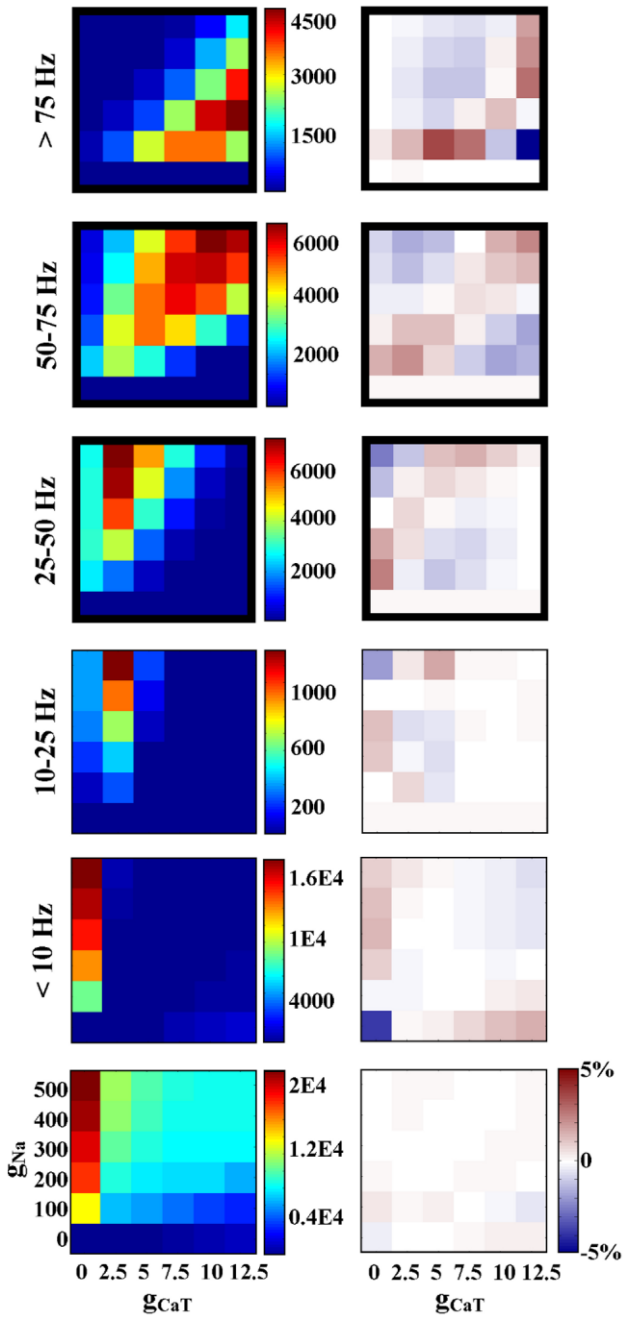

Figure 2.8: Values of g_{Na} and g_{CaT} are correlated for spiking models with a frequency greater than 25 Hz. Bold black borders indicate a correlation (χ^2>500 and |ρ|>0.2).

There was a strong presence of calcium conductance correlations in this database (Figure 2.6A). In the model sub-populations we investigated, there were 140 correlations involving one or both calcium conductances, compared to only 34 that did not involve

either calcium conductance. All conductances showed correlations with at least one of the calcium conductances. The g_{KCa} and g_{CaS} conductance pair had the highest number of correlations and was strongly correlated in several activity types.

In contrast with populations based on a single criterion, there was no straightforward trend in the appearance or disappearance of correlations when multiple activity criteria were used to generate a population. Individually, each population based on a single pacemaker criterion has a unique set of correlations (Figure 2.6B, bottom row). When criteria are combined, however, correlations appear or disappear with a seeming disregard to those seen in the "parent" populations. For example, starting with the population based on slow wave amplitude (SWA) between 10 and 30 mV, adding the slow wave peak (SWP) range as a criterion leads to a loss of the g_{CaT} vs. g_{leak} correlation. Adding duty cycle as a criterion brings back the g_{CaT} vs. g_{leak} correlation, even though the duty cycle parent population does not use it. Adding burst period again leads to loss of that correlation. There is no path from bottom to top in Figure 2.6 along which the number of correlations increases steadily with an increase in criteria. When all 5 criteria were used, no correlations were found, though this may be influenced by the small number of models that fit all 5 criteria (56).

Correlation-based Populations

Finally, defined correlations were used to create correlation-based sub-populations of models as described in the Methods section. A correlation-based population was, in all cases, found to have a larger percentage of models of the desired activity type than the original database. We found a 2.3 fold increase for individual correlations, on average ($\sigma = 0.9$). Individual correlations ranged from having a small positive effect on success rate to increasing it 5 fold (Figure 2.9).

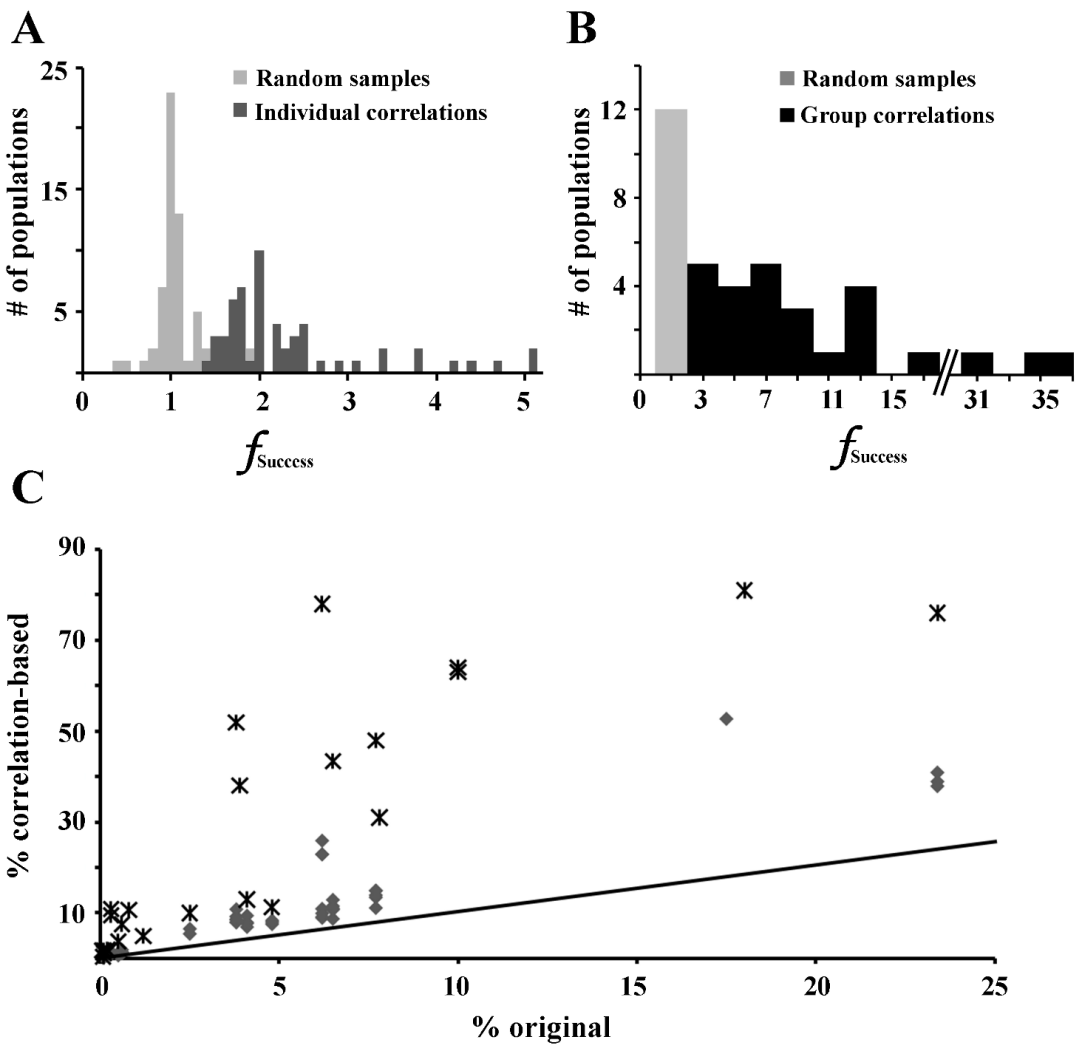

Figure 2.9: Correlation-based populations increased the percentage of models with a desired activity type. (A) Implementation of correlations individually had a modest, but always positive, effect on the percentage of models with the desired intrinsic activity type (%Success), contrary to the random-sample controls. Histograms are stacked in the rare case of overlap. Bin size is 0.1%. (B) Implementation of all correlations seen in an activity type increased %Success by as much as 37 fold. Bin size is 1%. (C) The percentage of a particular activity type in the original database (% original) is plotted against the percentage of models of that activity type in a correlation-based population (% correlation-based). Both single-correlation based populations (grey diamonds) and multiple-correlation based populations (black stars) are shown. Unity line is shown for scale.

This is in contrast to the control condition of random conductance relationships, in which decreases in success were as likely as increases. On average, there was no difference between the control condition and the original database (average $f_{Success} = 0.98$, $\sigma =$

0.2).The difference between control and correlation-based populations was even larger when multiple correlations were used to generate each population. When the set of all correlations for an activity type was used to create a population of models, the percent success increased 10 fold on average (Table S3). In contrast, the average $f_{Success}$ for the control case with multiple random conductance distributions was below 1 ($\mu = 0.89$, $\sigma = 0.17$).

Discussion

Our results illuminate the functional benefit of linear conductance correlations for maintaining activity type. When a population of models was gathered based on adherence to a correlation rule, there was always an increase in a particular feature of activity. In some cases, this increase was admittedly modest, particularly when the population was based on a single correlation. However, there were several cases in which the constraint on activity type was impressive (Figure 2.9). In one case, imposing a single correlation caused an increase in the desired activity type from 18% (in the original database) to 53% (in the new, correlation-based population). Another population increased its percentage of a single activity type by 72% when multiple correlations were used. Put another way, the combined correlation-based populations demonstrated up to 81% of a single activity type. We find this to be a notable contribution to robustness of activity.

This model implicates two types of correlations not previously seen in experiments. As of this writing there have been no published calcium conductance correlations. We have shown that calcium correlations are plausible, and if implemented by a cell, would assist maintenance of a wide range of activity types. This is also true of correlations with a negative slope, which have not yet been seen experimentally. Thirty percent of all correlations seen (56/174) were negative, spanning 10 out of the 23 conductance pairs with correlations in this study (see Table A.1). Though the mechanisms underlying biological correlations are uncertain, and not represented in the

details of our model, our results suggest that negative correlations can be just as useful as positive ones for maintaining cellular activity.

Negative correlations have been hypothesized for conductances that may compensate for one another. For example, a study of the solution space of a multi-compartment cerebellar Purkinje cell model reports negative correlations between several pairs of conductances, including two calcium conductances that appear to be anti-correlated so as to preserve the total calcium influx into the cell (Achard and De Schutter, 2006). When fitting model neuron parameters to reproduce specific experimentally recorded neuronal voltage traces, such functionally compensatory conductances can lead to irreducible model parameter uncertainty (Huys et al., 2006). An analysis of the correlation between the two potassium conductances g_{KCa} and g_A shows this type of relationship in our model. The Ca^{2+}-dependent K^+ current is often associated with bursting cells, and contributes in our model to determining burst length. Keeping all other conductances constant in a bursting model neuron, a higher value of g_{KCa} will correspond to a shorter burst length (Sun and Dale, 1998). The A current is also a K^+ current, though it is not calcium dependent and it acts on a much faster time scale. Keeping all other conductances constant in a bursting cell, a higher value of g_A will result in a slower spike rate, or fewer spikes per burst (Tierney and Harris-Warrick, 1992). The effects of these conductances appear to sum for bursting neurons with a duty cycle between 0.2-0.6 (Figure 2.7). To maintain duty cycle in this range, a model needs a minimal amount of one or both conductances to counter-balance depolarizing (inward) currents. The exception to this rule is a small population (~300 models) of elliptic bursters in the 0.4-0.6 duty cycle group. These models all have the same low value of g_{Na} (100 mS/cm^2), which may allow the absence of both g_{KCa} and g_A. Interestingly, bursting models with a low duty cycle show no dependence between g_A and g_{KCa}.

A second type of negative correlation was seen between g_{Na} and g_{Kd}. Initially, this negative correlation was surprising. Both conductances are involved in generation of the

action potential and would therefore be expected to require balance via a positive correlation. Instead, only negative correlations were seen, and they appeared in two activity subsections: spiking models with frequency greater than 75 Hz, and bursting neurons with a duty cycle less than 0.05. We found, based on where these correlations appeared, that a negative relationship between these two conductances was useful for maintaining very fast spiking. If a model in either of these activity groups was adjusted to make both conductances very low, then the model became silent. If both conductances were very high, the spike would broaden and the spiking frequency would decrease. It is interesting to note that both the conductance pairs discussed so far have been found to be positively correlated experimentally in stomatogastric neurons (Schulz et al., 2007). However, the activity types found to have these correlations in the database are not typical of stomatogastric intrinsic activity types (Heinzel and Selverston, 1988; Harris-Warrick et al., 1992; Bal et al., 1994) and thus should not be compared directly to experiment.

There are several reasons why directly relating our results to the published experimental data is a challenge. First, conductance is not directly measured in experiments. Mapping conductance (used in the database) to mRNA copy number or current density involves several tenuous assumptions. For example, conversion between mRNA copy number and conductance value has been studied for three conductance types in the STG, of which only two were found to relate linearly (Baro et al., 1997; Schulz et al., 2006). Therefore, it cannot be assumed that the other 5 conductances types used in this model have a linear relationship between mRNA copy number and conductance value. A larger problem is the choice of comparison: which activity characteristics should be assigned to a biological cell in a particular experiment? Our analysis of activity type of the model did not consider the effects of current injection or neuromodulation, and therefore should be compared to intrinsic activity of the biological cells. Unfortunately, there are conflicting accounts of the intrinsic activity of cells in the

stomatogastric ganglion. While they have reliable and identifiable activity types in the intact circuit, isolating a cell to measure intrinsic activity often involves direct harm to its own processes or neighboring cells. The method of isolation may influence activity in unknown ways. For example, when the PD neuron is cut off from all synaptic input and neuromodulation it can be spontaneously silent (Panchin et al., 1993), spike tonically (Bal et al., 1988; Panchin et al., 1993), burst with a periodic rhythm (Panchin et al., 1993) or burst irregularly (Bal et al., 1988). The one exception in the STG is the AB neuron, which is an intrinsic burster and has the same intrinsic and network behavior. Unfortunately, no experiments have been done examining conductance correlations in the AB neuron. For these reasons, we chose to avoid comparing our results for a particular activity type with the experimental data for a single cell type.

Even so, there are general comparisons that can be made between our results and experiment. For instance, we found differences in slope for the same correlation in different activity types (Figure 2.7). This is reminiscent of the cell-type specific correlations found by Schulz et al.; the correlation slope for a single conductance pair was different in each cell type (Schulz et al., 2007). In addition, we saw correlations which maintained slope but differed between activity types with regard to intercept (Figure 2.8). We can predict from this result that the general location within the conductance space is also important for determining activity, which has been suggested before (Goldman et al., 2001b). Furthermore, each identified cell type studied by Schulz et al. had a unique combination of correlated conductance pairs, similar to our results (see Table A.1). This suggests that not only the slope and location of correlations, but the combinations in which they are used, are important for definition of cellular identity. This view is bolstered by our results with correlation-based populations. We showed that combinations of correlations, drawn from a particular activity type, generated much larger increases in percent success compared to individual correlations or controls (Figure 2.9).

Another important comparison to experiment involves the hyperpolarization-activated inward conductance, g_H. Correlations involving this conductance were only found when the slope of the slow wave was used to identify activity type (Figure 2.6C). We found this result to be particularly interesting because correlations involving g_H have been found repeatedly in experiments in the stomatogastric ganglion (MacLean et al., 2003, 2005a; Khorkova and Golowasch, 2007; Schulz et al., 2007). In experiments on STG PD and LP cells, both the slope of the slow wave and the ratio of I_A to I_H were shown to be conserved after injection of shal mRNA (MacLean et al., 2005a). This implies that the correlation between the values of I_A and I_H may have something to do with maintaining the shape of the slow wave. In these experiments, the average slope of the rising phase of the slow wave was found to range, roughly, from 0.02-0.08 mV/ms. We found this correlation in a slightly higher range when looking at the central 50% of the rise phase (>0.1, see Table A.1). Though these results are slightly different, both correlations were positive and both suggest that I_H is involved in maintaining a specific activity characteristic: inter-burst dynamics. Interestingly, I_H was not correlated in any other activity types. We hypothesize that this is because the other activity types are defined more by conductances which are active during the depolarized phase of the spike or burst. If this is the case, it would follow that correlations involving I_H would be more prevalent if response to hyperpolarizing current injection were used as a metric for defining activity type. For cells dependent on inhibitory network connections for a bursting phenotype, such as LP and pyloric (PY) neurons in the STG, this may be the case and should be an interesting area of further research.

Recently, Taylor et al published a study of a population of LP neuron models, constrained by 9 activity characteristics, in which no strong linear correlations were found. We report a similar result in that the usefulness of correlations for supporting activity characteristics did not scale up as we expected. When multiple biologically-realistic activity criteria were used to generate a population of models, the appearance

and disappearance of correlations was not easily explained by the correlations found in the "parent" single-criteria populations. This suggests that the correlations which would be helpful for each feature individually might interact in complex ways, inhibiting or enhancing the influence of the other, when multiple activity characteristics are imposed on a group. In our case, a likely explanation for these results lies in the complexity of the conductance space. The conductance plots we analyzed were 2D approximations of an 8-dimensional space. This means that a perfect linear correlation between two parameters will appear as such. However, dependencies between multiple parameters will form subspaces within the overall conductance space that may, or may not, be detectable in a flattened 2D analysis. Furthermore, the perfect population definition for one conductance pair may not be ideal for another conductance pair, resulting in the occasional conductance plot that contains two local dependency rules (see Figure 2.5A for a possible example). Finally, the scale of analysis is important. We had the opportunity to examine raw experimental data from correlations published by Schulz et al. (Schulz et al., 2007). It has been previously shown that every STG cell type has a unique range of conductance values (Baro et al., 1997; Schulz et al., 2006). By binning the experimental data based on the conductance ranges of each cell type, it was apparent that bin size could contribute to the appearance of correlations (analysis not shown). For example, when binning conductance measurements from the gastric mill (GM) cell type based on the range of conductance values present in the PD cell type, otherwise apparent correlations are lost. Our model database is limited in this way, due to the grid structure of the conductance space, which can be interpreted as a type of binning. Combined, this complex behavior can easily give rise to situations in which correlations appear, or disappear, as the population of models is further reduced. Though this result highlights the inability of our analysis to capture all possible linear dependencies between conductances, it is important to note that it does not shed doubt on the correlations we did find.

Though our set of apparent correlations should not be considered an inclusive list for these activity types, the correlations found in our database are useful for considering the possible effects of conductance relationships on activity. We argue that the presence of a large number of defined conductance relationships lends to the validity of the database as a tool for investigating correlation utility. With this tool, we have shown that linear conductance correlations can shape neuronal activity. Furthermore, we made specific predictions about the presence of negative or g_{Ca} correlations and situations in which they might be useful.

CHAPTER 3

CHONDROITIN SULFATE PROTEOGLYCANS AND ACTIVITY MAINTENANCE IN THE STOMATOGASTRIC GANGLION

Introduction

The question of how diverse cellular processes converge to regulate stable neuronal activity is an open, and complicated, problem. In recent years, there has been an abundance of evidence that the extracellular neural environment is participating in a variety of cellular functions, including structural and synaptic plasticity, memory consolidation, LTP/LTD, receptor membrane diffusion and homeostasis. Furthermore, many of the components of the extracellular matrix (ECM) are produced and organized in an activity-dependent manner, which has led to idea that the ECM is an interesting candidate for participation in long-term regulation of neuronal activity because it offers both the opportunity for monitoring of cellular activity and the tools for control of cellular functions (Dityatev and Fellin, 2008; Kazantsev et al., 2012). One family of extracellular proteoglycans called chondroitin sulfate proteoglycans (CSPGs) has been particularly well studied, and demonstrates many of the properties ideal for coordination of activity maintenance.

The CSPG family contains a diverse array of structure and function. CSPGs have two common structural features – the polysaccharide side chains made up of chrondroitin dimers and the protein 'backbone' to which they are attached. Other features vary and contribute to the structural and functional diversity within the family, including the identity of the protein backbone, the number of chondroitin side chains and the degree and location of sulfation of the chondroitin side chains (reviewed in (Sugahara and Yamada, 2000)). This variability has been shown to be cell-type specific (Lander et al.,

1997). There is evidence that CSPGs are produced locally by both neurons and glia (Giamanco and Matthews, 2012), with dependence on cellular activity patterns (Lander et al., 1997) via Ca^{2+} influx (Dityatev et al., 2007). Highly organized extracellular structures called perineuronal nets (PNN), of which CSPGs are a large and vital component, have also been shown to be activity-dependent and cell-type specific (reviewed in (Galtrey and Fawcett, 2007)). The type-specificity and activity-dependence of CSPG localization is thought to contribute to its role in cell fate determination (Von Holst and Faissner, 2009), neuroprotection (Egea et al., 2010; Martin-de-Saavedra et al., 2011), and homeostasis (Dityatev et al., 2010; Kazantsev et al., 2012).

CSPGs have been implicated in neuronal systems relating to control of function, such as structural plasticity, binding and presentation of growth factors and modulation of ion channel properties. Depending on whether they are bound and the pattern of sulfation they present, CSPGs can alternately encourage or discourage growth cone advance in axonal pathfinding (Snow et al., 1994; Fongmoon et al., 2007). Furthermore, CSPGs coalesce into PNNs during the closure of a critical period for structural and functional plasticity in several systems (Balmer et al., 2009; Gogolla et al., 2009; Kwok et al., 2012), and prevention of PNN formation with CSPG removal via an enzyme that degrades the CS side chains of CSPGs called chondroitinase ABC (chABC) will prolong the period of plasticity. Some have suggested that this activity is mediated by the tendency of CSPGs to bind growth factors or pathfinding molecules such as cytokines (Galtrey and Fawcett, 2007). Others have shown that CSPGs, or the PNNs of which they are a part, can alter ion channel properties and neuronal activity patterns in a variety of systems, particularly via Ca^{2+} channels (Snow et al., 1994; Dityatev et al., 2007; Vigetti et al., 2008; Vargas and De-Miguel, 2009; Maroto et al., 2013). This is interesting because Ca^{2+} transients are important in the process of pathfinding, but also for a host of other cellular functions, such as cellular and synaptic homeostasis and gene expression (Fields et al., 2005; Gomez-Ospina et al., 2006; Greer and Greenberg, 2008).

The presence of CSPGs, or the PNNs of which they are a part, have been shown to alter activity patterns in several systems. In cultured embryonic hippocampal neurons, free chondroitin sulfate (CS) induced Ca^{2+} currents mediated by AMPA and Kainate receptors (Maroto et al., 2013). In chick dorsal root ganglion neurons, anchored CSPGs induced intracellular Ca^{2+} transients that were not present when a similar concentration of soluble CSPG was introduced (Snow et al., 1994). In cultured postnatal mouse hippocampal neurons, chABC increased excitability of already fast-spiking interneurons by altering the firing threshold and afterhyperpolarization of spikes (Dityatev et al., 2007). In *Xenopus laevis* photoreceptors, CS solutions had various effects on the activation curves of the H current and voltage gated calcium channels, depending on the sulfation pattern of the CS used (Vigetti et al., 2008). The diversity of the CSPG family and the model systems used to study them does not allow strong conclusions about a unified role in neuronal circuit regulation; however, a common theme of several of these studies includes CS influence on neuronal activity characteristics, particularly via Ca^{2+} currents. Because Ca^{2+} is such an important cellular messenger, these studies suggest a role for CSPGs in coordination of neuronal regulatory pathways.

Taken together, the evidence suggests that CSPGs provide a mechanism for cell-type specific information storage about the history of activity patterns, and the potential for providing feedback to cellular regulation systems using that information. However, this connection has not been verified in one system. Here, we propose the use of invertebrate systems to study CSPGs and their role in neuronal activity maintenance. CS is structurally conserved between invertebrate and vertebrate systems (Medeiros et al., 2000) and there is reason to believe invertebrate CS behaves similarly as in mammalian neurons (Fongmoon et al., 2007).

The stomatogastric ganglion (STG) of decapod crustaceans, such as lobsters and crabs, is an ideal system to study the regulation and maintenance of stable ongoing neuronal activity. The STG is comprised of approximately 30 neurons that control the

rhythmic movement of the animal's foregut musculature, which includes a small pattern generating circuit known as the pyloric circuit. Many pyloric neurons are readily identifiable, meaning that individual neurons can be identified as serving a unique and necessary function in every animal (Selverston et al., 1976), and each of the identified neurons has robust, stereotyped activity and connectivity patterns that are invariant both between animals of each species and over the life of each animal. The STG is part of the larger stomatogastric nervous system (STNS) which includes connections to three other ganglia and the brain, but the STG is easily isolated from all projection neurons and neuromodulatory input via a single nerve called the stomatogastric nerve (*stn*). If the *stn* is blocked or cut, a technique known as decentralization, the pyloric rhythm is disrupted via a dramatic slowing or cessation of bursting activity within minutes (Thoby-Brisson and Simmers, 1998). Over a period of days the activity is spontaneously restored in a homeostatic direction via cell-type specific changes in conductance levels (Haedo and Golowasch, 2006) and synaptic strength (Thoby-Brisson and Simmers, 2002), but the full mechanistic details of what drives these transitions remain an interesting area of study. Due to the relatively simple circuit architecture with identifiable neurons, the compact isolatable nature of the ganglion, and the reliable network output, the pyloric network continues to be a fruitful system for study of circuit dynamics, cellular identity, neuromodulation, homeostasis and activity maintenance. Here we show evidence of neuronal CS in the brain and STG of *Cancer borealis* using immunochemical methods. We then use long-term organ culture and electrophysiology techniques to show that removal of CS from the STG via chABC alters regulation of activity maintenance in the pyloric circuit after removal of neuromodulatory input via decentralization.

Methods

Animals

All experiments were performed using the STNS of the crab, *Cancer borealis*. Live animals were purchased from The Fresh Lobster Company (MA, USA), shipped overnight to Atlanta, GA, and housed in 10-12 ^{o}C artificial seawater until use. Animals were anesthetized by placing on ice for 45 minutes and the intact STNS was removed from surrounding tissue as previously described (Gutierrez and Grashow, 2009).

Westerns

Cancer borealis brains were removed and set aside during STNS dissection and flash frozen in liquid nitrogen. Brains were pooled and processed as previously described (Deepa et al., 2006). Briefly, tissue was crushed and homogenized in 1ml of extraction buffer 1 (50mM TBS, pH 7.0, 2 mM EDTA, 10 mM N-ethylmaleimide, 2 mM phenylmethylsulfonyl fluoride, and one cOmplete EDTA-free protease inhibitor cocktail tablet, Roche) before centrifugation at 15000 rpm at 4 ^{o}C for 30 minutes. Supernatant was carefully removed and the remaining pellet was resuspended before additional centrifugation. Extraction in this manner was continued sequentially: three times with buffer 1 after which the first two supernatants were pooled (extract 1) and the third was discarded, three times with buffer 2 (buffer 1 containing 0.5% Triton X-100) after which all buffer 2 supernatants were pooled (extract 2) and twice with buffer 3 (buffer 2 containing 6 M urea) after which both buffer 3 supernatants were pooled (extract 3). Extract 3 was dialyzed overnight against phosphate buffered saline (PBS). All extracts were quantified with a BCA protein assay kit (Pierce). Extracts were stored at -20 ^{o}C. Decorin (Sigma, MO, USA) was used as a positive control. A subset of samples were preincubated with 2.5 U/ml protease-free chondroitinase ABC (chABC, Sigma) for 2 hours at 37 ^{o}C before use in a Western blotting protocol as follows.

10 to 20 µg of STNS extracts were electrophorised on a 4-20% gradient mini-Protean precast polyacrylamide gel (BIO-RAD) then electroblotted onto a nitrocellulose

sheet (I-blot, Invitrogen). Ponceau S staining was used to visualize transfer of protein to the nitrocellulose, by incubating with 0.1% Ponceau S for one minute and rinsing with DI H_20. Ponceau S stain was removed with two five-minute rinses with Tris-buffered saline with 0.1% Tween 20 (TTBS) before continuing with a Western-blot protocol. Western-blot was performed using mouse anti-chondroitin sulfate IgM CS-56 (1:10000, Sigma) or mouse anti-chondroitinase-generated C-4-S neoepitope 2b6 (3:10000, MD Bioproducts) as primary antibody then respectively goat anti-mouse IgM (1:5000, KPL, MD, USA) or goat anti-mouse Ig was used with 2b6 (1:10000, BD Pharmingen) as secondary. Blocking was performed in 5% bovine non-fat dry milk in TTBS at 37^{o}C for 30 minutes. Primary antibody was incubated overnight at 4 ^{o}C and secondary antibodies 1h at room temperature (RT) with constant agitation. All antibody dilutions were done in TTBS-5% milk. Between each incubation the membrane was washed three times 5 minutes in TTBS. Blots were developed using Supersignal West Femto chemiluminescent substrate (ThermoScientific) for 30 seconds and developed with blue basic autorad film (GeneMate).

Immunohistochemistry

The desheathed stomatogastric ganglion (STG) was cut from the rest of the STNS and pinned in a Sylgard-coated 24-well plate. STGs were fixed using 4% paraformaldehyde in standard physiological crab saline for 1 hour. All incubations were done at RT using constant agitation at 30 rpm, unless otherwise stated. After fixation, tissue was rinsed 8X15 minutes in PBS. In some preparations, the STG was treated with 4U/ml chABC for 2 hr at 37 ^{o}C at this stage. The tissue was then blocked with 2.5% bovine serum albumin (Sigma) in PBS for 1 hour, after which the primary antibody (mouse anti-chondroitin sulfate IgM CS-56, 1:50) was allowed to incubate for at least 12 hours at 4 ^{o}C. All primary and secondary antibodies were diluted in serum block. The tissue was washed 8 X15min with PBS, before the goat anti-mouse IgG+IgM Alexa Fluor 594-conjugate (1:200, JacksonImmuno) was added and allowed to incubate for 2

hours. The tissue was washed 8X15 minutes with PBS. STGs were dehydrated with 5 minute washes of 30, 50, 70, 90 and 100% ethanol, in that order, plus an additional two 5 minute washes with 100% ethanol. The Sylgard under each pinned STG was cut from the dish in order to place still-pinned tissue in a solution of 1:1 ethanol to methyl salicylate for 1 hour. The tissue was then transferred to a glass microscope slide for mounting. Methyl salicylate was used as a mounting medium. An Olympus IX81 DSU spinning disk confocal microscope was used for fluorescent imaging of 2 µm optical slices, and Slidebook software (Intelligent Imaging Innovations, CO, USA) was used for image capture and deconvolution.

Organ Culture and Long-term Electrophysiology

The intact stomatogastric nervous system (STNS) was carefully removed from the crab *Cancer Borealis*, as described above. Each STNS was pinned in a sterile Sylgard-coated glass petri dish, and covered with fluorinated ethylene propylene gas-permeable membrane (American Durafilm, MA, USA), through which bleach-sterilized stainless steel wire electrodes could be threaded and secured in the Sylgard coating. Recordings were amplified with a differential AC amplifier (Model 1700, A-M Systems, WA, USA) and converted from analog to digital at 2 kHz using a National Instruments data acquisition board (PCI-6052E). MATLAB and Simulink software (Mathworks, MA, USA) was used, and custom scripts were written for data acquisition and analysis. Long-term cultures were maintained at 13 ^{o}C in filter sterilized L-15 medium supplemented with 40 U/ml penicillin, 40 µg/ml streptomycin (Sigma) and 1 g/L glucose. After verification of a stable rhythm (30-60 minutes), 4 U/ml of chABC in media was added to a Vaseline well around the desheathed STG, and allowed to sit undisturbed for 12-18 hours. Alternatively, media-only or denatured chABC (DNchABC) were used as controls. After this incubation, the enzyme was removed by rinsing the Vaseline well around the STG three times with media. In some experiments, the *stn* was cut to isolate the STG from neuromodulatory input at this time. Sterile media was replaced every 12 to

24 hours, and the activity of the STG was monitored for at least 5 days after decentralization. To denature chABC, the powdered form was partially reconstituted in a small amount of crab saline and heated to 90 C for 10 minutes. This denatured enzyme was then fully reconstituted with media, and used in the above protocol. Similar protocols for denaturing chABC have been previously described (Morriss-Kay and Tuckett, 1989).

Enzyme samples were tested for relative enzymatic activity using a standard dimethylmethylene blue (DMMB) protocol (Lee et al., 2010). Briefly, 50 µl of 4 U/ml chABC in media was added to 50 µl of 1mg/ml decorin in 50mm Tris-HCL (for a total of 50 µg of decorin per sample). Concurrently, a standard curve was prepared, spanning from 0-60 µg of decorin in 10 µg increments, in the same buffers and total volumes as the chABC samples. All samples were incubated at 37 ^{o}C for 4 hours, after which 50 µl of the chABC/decorin mixture was added to 150 µl of the DMMB solution (95 ml 0.1 N HCL, 16 mg DMMB, 2.37 NaCl , in 1L diH20) and absorbance was measured on a Microplate Reader (BIO-TEK Instruments, Inc) at 525 nm. Controls included newly reconstituted chABC and one without decorin. Percent activity was calculated by comparison to the standard curve.

Data analysis was done with custom MATLAB scripts. Several metrics of activity were compared between STGs that had been treated with enzymatically active chABC and those that had not. In most cases, the burst frequency of the PD neuron as recorded on the *pdn* was used as a proxy for pyloric frequency. If the *pdn* was not available, burst frequency of the LP neuron (if present) or PD neuron was recorded on the *lvn*. Time to half maximal activity ($t_{1/2}$) was defined as the time from decentralization to the time at which median-filtered (order 3) pyloric frequency first dipped below half of the pre-decentralization pyloric frequency. Pre-decentralization frequency was the average frequency in the 10 hours before decentralization. Bouts were defined as at least 3 pyloric cycles with an instantaneous frequency 40% above the baseline frequency, as previously described (Zhang et al., 2009). Baseline frequency was defined as the average frequency

of either the previous 7 minutes or a minimum of 50 pyloric cycles. Time to first bout (t_{bout}) was defined as the time from decentralization to time of the first recorded bout that occurred after $t_{1/2}$. Stable pyloric activity for intact STNS was defined as continuous bursting activity in which pyloric frequency did not go below 0.2 Hz. Maximum average pyloric frequency (F_{max}) after decentralization was defined as the maximum value of a 5-hour moving average which scanned from 10 hours after decentralization to the last recording. Averages drawing upon less than 500 data points were excluded from comparison in order to focus analysis on sustained activity. Student's t-tests, single-factor ANOVA, and Tukey-Kramer tests were used for statistical analysis. Standard error was used for reported confidence measures.

Results

Chondroitin Sulfate in the STG

Cancer borealis brains were homogenized and exposed to a series of three extraction buffers. These buffers have previously been shown to separate diffuse ECM (buffers 1 and 2) from more stable and cell-type specific perineuronal nets (buffer 3) in mammalian systems (Deepa et al., 2006; Carulli et al., 2010). Extracts, with or without chABC pretreatment, were subjected to SDS-PAGE gel electrophoresis and subsequent western blotting using an antibody specific to chondroitin sulfate (CS-56) (Figure 3.1).

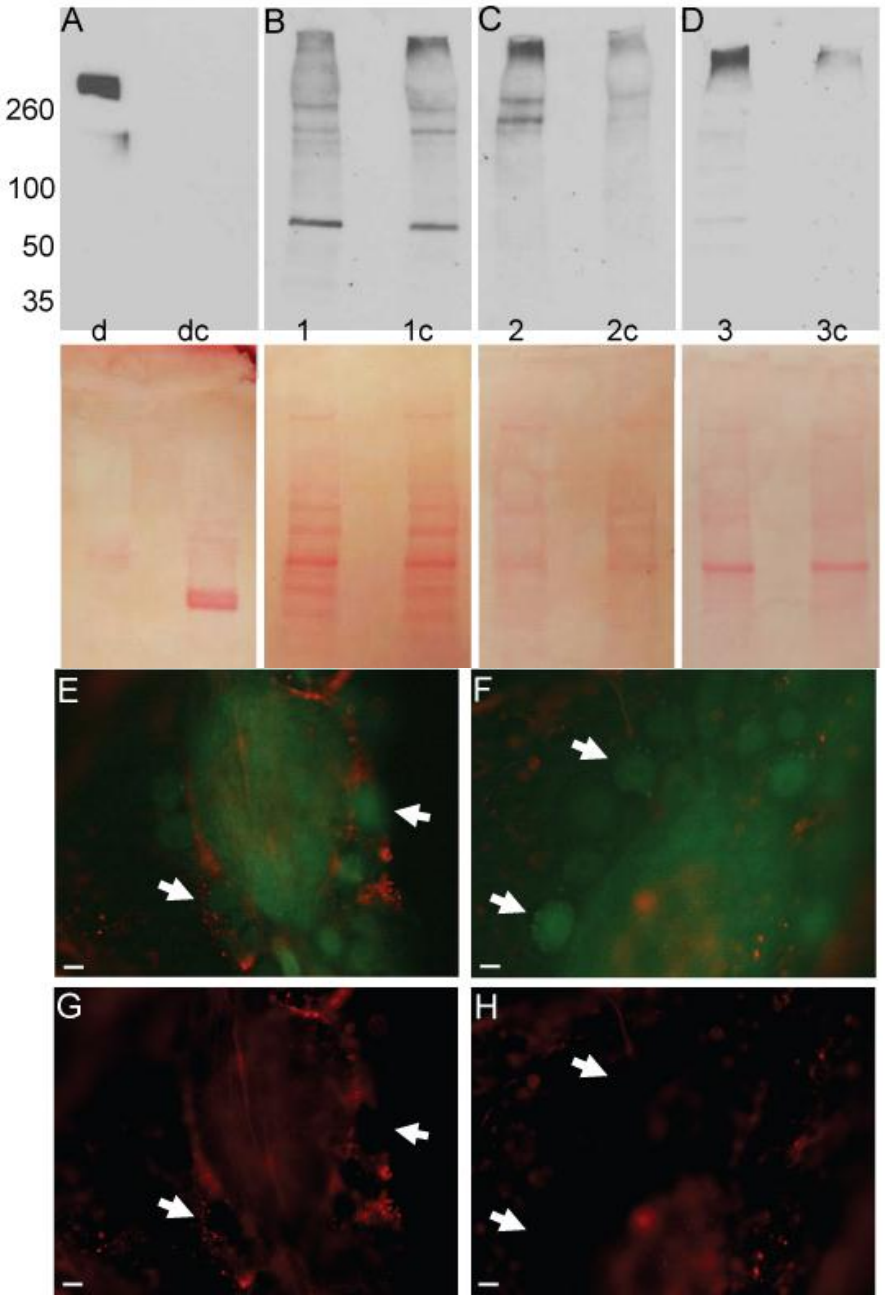

Figure 3.1: Anti-CS immunoreactivity in *Cancer borealis* brain. (A-D) Top row: Western blots using anti-CS (CS-56) primary antibody. Bottom row: Ponceau S stain of the same blot as pictured in the top row, to demonstrate general protein levels of each lane. (A) Decorin (d) was used as a positive control. Decorin treated with chABC (dc) was used as a negative control. (B-D) Crab brain samples treated sequentially with buffers 1, 2 and 3 (see methods) adjacent to the same samples treated with chABC (1c, 2c, 3c, respectively). (E-H) Anti-CS immunostaining in the STG (red) and autofluorescence (AF,green) to demonstrate cell and neuropil orientation. (E,F) Anti-CS and AF overlay. (G,H) Anti-CS only. (E,G) Untreated STG. Arrows indicate cell bodies with extracellular anti-CS staining. (F,H) chABC treated STG. Arrows indicate cell bodies without anti-CS staining. Scale bars indicate 20 µm.

Extract 1 appeared to have few differences in CS-56 binding between chABC-treated and untreated extracts, suggesting non-specific binding of the primary antibody in this fraction. Extracts 2 and 3 showed greater differences between chABC-treated and untreated extracts. Extract 2 shows clear bands around 260 kD and at high molecular weights (MW) that are greatly reduced in the chABC-treated sample. Extract 3 has a single large band at high MW that is absent after chABC-treatment. The mammalian CSPG decorin was used as a positive control, and showed a clear high MW band before chABC treatment and no staining after treatment, as expected. An antibody specific for the chondroitinase-generated C-4-S neoepitope 2b6 epitope (2b6) was also used, and appears to have no specificity for crab neural tissue using the described Western or IHC protocols (not shown).

CS stain was seen throughout the sheath surrounding STG neurons and within the neuropil of the STG. In most control preparations (5/6), a subset of STG neurons showed strong pericellular staining around the cell body (Figure 3.1E,G). This pericellular stain was absent from most STGs (5/6) that had been treated with chABC (Figure 3.1F,H). However, variability was seen in these staining patterns and each group had one clear outlier. In the control group, there was one STG that showed no pericellular stain and in the treatment group, there was one STG that showed clear pericellular staining. The lack of consistency in staining outcomes could be due to natural variability in the CSPG arrangements in the STG, or could be a consequence of the non-specific binding of the CS-56 antibody in crab neural tissue, or a combination thereof. In the western blot results, we saw that the majority of extracted protein was found in extract 1, which showed a greater proportion of CS-56 binding that did not respond to chABC treatment. Therefore any CSPG-specific signal seen in the STG using this antibody has the potential to be overwhelmed by non-specific staining.

Chondroitinase Does Not Interrupt the Ongoing Pyloric Rhythm

Intact stomatogastric nervous systems (STNS) were carefully removed from surrounding tissue and maintained in organ culture. Electrical activity of the *pdn* and *lvn* was recorded with steel extracellular electrodes over a period of 5-7 days. In the first hour of organ culture, treatment (chABC in media) or sham (media only, or denatured chABC (DNchABC) in media) solutions were added to a water-tight well surrounding the STG. These solutions were allowed to sit overnight (12-18 hours) before they were rinsed and replaced with media. No difference between treatment groups in the nature or progression of pyloric circuit activity from intact STNSs was seen over the duration of organ culture (Figure 3.2).

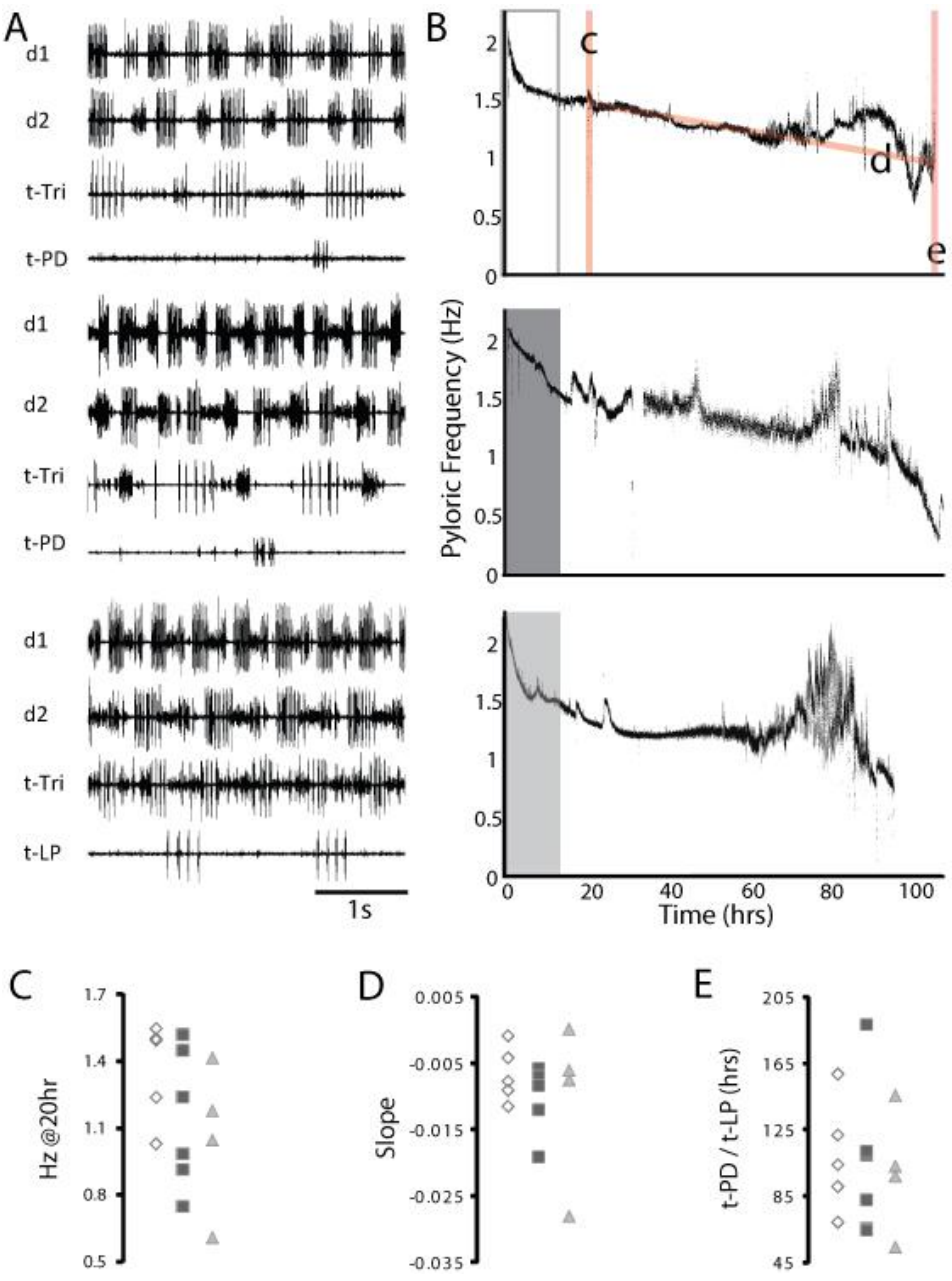

Figure 3.2: chABC treatment has no measureable effects on pyloric rhythm in long term organ culture. (A,B) Top row, untreated, n=5; Middle row, chABC-treatment, n=6; Bottom row, DNchABC-treatment, n=4. (A) Example extracellular recordings of the *lvn* nerve at days 1 (d1) and 2 (d2), and at the approximate location of last triphasic activity (t-Tri) and last stable bursting activity seen with either the PD neurons (t-PD) or LP neuron (t-LP). Scale bar is 1 second. (B) Pyloric frequency vs. time in culture. Shading indicates treatment condition and duration. (C,D,E) White diamonds, untreated; dark grey squares, chABC-treatment; light grey triangles, DNchABC-treatment. (C) Pyloric frequency after 20 hours in culture. (D) Slope between pyloric frequency at 20 hr and frequency of last stable bursting activity. Example shown in inset in B. (E) Time at last stable bursting activity.

All treatment groups demonstrated a quick decline in pyloric network frequency within the first 5 hours of culture. Frequency continued to decline thereafter, but at a much slower pace. After an average of 4 days in culture, most preparations ceased rhythmic activity. The last cell type to stop bursting is often the PD, as recorded on the *pdn* (Figure 3.2A). There was only one case of an intact preparation in which the LP neuron was the last to stop bursting (Figure 3.2A, bottom row). On average, the last stable bursting activity of either cell type occurs 8 hours after the last triphasic activity seen on the *lvn*. The time and frequency of the last stable bursting activity was recorded and compared between groups (Figure 3.2E). Quantitative measurements of pyloric frequency at 10 and 20 hours in culture were compared between treatment groups and no differences were seen (Figure 3.2C). There were also no significant differences in the slope between the frequency at hour 20 in culture and the frequency at the last PD bursting activity (Figure 3.2D). LP-on phase, defined as previously described (Luther et al., 2003), was calculated for the first hour of culture, 10 hours of culture, and after 20 hours (not shown). No significant differences were seen in any of the three treatment conditions for any of the investigated activity metrics, and no qualitative differences in activity pattern were observed to warrant further investigation.

Chondroitinase Treatment Prevents or Delays Classical Recovery

STNSs were cultured as described for intact preparations; however, in these experiments the *stn* was cut shortly after replacing the treatment solutions with media (12-18 hours into culture). This removes neuromodulatory input to the pyloric circuit and causes the pyloric rhythm to dramatically slow or stop within minutes of the cut. In some cases, bursting activity goes through a period of bouting beginning 5-25 hours after the cut. Bouting is defined as alternating periods of time, on the order of minutes, in which the rhythm gets faster and slower (see methods). Stable bursting activity returns an average of 3 days after decentralization (72.8 +/- 14.8 hrs) at a post-decentralization

maximum average frequency (F_{max}) approximately half of the original value (0.66 +/- 0.09 Hz) (Figure 3.3).

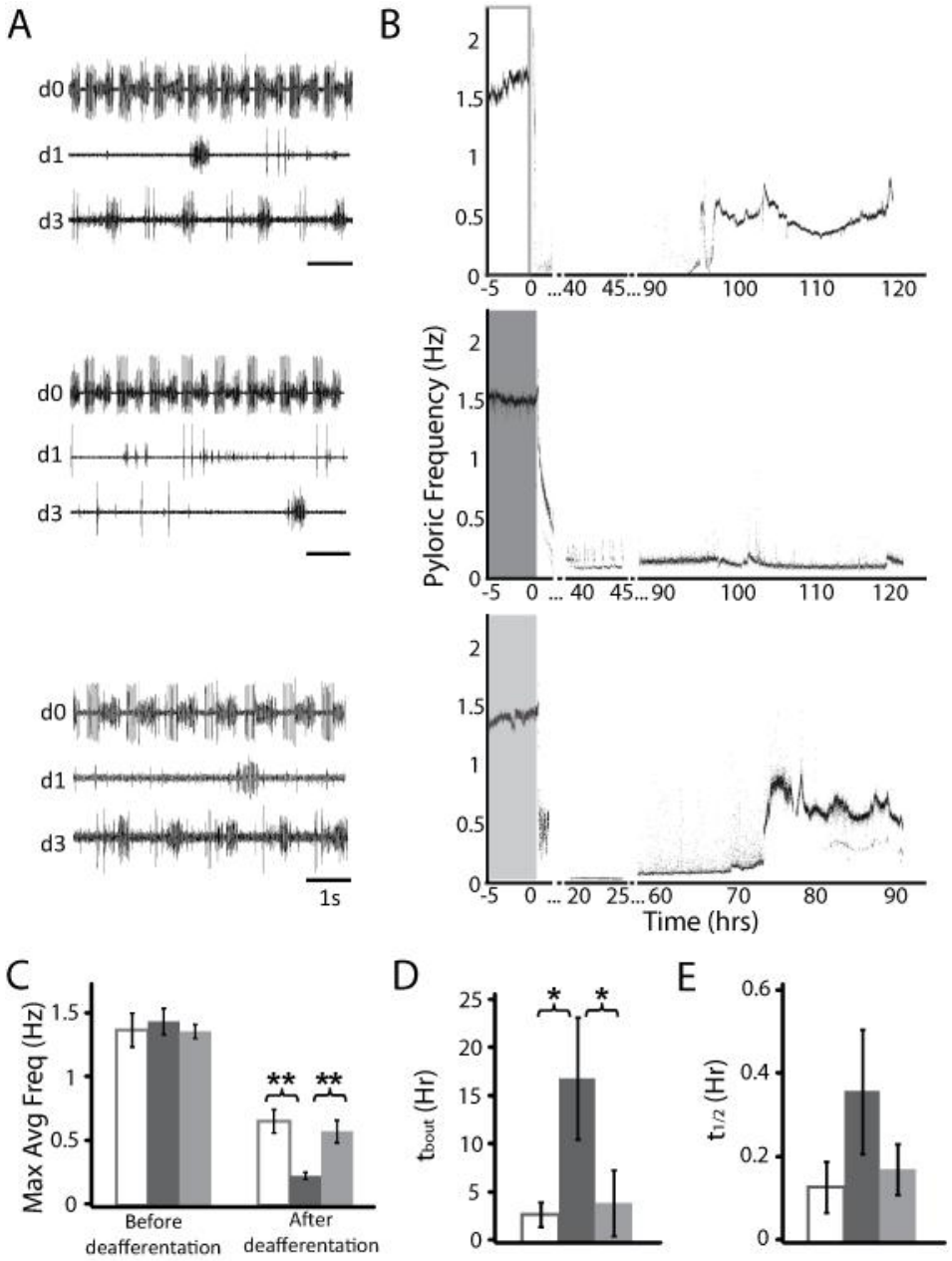

Figure 3.3: chABC treatment alters recovery of the pyloric rhythm after removal of neuromodulator via decentralization. (A,B) Top row, untreated, n=6; Middle row, chABC-treatment, n=8; Bottom row, DNchABC-treatment, n=8. (A) Example extracellular recordings of the *lvn* nerve (d0, before decentralization, d1, within 24 hours of decentralization, d3, 72-96 hours after decentralization). Scale bar is 1 second. (B) Pyloric frequency vs. time in culture. Decentralization occurs at t=0. Recordings (and treatment, if applicable) began 12-18 hours earlier (data not shown in entirety). Shaded areas indicate treatment duration (white outline – no treatment, dark grey-chABC, light grey-DNchABC). (C) Average pyloric frequency immediately before decentralization and maximum average pyloric frequency between 10-120 hours after decentralization as measured by PD burst frequency. (D) Time to first bout (E) Time to half max pyloric frequency. Error bars represent standard error. **p<0.01 *p=0.075

Chondroitinase treatment before decentralization significantly delayed the time to maximum average burst frequency after decentralization, but did not significantly alter other activity metrics. There was no significant differences in the time needed to reach half maximal frequency after decentralization ($t_{1/2}$) for any of the 3 conditions as determined by ANOVA (Figure 3.3E, p=0.28). The time from decentralization to first bout (t_{bout}) was also not significantly different between the three conditions when a 95% confidence interval was used; however, the p value was notably low at p=0.075 (Figure 3.3D). The F_{max} of all control pyloric circuits occurred within the first 100 hours after decentralization. During this time frame, chABC-treated preparations recovered bursting activity, however the F_{max} values were significantly lower (0.23 +/- 0.03 Hz) when compared to untreated activity and those treated with denatured chondroitinase ($p<0.01$) (Figure 3.3). Denatured chondroitinase and control preparations were not significantly different, suggesting that it is the enzymatic activity of chABC that is mediating the effects of the active chABC. There was no difference in the incidence of triphasic recovery patterns – fifty percent of pyloric circuits demonstrated triphasic activity after decentralization regardless of treatment conditions – or the qualitative appearance of bursting activity after recovery between groups.

To determine if the difference in post-decentralization frequency between active chABC treatment and the control groups was a permanent change or simply a delay, chABC-treated preparations were allowed persist in culture beyond 120 hours (Figure 3.4).

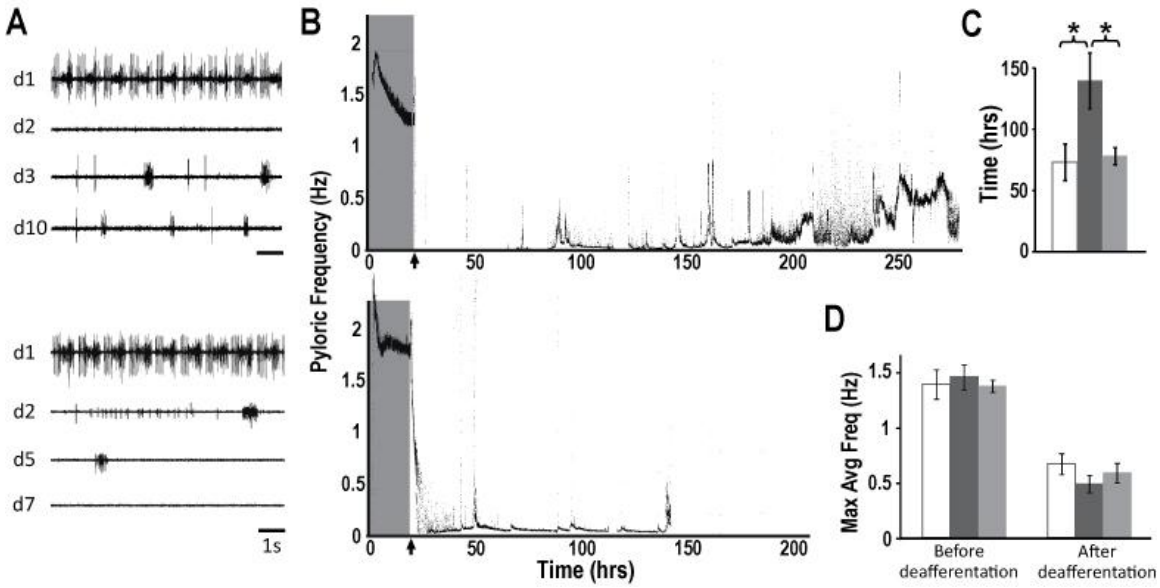

Figure 3.4: Recovery profiles after CSPG degradation fall into two categories. (A) Example extracellular recordings of the *lvn* nerve (d1, before decentralization, d2, within 24 hours of decentralization, dX, day X after decentralization). Scale bar is 1 second. (B) Pyloric frequency vs. time in culture. Arrow indicates decentralization. Shaded areas indicate treatment duration with chABC. (C) Average time to F_{max}. (D) Average pyloric frequency immediately before decentralization and maximum average pyloric frequency from 10 hours after decentralization to the last activity recorded in each experiment, as measured by PD burst frequency. *p<0.05 Error bars represent standard error.

In 3 out of 8 chABC-treated STGs, the pyloric activity did not increase in frequency past 120 hours after decentralization. These preparations show a "flat" recovery profile after decentralization, meaning that pyloric activity remains consistently very slow after decentralization, and eventually stops. In the remaining 5 cases, activity eventually returned to control recovery values of up to half the original frequency. These preparations show a "slow ramp" recovery profile, meaning that the pyloric frequency starts slow after decentralization, and very gradually becomes more active. The average F_{max} value after decentralization for chABC-treated pyloric circuits (0.48 +/- 0.08 Hz) was not significantly different from F_{max} values for untreated (0.66 +/- 0.09 Hz) or DNchABC-treated controls (0.62 +/- 0.09 Hz) when no time constraints were placed on the analysis period. However, the time needed for chABC-treated preparations to reach

these values was significantly greater (139 +/- 23 hrs) than both untreated and DNchABC-treated circuits ($p<0.05$).

Discussion

The present report is the first that demonstrates the presence of CS in *Cancer borealis* neural tissue. The presence of sulfated glycosaminoglycans (GAGs) in the crustacean nervous system is known (Abbott, 1979), but to the author's knowledge has not been studied in detail, and the presence of neural CS in particular has not been confirmed. CS has previously been described in the cartilage of decapod crustaceans (Gomes et al., 2011). *Tachypleus tridentatus* (horseshoe crab or king crab) gill cartilage contains a mixture of chondroitin sulfate variants with unusual GlcA3S-containing disulfated disaccharide units, including [GlcA3S–GalNAc4S], [GlcA3S–GalNAc6S], and [GlcA3S–GalNAc4S,6S], in addition to one of the monosulfated disaccharide units [GlcA–GalNAc4S] commonly seen in mammalian brain tissue (termed CS-A). The novel [GlcA3S–GalNAc4S] variant (termed CS-K) was particularly prevalent in crab cartilage at 54% of total disaccharide units (Fongmoon et al., 2007), and though it has not been well studied in mammalian systems, it is also thought to be present in human peripheral nerves as detected by the HNK-1 antibody (Chou et al., 1986; Ariga et al., 1987).

CS-K from crab cartilage has been shown to be susceptible to digestion by chABC (Fongmoon et al., 2007), but its immunoreactivity with common anti-CS antibodies is unclear. In this study we used an antibody which binds to the chondroitin sulfate family of molecules generally (monoclonal CS-56) and an antibody specific to a neoepitope generated on CS-A after chABC treatment (monoclonal 2b6). We did not see any immunoreactivity with the 2b6 antibody in either western blotting of brain tissue or immunochemistry in the STG, which is puzzling because the CS-A disaccharide has been seen in crab cartilage and the presence in neural tissue would be a natural assumption. Nonetheless, it is possible that CS-A is not present in crab neural tissue or that there are

species-specific differences in CSPG structure which would prevent binding of this antibody in our system, such as the connection region of CS-A polysaccharide to the protein backbone or the diversity of CS variants within one chain. On the other hand, the CS-56 antibody displayed an abundance of immunoreactivity in both crab brain and the STG. This binding was not entirely specific to chondroitinase-susceptible molecules in the saline-eluted fractions of brain tissue, suggesting either non-specific binding in this system or the presence of a CS variant not degraded by chABC. However, western blotting of detergent and urea fractions contained clear staining that was not present after treatment with chABC, demonstrating the presence of chABC-sensitive CS. This result was not as clear in immunostaining of the STG, possibly due to the large proportion of non-specific binding of saline-soluble molecules. One avenue of future research could be the use of the same elution buffers on tissue before immunostaining, to minimize the possibility of this non-specific binding (Deepa et al., 2006).

Ours is also one of very few reports describing invertebrate CS acting on invertebrate neurons. Crab cartilage CS-K promoted neuritic outgrowth of cultured murine hippocampal neurons (Fongmoon et al., 2007), but no studies to date have demonstrated similar action on invertebrate neurons. A study of cultured leech anterior pagoda neurons used peanut lectin (PNA) to bind to, and presumably block the effects of, native cell-surface extracellular GAGs. This binding caused changes in neurite outgrowth patterns, and an increase in the amplitude and duration of action potentials (Vargas and De-Miguel, 2009). PNA binding has been shown to be knocked down after chondroitinase treatment, suggesting that at least some of the effect seen in this study could have been mediated by CS-containing GAGs (Johnson and Hageman, 1987). The long-term nature of our study necessitated extracellular recordings; we chose extracellular recordings to prevent cell death that would be inevitable over such long term recordings if we had attempted intracellular recordings. The resulting recordings are a clear record of when action potentials occur (Figures 3.2A, 3.3A and 3.4A), but they do

not allow a detailed analysis of electrophysiological features such as the shape of the action potential or sub-threshold activity. An interesting follow up to our study would be to look at the effect of chABC treatment on the action potential in STG neurons. These types of experiments could give valuable insight into cellular mechanisms that give rise to the long-term network effects.

Our results show a role for CS in regulation of pyloric activity, perhaps via an activity-dependent mechanism. First, we demonstrated that degradation of CS in the STG of the intact STNS does not affect ongoing network activity over the long term, up to a week after treatment. There were no differences in ongoing burst frequency or phase relationships between cell types, suggesting that ongoing activity does not require involvement of extracellular CS. Next, we showed that extracellular CS is involved in the process of recovery of pyloric activity after a perturbation. Removal of CS via chABC prevented classical recovery within the first 5 days after decentralization. However, chABC treated pyloric circuits eventually recovered bursting activity with a frequency near control values 5-10 days after decentralization. The significant delay in time needed to reach control F_{max} values suggests that some component of the recovery mechanism is being interfered with temporarily; from this data we hypothesize that degradation of CS by chABC treatment is followed by synthesis and secretion of CS by STG neurons and glia to replace what was lost. CSPGs in mammalian systems are replenished on the order of days to weeks after chABC treatment, so secretion by STG neurons and glia is a possibility and would fit the time line of this experiment. Furthermore, there was a suggestive ($p<0.1$), though not significant, difference in the time to first bout between chABC-treated and control (untreated or DnchABC-treated) STGs. On average, the chABC-treated circuits took longer to produce bouting activity than the controls, which reinforces the hypothesis that intact CS is needed for post-decentralization activity, and that it is replaced over time such that treated STGs eventually go through periods of bouting and recovery. Previous work on recovery

mechanisms of the pyloric circuit has shown that cessation of pyloric activity before decentralization via PD hyperpolarization or application of low-Na+ saline causes an advance in the time to first bout, suggesting that t_{bout} is an indicator of an activity-dependent regulatory mechanism (Zhang et al., 2009). We saw no change in pre-decentralization activity with chABC treatment, but we did see a delay in t_{bout}. Though only suggestive and not a statistically significant finding, this result hints at a role for CS in activity-dependent regulation. Our results will be compared to what is already known about the mechanisms of recovery in the STG and the effects of CSPGs in other systems in the following paragraphs. This analysis may imply several possible mechanisms of action of CS on pyloric neurons, but all will require further experiments for verification. One such experiment could measure CS levels of treated and untreated STGs over time to determine if CS is being replenished after treatment, and if CS levels are being changed endogenously during normal recovery, perhaps in an activity-dependent manner.

The current understanding of network activity recovery after decentralization in the STG provides a good description of cellular and synaptic changes, but does not fully address what is driving these changes or controlling their trajectory. It has been shown that changes in intrinsic K^+ and Ca^{2+} conductances and synaptic efficacy occur during the hours after decentralization until activity is restored (Thoby-Brisson and Simmers, 2002; Haedo and Golowasch, 2006). Furthermore, some conductance changes during the course of recovery are activity-independent (Khorkova and Golowasch, 2007), in that they will occur with or without bouting activity. Also, conductance changes are mostly independent of synaptic input patterns, suggesting that the absence of neuromodulator is the major driver of network recovery (Temporal et al., 2012). However, the time course of bouting onset after decentralization can be manipulated depending on the history of activity patterns of the network before decentralization or the application of neuromodulators which alter network activity patterns before decentralization, suggesting that recovery requires coordinated action of both activity and neuromodulator-dependent

pathways (Zhang et al., 2009). Furthermore, changes in three K currents of pyloric cells over a period of hours are Ca^{2+} dependent (Golowasch et al., 1999), which strongly suggests a role for activity in driving these changes because intracellular Ca^{2+} concentration has long been thought to be a good measure of neuronal activity (Ross, 1989). Theoretical work has suggested that activity-dependent control of ion channel distributions could be working in concert with a neuromodulator-dependent intracellular Ca^{2+} buffering system (Zhang and Golowasch, 2011), though no experimental verification of the involvement of any intracellular regulatory cascades has been published to date. These models assume a black-box intracellular Ca^{2+} sensor as the integrating component for long-term observations of activity and feedback to the system – but there is no particular reason that this component of the system need be intracellular if the condition of feedback on ion channel activity is met. In fact, compartmentalization of this sensory-feedback component to the outside of the cell may be an advantage for network-wide regulation or prevention of unintended interference in other intracellular pathways. CSPGs and associated ECM molecules may be good candidates for this, as demonstrated in recent theoretical work (Kazantsev et al., 2012).

Across a variety of model systems, most of the neuronal effects of CSPGs fall into two main categories – structural plasticity and neuronal excitability. CSPGs are known to inhibit structural plasticity via their role in the glial scar after injury, axonal pathfinding and synapse formation during development (reviewed in (Kwok et al., 2011)) . There are some known changes in synaptic strength during normal recovery of the pyloric rhythm, but these changes appear to be homogeneous and do not affect the relative strength or overall wiring pattern of the circuit, and are therefore not thought to be an important factor in recovery (Thoby-Brisson and Simmers, 2002). For that reason, any interference in or exacerbation of these changes due to the absence of CSPGs would likely not prevent or delay recovery, unless they also resulted in large changes in structural plasticity or the wiring of the network. That scenario would likely result in non-

functional network activity in both the intact and decentralized pyloric circuit, which we did not observe. We take that as evidence that structural or synaptic changes due to chABC treatment are not a factor in the pyloric network, but further experiments measuring the synaptic strengths of identified synapses before and after treatment with chABC would further inform this hypothesis.

We suggest that CSPG-mediated effects on neuronal excitability present a more likely mechanism of action in the pyloric circuit. Though it is still unclear how CSPGs mediate their effects on neuronal excitability, there are three main categories of evidence for potential mechanisms in other systems: cation buffering (Vigetti et al., 2008; Hrabětová et al., 2009), direct interaction with cell-surface receptors or channels (Snow et al., 1994; Maroto et al., 2013), and binding of growth factors for later presentation to cellular receptors (Deepa et al., 2002, 2004; Kantor et al., 2004). The lack of a clear change in the ongoing pyloric rhythm in the intact STNS after chABC treatment suggests that ion buffering is an unlikely mechanism in our system. However, a detailed study of current parameters, including reversal potential, before and after treatment would address this possibility. Direct channel or receptor binding by free CS is another possibility. If enzymes released by the cell after decentralization, or in times of activity-related stress, free CS from the cellular environment in proportion to the available CSPG stores, this could be a clear way for stored cell-type specific information to feed back onto the cell. This hypothesis addresses both the lack of change in ongoing activity and the delay in recovery metrics in the treated pyloric circuit, if we assume that CSPGs are slowly replenished after chABC treatment, as discussed. Alternatively, the same effect could be generated if it was CS-bound growth factors or other soluble factors being released by secreted enzymes after decentralization. This hypothesis would require the assumption that endogenous enzymes release bound growth factors in a way that makes them available for binding to cellular receptors, whereas chABC does not, else the lack of effect of chABC on ongoing activity cannot be explained. To address the delay in

recovery seen in our results, this hypothesis would also require post-decentralization production of both CS and the required factors by STG neurons to replenish what was lost after chABC treatment.

We have demonstrated the presence of chondroitin sulfate in the nervous system of *Cancer borealis*, and its involvement in activity maintenance after decentralization. As described, the STG is ideally suited for further study of the mechanisms by which CSPGs might be involved in activity maintenance and homeostasis, and the described results suggest several specific avenues of future research.

CHAPTER 4

DISCUSSION

Every neuron needs to maintain a careful balance between the changes implicit in experience and the demands of stability required by its function. This balance tips depending on the neuronal system, but in any role, disease or neural disorders can develop when the regulatory mechanisms involved in neuronal stability fail. The pyloric circuit of decapod crustaceans has long been recognized as an excellent model system in which to study neuronal network stability, particularly for its reliable stereotyped output which implies reliable regulatory mechanisms. In addition, the phenomenon of network recovery after removal of top-down neuromodulatory input via decentralization is seen as a classical model of homeostatic change after injury. However, as more is discovered about the regulatory mechanisms controlling pyloric activity, it is increasingly difficult to say whether this system relies on homeostatic feedback in the classical sense or if more deterministic feed-forward mechanisms dominate.

The Case for Feed-forward Control: Conductance Correlations

We now know that a major mechanism constraining ongoing pyloric activity is dependent on the presence or absence of neuromodulator. In chapter 2 we demonstrated that the implementation of conductance correlations will constrain activity at the individual neuron level. This result verifies the functional significance of experimentally observed conductance correlations; these biological correlations constrain activity in the face of conductance variability, allowing neuronal populations the flexibility to navigate the conductance space while reducing the risk of non-functional activity. Neuromodulation of the STG originates in anterior ganglia which appear to exert top-down control on pyloric circuit activity. By studying current density levels and mRNA

levels coding for membrane ion channels in STG neurons before and after decentralization, it has been shown that neuromodulation controls conductance correlations. Population-wide conductance correlations have been shown to appear or disappear after the removal of neuromodulatory input in the STG (Khorkova and Golowasch, 2007; Temporal et al., 2012). These changes do not rely on the presence of a particular pattern of either synaptic (Temporal et al., 2012) or intrinsic (Khorkova and Golowasch, 2007) activity; though no experiments have been done to definitively show that the quick cessation of activity is not needed for these changes. Nonetheless, it has been repeatedly shown that neuromodulators are necessary to control population-wide conductance correlations in a cell-type specific manner at the mRNA and conductance levels (Schulz et al., 2006; Khorkova and Golowasch, 2007; Tobin et al., 2009; Temporal et al., 2012; Zhao and Golowasch, 2012). Therefore, the current understanding is that conductance correlations controlled by neuromodulators are an example of top-down control, not homeostatic regulation of activity.

While it is clear that conductance correlations are dependent on neuromodulation, it is easy to misinterpret these results as evidence that conductance *changes* are dependent on presence or absence of neuromodulator. In contrast, most reported correlations are population correlations, which means that no one cell is monitored before and after removal of neuromodulators. Instead, populations of cells are monitored at each time point which results in a general picture of how conductance levels correlate over time, but not how one cell manages its conductance values over time. The data on population correlations gives us the impression that conductances are non-changing before decentralization, and changing thereafter. But we could also interpret these results within a context wherein conductances are continually changing in an activity-dependent manner, but the types of changes they undergo are constrained by rules laid down by neuromodulators. In fact, there is data to suggest that the cellular changes that occur with

network recovery after decentralization are due to a synergy of neuromodulator-dependent and activity-dependent mechanisms.

The Case for Homeostatic Feedback: The Old Story and New Evidence

Before conductance correlations were discovered, the best mechanistic hypothesis for recovery after decentralization relied on activity-dependent homeostasis. Initial data demonstrated that injected current in a rhythmic pattern over a period of hours can induce changes in stomatogastric currents and the resulting activity type of STG neurons, and that these changes are Ca^{2+} dependent (Turrigiano et al., 1994; Golowasch et al., 1999; Haedo and Golowasch, 2006). However, for strong conclusions these kinds of studies necessitate individual cell isolation, and were often done in cell culture. Unfortunately the results did not translate to network-wide homeostasis studies; in fact, it was quickly deduced that network recovery would occur regardless of forced activity (via elevated K^{+}) or forced inactivity (via TTX) (Thoby-Brisson and Simmers, 1998). So attention turned to alternative theories of recovery such as top-down control.

In recent years, however, attention has turned to a synergistic approach. It is possible that both activity-dependent and activity-independent mechanisms contribute to recovery after decentralization. The time course of loss of activity and bouting onset after decentralization can be manipulated depending on the history of neuromodulator application or activity patterns of the network before decentralization, suggesting that recovery requires coordinated action of both activity and neuromodulator-dependent pathways (Zhang et al., 2009). Theoretical work has suggested that activity-dependent control of ion channel distributions could be working in concert with a neuromodulator-dependent intracellular Ca^{2+} buffering system (Zhang and Golowasch, 2011), though no experimental verification of the involvement of any intracellular regulatory cascades has been published to date.

In chapter 3 we describe a new player in the recovery mechanisms field. The extracellular environment has not previously been considered as important in the process of activity maintenance, but we show evidence that extracellular CS is needed for classical recovery after decentralization. We describe several possible mechanisms of action that would fit with both what is known about CS in other systems, and what is known about the recovery process in the STG. Our data suggest that this mechanism is likely activity-dependent. This presents a wide range of possible follow up experiments for exploring the details of the molecular cascades underlying network and cellular activity maintenance in the STG. Not only does this work have implications for activity regulation in the STG, but it also suggests that there may be more to CSPG and PNN function in vertebrate systems than is currently appreciated. PNNs are often cited as being potentially neuroprotective, and recent evidence suggests their involvement in synaptic homeostasis, but it is also possible that the extracellular environment is participating in intrinsic homeostasis and activity maintenance in a cell-type specific manner. CS is highly conserved across the kingdom animalia, and our results suggest that crustacean neuronal CS may also have some aspects of conserved or parallel function. The described future directions may offer heretofore unknown insight into one of the most basic and important aspects of neuronal function – regulation of activity.

Conclusions and Future Directions

Aim 1 – Conductance Correlation and Cellular Identity

Modeling is an excellent way to explore the theoretical implications of experimental work, and to answer questions that would be cost-prohibitive or technically challenging to pursue experimentally. In aim 1, we answered just such a question. By using a database of 1.7 million model neurons, we asked if varying conductance parameters within pairwise ratios would maintain features of activity, and we showed theoretical evidence that it will. This large-scale experiment would have been both cost-

prohibitive and technically challenging if biological neurons were used. Since publishing our work, our lab and others have expanded on it by using the same or similar models to investigate cellular parameter correlations and their role in constraining cellular identity. Using the same database and similar techniques, Soofi et al. showed that conductance ratios can support phase maintenance (Soofi et al., 2012), which is a feature of activity that has been shown to be tightly monitored in STG neurons experimentally. The Golowasch lab recently published a study in which they used dynamic clamp technique to force STG neurons to adhere to specific pairwise conductance correlations of their choosing (Zhao and Golowasch, 2012). They then measured the resulting activity attributes to determine if any remained invariant. They also found that several aspects of the phase relationships remained invariant when conductances were varied in a correlated manner. Our work has therefore informed future studies in two ways: first to demonstrate techniques for identifying correlations in model database with an evenly spaced grid-like conductance space, and second, to identify specific correlation pairs that are worthy of costly and time intensive further experimental study, based on their theoretical relationship to biologically constrained activity characteristics.

In addition to characterization of the biologically important correlations, another avenue of future work will undoubtedly include determination of the mechanisms that create the correlations, or in some cases, co-regulation. Correlations have also been seen on the mRNA level, suggesting that there is some element of genetic regulation at work. Furthermore, the signaling cascades that allow neuromodulation to control the presence or absence of some correlations has yet to be determined, and would be an interesting area of future research.

Finally, we have contributed to the burgeoning field of cellular identity characterization by showing that a cell-type specific subset of conductance correlations may be enough to determine broad features of activity type. Furthermore, we have contributed to the knowledge that the numerical value of each cellular property may not

contain as much information as the relationships between properties. With this in mind, genetic methods of identification appear to be universally appealing as the next frontier in neuronal circuit analysis because they may provide a much larger repertoire of identifying characteristics. Work is underway to identify cell-specific transcription factors, promoters, surface receptors, or other molecular machinery that can be used to target a subset of cells in a circuit. For example, fluorescence-activated cell sorting of retrograde-labeled cells has identified several cell type-specific molecular markers in mammalian cortical and cortico-spinal neurons (Shoemaker and Arlotta, 2010). Cell populations subjected to multiplex RT-PCR may also produce type-specific genetic profiles (Toledo-Rodriguez et al., 2004). In transgenic animals, this kind of cell type-specific genetic information has proven to be an invaluable tool for reproducibly identifying neurons, tracking connections, and directing perturbations in cellular activity (Kiehn, 2006; Luo et al., 2008; Brown and Hestrin, 2009). In invertebrates that take years to mature, such as the lobster and crab, transgenics are impractical; however, work has recently been done utilizing electroporation, viral transduction, or direct injection of genetic material into adult neurons (Haas et al., 2001; Saito and Nakatsuji, 2001; Callaway, 2005; MacLean et al., 2005b; Lovell et al., 2006). As this work progresses, the presence or lack of molecular differences between cells may reveal a more detailed picture of how functional cellular identity is achieved and maintained and may answer some lingering questions about the nature of cellular identity. Are two cells with identical circuit function also identical in their patterns of gene expression and molecular makeup? If not, are the differences consistent and identifiable between animals of a species? We expect the concepts of cell type and identity to continue to evolve, depending on the answers to these questions.

Aim 2 – CSPG Regulation of Homeostasis in the STG

The phenomenon of pyloric network recovery after removal of top-down neuromodulatory input, a process termed decentralization, is seen as a classic model of

homeostatic change after injury. Our results are the first to demonstrate the presence of chondroitin sulfate (CS) in the crustacean nervous system via immunochemistry. Furthermore, our results are the first to show that CS has a role in neuronal activity maintenance in crustaceans. We show that while ongoing activity is not disrupted by chABC treatment, recovery of pyloric activity after decentralization was significantly delayed without intact extracellular CS. Our results suggest that CS may be involved in initiating or directing activity maintenance in a homeostatic direction. Furthermore, we have suggestive evidence that this involvement may be activity dependent.

This work opens up a wide range of possible new directions for crab homeostasis research. While it does not contradict any of the known mechanisms involved in recovery of the pyloric circuit, it certainly adds a new dimension to the field that was not considered previously. This is the first report of any involvement of the extracellular space in homeostasis in the STG. Of the possible future directions, determining if CSPGs are degraded by endogenous enzymes during recovery is an important first step. This could be accomplished by immunochemical methods, particularly if an antibody better matched to crustacean CSPGs is found or made. Alternatively, characterization of the molecular nature of the CS or CSPGs via mass spectrometry would allow a more quantitative measure of the levels of CS before and after decentralization, with the added benefit of describing the molecular structure of the CS involved. Another way of determining endogenous use of CSPGs by cells for activity maintenance would be to measure levels of enzymes, perhaps matrix metalloproteinases, which could be working to degrade the CSPGs. If these types of enzymes are found to have greater activity before or after decentralization, this would be good evidence to support the hypothesis laid out in Chapter 3.

If it can be shown that manipulation of CSPGs is an endogenous mechanism in the STG, then there are several interesting future directions for this line of research that

would add to our understanding of cellular regulation of activity maintenance. For example, an interesting next step would be to investigate whether CSPG effects are activity dependent. This could be accomplished with electrophysiology protocols similar to those described in (Zhang et al., 2009). Furthermore, it would be interesting to investigate if CSPGs are interacting with known recovery mechanisms and in what way. For example, are CSPGs required for maintaining conductance correlations, or for the loss of those correlations after decentralization? Finally, one of the great advantages of the stomatogastric nervous system is the wealth of knowledge available about the reliably identifiable component cells of this circuit. Our preliminary immunohistochemistry is inconclusive, but suggests that some cells may have more CS stain than others, particularly around the cell body. If found true, it would be extremely interesting to investigate which cells required additional CS, and if there were cell-type specific complements of CSPG types, as seen in some vertebrate studies.

Significance

Our results represent a step toward a general understanding of the mechanisms by which neuronal regulation of activity maintenance occurs in the STG. Aim 1 adds the weight of theory to experimental observations, and demonstrates that implementation of conductance correlations can constrain activity. Forced implementation of conductance correlations via gene therapy may someday be a clinical strategy for disorders of neural control such as epilepsy, though there is still much multidisciplinary research that needs to be done to reach that goal. Aim 2 opens up the possibility of a paradigm shift in current concepts of how cellular regulation of activity is achieved. Presently, most known regulatory mechanisms are intracellular; here, we demonstrate evidence for extracellular regulatory mechanisms. As with any new area of research there are many more questions than answers, but this too may prove to be a fruitful area for the identification of clinical targets or a greater understanding of the big unanswered questions in neuroscience.

APPENDIX A

SUPPLEMENTARY TABLES

Table 2.1: Linear conductance relationships (χ^2>500 and |ρ|>0.2) by activity type. Any correlation with a |ρ|>0.4 is shown in bold, and any correlation with a |ρ|>0.6 is shown in red.

DATASET (# of models)	gleak	gH	gKd	gKCa	gA	gCaS	gCaT	gNa
Silent (286400)						gCaT-	gCaS-	
BURSTING MODELS								
Non-periodic bursters (55010)			gKCa+	**gNa+** gCaS+ gKd+ gCaT-		gKCa+	gKCa-	**gKCa+**
One-spike bursters (322679)								
All periodic bursters (712793)								
Periodic with duty cycle < 0.05 (392399)			gCaT+ gNa -	gNa+			gKd +	gKCa+ gKd -
Periodic with 0.05 <= duty cycle < 0.1 (129814)			**gCaT+**	gCaS+	gCaS +	gKCa+ gA+ gCaT-	**gKd +** gNa + gCaS-	gCaT+
Periodic with 0.1 <= duty cycle < 0.2 (109781)			gCaT+	**gCaS+** gCaT-	gCaS +	**gKCa+** gA + gCaT-	gKd + gNa+ gCaS- gKCa-	gCaT+
Periodic with 0.2 <= duty cycle < 0.4 (68237)			**gKCa+**	**gKd+** **gCaS +** gA- **gCaT-**	gKCa-	**gKCa+**	**gKCa-**	
Periodic with 0.4 <= duty cycle < 0.6 (10790)			**gKCa+**	**gKd+** gNa+ **gCaS +**	gKCa-	**gKCa+** gCaT-	**gKCa-** gCaS-	gKCa+

				gA- **gCaT-**				
Periodic with 0.6 <= duty cycle (1772)				**gCaS+**		**gKCa+**	**gNa+**	**gCaT+**
Periodic with average slope of the rise phase of the slow wave < 0.049 (306812)					gCaS+	gCaT- gA +	gCaS-	
0.049 <= slope < 0.059 (54543)			gCaT+	gCaS+	gCaS+	gCaT- gA + gKCa+	gCaS- gKd +	
0.059 <= slope < 0.072 (77577)	gCaS+		gCaT+	gCaS+	gCaS+	gCaT- gA + gKCa+ gleak+	gCaS- gKd +	
0.072 <= slope (270500)	gCaS+ gH-	gleak-	gCaT+	gCaS+		gKCa+ gleak+	gKd +	
Periodic with first quarter slope of rise phase of slow wave < 0.04 (117978)								
0.04 <= slope < 0.06 (92608)	gH-	gleak-				gCaT-	gCaS-	
0.06 <= slope < 0.08 (115859)						gCaT-	gCaS-	
0.08 <= slope < 0.1 (153965)						gCaT-	gCaS-	
0.1 <= slope < 0.12 (133708)			gCaT+		gCaS+	gCaT- gA +	gCaS- gKd +	
0.12 <= slope (95313)	gCaT+		gCaT+	gCaS+		gKCa+	gKd + gleak+	
Periodic with central slope of rise phase of slow wave < 0 (502)				**gCaS+**		**gCaT- gKCa+**	**gCaS-**	
0 <= slope < 0.04 (331386)	gCaS+				gCaS+	gCaT- gA+ gleak+	gCaS-	
0.04 <= slope < 0.06 (91778)	gH+ gCaS+	gleak+	gCaT+	gCaS+	gCaS+	gA+ gKCa+ gleak+	gKd+	
0.06 <= slope < 0.08 (103874)	gCaS+		gCaT+	gCaS+	gCaS+	gA+ gKCa+ gleak+	gKd+	
0.08 <= slope < 0.1 (119006)	gH- gCaS+ gA-	gleak- gCaS-	gCaT+		gleak-	gleak+ gH-	gKd+	
0.1 <= slope (62886)	**gH-** gCaS+	**gleak-** gCaS-	gCaT+ gNa-	gKd+ gleak-	gleak- gH+	gleak+ gH-	gKd+	gKd- gleak+

	gA- gNa+ gKd- gKCa-	gA+	gKCa+ gleak-					
SPIKING MODELS	**gleak**	**gH**	**gKd**	**gKCa**	**gA**	**gCaS**	**gCaT**	**gNa**
Non-periodic spikers (8694)	gCaS+ gKCa+ gKd-		gKCa+ gA+ gleak- gCaS+	gKd+ gleak+	gKd+ **gCaS+**	gKd+ **gA+** gleak+		
All periodic spikers (294040)								
Periodic with frequency < 10 Hz (79747)	**gCaS+**		gCaS+		gCaS+	gKd+ **gleak+** gA+		
Periodic with frequency 10-25 Hz (5389)			gCaT+	**gCaS+**	**gCaT+**	**gKCa+** **gCaT-**	gKd+ **gA+** **gCaS-**	
Periodic with frequency 25-50 Hz (63465)			gCaT+	**gCaS+** gA-	**gCaT+** gKCa-	**gKCa+** gCaT-	gKd+ **gA+** gNa+ gCaS-	gCaT+
Periodic with frequency 50-75 Hz (103568)			gCaT+ gKCa+	gKd+ gCaS+ gA-	gCaT+ gKCa-	gKCa+ gCaT-	gKd+ gA+ gNa+ gCaS-	gCaT+
Periodic with frequency > 75 Hz (41871)			**gNa-**				**gNa+**	**gCaT+** **gKd-**

Table 2.2: Conductance relationships that fit statistical criteria for correlations, but do not appear to have a linear relationship.

DATASET (# of models)	**gleak**	**gH**	**gKd**	**gKCa**	**gA**	**gCaS**	**gCaT**	**gNa**
Silent (286400)	**gH**	**gleak**	**gKCa**	**gKd** **gCaT**			**gKCa**	
BURSTING MODELS								
One-spike bursters (322679)			**gNa**					**gKd**
Periodic with first quarter slope of rise phase of slow wave < 0.02 (117978)	**gCaT** **gCaS** **gA** **gKCa** **gKd**		**gleak**	**gleak**	**gleak**	**gleak**	**gleak**	
SPIKING MODELS								
Non-periodic spikers (8694)				**gCaT**			**gKCa**	
All periodic spikers (294040)				**gCaT**			**gKCa**	
Periodic with frequency < 10 Hz (79747)	**gCaT**		**gCaT**	**gCaT**		**gCaT**	**gNa** **gCaS** **gKCa** **gKd** **gleak**	**gCaT**

Table 2.3: Percent success increased an average of 10 times the original value when model populations were defined by correlations. Correlation-based populations were generated using the complete set of correlations that define that activity type in the original database (See Table S1).

Activity type		% Success		$f_{Success}$
		Original	**Correlation**	
Bursting	< 0.05	23.4	76.0	3.2
	0.05-0.1	7.7	48.0	6.2
	0.1-0.2	6.5	43.4	6.7
	0.2-0.4	4.1	13.0	3.2
	0.4-0.6	0.6	7.5	12.5
	> 0.6	0.1	1.2	12.0
Spiking	Irregular	0.5	3.7	7.4
	< 10 Hz	4.8	11.2	2.3
	10-25 Hz	0.3	10.9	36.3
	25-50 Hz	3.8	51.9	13.7
	50-75 Hz	6.2	78.0	12.6
	> 75 Hz	2.5	10.0	4.0
	Average	**5.0**	**29.6**	**10.0**
	St. dev.	6.4	28.3	9.3

REFERENCES

Abbott NJ (1979) Primitive forms of brain homeostasis. Trends in Neurosciences 2:91–93.

Achard P, De Schutter E (2006) Complex Parameter Landscape for a Complex Neuron Model. PLoS Comput Biol 2:e94.

Ariga T, Kohriyama T, Freddo L, Latov N, Saito M, Kon K, Ando S, Suzuki M, Hemling ME, Rinehart KL (1987) Characterization of sulfated glucuronic acid containing glycolipids reacting with IgM M-proteins in patients with neuropathy. The Journal of biological chemistry 262:848–853.

Bal T, Nagy F, Moulins M (1988) The pyloric central pattern generator in crustacea - A set of conditional neuronal oscillators. Journal of Comparative Physiology a-Sensory Neural and Behavioral Physiology 163:715–727.

Bal T, Nagy F, Moulins M (1994) Muscarinic modulation of a pattern-generating network - control of neuronal properties. Journal of Neuroscience 14:3019–3035.

Balmer TS, Carels VM, Frisch JL, Nick TA (2009) Modulation of perineuronal nets and parvalbumin with developmental song learning. J Neurosci 29:12878–12885.

Baro DJ, Cole CL, Zarrin AR, Hughes S, Harriswarrick RM (1994) Shab gene expression in identified neurons of the pyloric network in the lobster stomatogastric ganglion. Receptors & Channels 2:193–205.

Baro DJ, Levini RM, Kim MT, Willms AR, Lanning CC, Rodriguez HE, HarrisWarrick RM (1997) Quantitative single-cell reverse transcription PCR demonstrates that A-current magnitude varies as a linear function of shal gene expression in identified stomatogastric neurons. Journal of Neuroscience 17:6597–6610.

Baro DJ, Quinones L, Lanning CC, Harris-Warrick RM, Ruiz M (2001) Alternate splicing of the shal gene and the origin of I-A diversity among neurons in a dynamic motor network. Neuroscience 106:419–432.

Bito H, Deisseroth K, Tsien RW (1997) Ca2+-dependent regulation in neuronal gene expression. Current Opinion in Neurobiology 7:419–429.

Brown SP, Hestrin S (2009) Cell-type identity: a key to unlocking the function of neocortical circuits. Current Opinion in Neurobiology 19:415–421.

Bucher D, Johnson CD, Marder E (2007) Neuronal morphology and neuropil structure in the stomatogastric ganglion of the lobster, Homarus americanus. Journal of Comparative Neurology 501:185–205.

Bucher D, Prinz AA, Marder E (2005) Animal-to-animal variability in motor pattern production in adults and during growth. J Neurosci 25:1611–1619.

Burdakov D (2005) Gain control by concerted changes in I-A and I-H conductances. Neural Computation 17:991–995.

Callaway EM (2005) A molecular and genetic arsenal for systems neuroscience. Trends in Neurosciences 28:196–201.

Carulli D, Pizzorusso T, Kwok JC, Putignano E, Poli A, Forostyak S, Andrews MR, Deepa SS, Glant TT, Fawcett JW (2010) Animals lacking link protein have attenuated perineuronal nets and persistent plasticity. Brain 133:2331–2347.

Celio MR, Blumcke I (1994) Perineuronal nets - A specialized form of extracellular-matrix in the adult nervous-system . Brain Research Reviews 19:128–145.

Chou DK, Ilyas AA, Evans JE, Costelloll C, Quarless RH, Jungalwalas FB (1986) Structure of sulfated glucuronyl glycolipids in the nervous system reacting with hnk-1 antibody and some igm paraproteins in neuropathy. J Biol Chem 261:11717–11725.

Colvis CM, Pollock JD, Goodman RH, Impey S, Dunn J, Mandel G, Champagne FA, Mayford M, Korzus E, Kumar A, Renthal W, Theobald DE, Nestler EJ (2005) Epigenetic mechanisms and gene networks in the nervous system. J Neurosci 25:10379–10389.

Crespo D, Asher RA, Lin R, Rhodes KE, Fawcett JW (2007) How does chondroitinase promote functional recovery in the damaged CNS? Experimental Neurology 206:159–171.

Deepa SS, Carulli D, Galtrey C, Rhodes K, Fukuda J, Mikami T, Sugahara K, Fawcett JW (2006) Composition of perineuronal net extracellular matrix in rat brain: a different disaccharide composition for the net-associated proteoglycans. The Journal of biological chemistry 281:17789–17800.

Deepa SS, Umehara Y, Higashiyama S, Itoh N, Sugahara K (2002) Specific molecular interactions of oversulfated chondroitin sulfate E with various heparin-binding growth factors. Implications as a physiological binding partner in the brain and other tissues. The Journal of biological chemistry 277:43707–43716.

Deepa SS, Yamada S, Zako M, Goldberger O, Sugahara K (2004) Chondroitin sulfate chains on syndecan-1 and syndecan-4 from normal murine mammary gland

epithelial cells are structurally and functionally distinct and cooperate with heparan sulfate chains to bind growth factors. A novel function to control binding of midkine, pleiotrophin, and basic fibroblast growth factor. The Journal of biological chemistry 279:37368–37376.

Dityatev A (2010) Remodeling of extracellular matrix and epileptogenesis. Epilepsia 51:61–65.

Dityatev A, Brückner G, Dityateva G, Grosche J, Kleene R, Schachner M (2007) Activity-dependent formation and functions of chondroitin sulfate-rich extracellular matrix of perineuronal nets. Developmental Neurobiology 67:570–588.

Dityatev A, Fellin T (2008) Extracellular matrix in plasticity and epileptogenesis. Neuron Glia Biology 4:235–247.

Dityatev A, Schachner M, Sonderegger P (2010) The dual role of the extracellular matrix in synaptic plasticity and homeostasis. Nat Rev Neurosci 11:735–746.

Egea J, Garcia AG, Verges J, Montell E, Lopez MG (2010) Antioxidant, antiinflammatory and neuroprotective actions of chondroitin sulfate and proteoglycans. Osteoarthritis and Cartilage 18:S24–S27.

Fields RD, Lee PR, Cohen JE (2005) Temporal integration of intracellular Ca2+ signaling networks in regulating gene expression by action potentials. Cell Calcium 37:433–442.

Fongmoon D, Shetty AK, Basappa, Yamada S, Sugiura M, Kongtawelert P, Sugahara K (2007) Chondroitinase-mediated degradation of rare 3-O-sulfated glucuronic acid in functional oversulfated chondroitin sulfate K and E. J Biol Chem 282:36895–36904.

Frischknecht R, Heine M, Perrais D, Seidenbecher CI, Choquet D, Gundelfinger ED (2009) Brain extracellular matrix affects AMPA receptor lateral mobility and short-term synaptic plasticity. Nat Neurosci 12:897–904.

Galtrey CM, Fawcett JW (2007) The role of chondroitin sulfate proteoglycans in regeneration and plasticity in the central nervous system. Brain Research Reviews 54:1–18.

Giamanco K a, Matthews RT (2012) Deconstructing the perineuronal net: cellular contributions and molecular composition of the neuronal extracellular matrix. Neuroscience 218:367–384.

Goaillard JM, Taylor AL, Schulz DJ, Marder E (2009) Functional consequences of animal-to-animal variation in circuit parameters. Nat Neurosci 12:1424–1430.

Gogolla N, Caroni P, Luthi A, Herry C (2009) Perineuronal Nets Protect Fear Memories from Erasure. Science 325:1258–1261.

Goldman MS, Golowasch J, Marder E, Abbott LF (2001a) Global structure, robustness, and modulation of neuronal models. Journal of Neuroscience 21:5229–5238.

Goldman MS, Golowasch J, Marder E, Abbott LF (2001b) Global structure, robustness, and modulation of neuronal models. Journal of Neuroscience 21:5229–5238.

Golowasch J, Abbott LF, Marder E (1999) Activity-dependent regulation of potassium currents in an identified neuron of the stomatogastric ganglion of the crab Cancer borealis. J Neurosci 19:RC33.

Golowasch J, Goldman MS, Abbott LF, Marder E (2002) Failure of averaging in the construction of a conductance-based neuron model. J Neurophysiol 87:1129–1131.

Golowasch J, Marder E (1992) Ionic currents of the lateral pyloric neuron of the stomatogastric ganglion of the crab. Journal of Neurophysiology 67:318–331.

Gomes M, Silva CS, Kozlowski EO, Cristina A, Silva ESDV (2011) Glycans in Diseases and Therapeutics Pavão MSG, ed. :159–184.

Gomez-Ospina N, Tsuruta F, Barreto-Chang O, Hu L, Dolmetsch R (2006) The C terminus of the L-type voltage-gated calcium channel Ca(V)1.2 encodes a transcription factor. Cell 127:591–606.

Greer PL, Greenberg ME (2008) From synapse to nucleus: Calcium-dependent gene transcription in the control of synapse development and function. Neuron 59:846–860.

Gutierrez GJ, Grashow RG (2009) Cancer Borealis Stomatogastric Nervous System Dissection. J Vis Exp:e1207.

Haas K, Sin WC, Javaherian A, Li Z, Cline HT (2001) Single-cell electroporation for gene transfer in vivo. Neuron 29:583–591.

Haedo RJ, Golowasch J (2006) Ionic mechanism underlying recovery of rhythmic activity in adult isolated neurons. J Neurophysiol 96:1860–1876.

Harris-Warrick RM, Marder E, Selverston AI, Moulins M (1992) Dynamic Biological Networks: The Stomatogastric Nervous System Sejnowski TJ, Poggio TA, eds. Computational Neuroscience:328.

Heinzel HG, Selverston AI (1988) Gastric mill activity in the lobster. III. Effects of proctolin on the isolated central pattern generator. J Neurophysiol 59:566–585.

Hooper SL, Marder E (1987) Modulation of the lobster pyloric rhythm by the peptide proctolin. J Neurosci 7:2097–2112.

Hrabětová S, Masri D, Tao L, Xiao F, Nicholson C (2009) Calcium diffusion enhanced after cleavage of negatively charged components of brain extracellular matrix by chondroitinase ABC. The Journal of Physiology 587:4029–4049.

Hudson AE, Archila S, Prinz AA (2010) Identifiable cells in the crustacean stomatogastric ganglion. Physiology Bethesda Md 25:311–318.

Hudson AE, Prinz AA (2010) Conductance Ratios and Cellular Identity Gutkin BS, ed. PLoS Computational Biology 6:13.

Huguenard JR, McCormick DA (1992) Simulation of the currents involved in rhythmic oscillations in thalamic relay neurons. Journal of Neurophysiology 68:1373–1383.

Huys QJ, Ahrens MB, Paninski L (2006) Efficient estimation of detailed single-neuron models. J Neurophysiol 96:872–890.

Johnson BR, Kloppenburg P, Harris-Warrick RM (2003) Dopamine modulation of calcium currents in pyloric neurons of the lobster stomatogastric ganglion. J Neurophysiol 90:631–643.

Johnson L V, Hageman GS (1987) Enzymatic characterization of peanut agglutinin-binding components in the retinal interphotoreceptor matrix. Experimental Eye Research 44:553–565.

Kantor DB, Chivatakarn O, Peer KL, Oster SF, Inatani M, Hansen MJ, Flanagan JG, Yamaguchi Y, Sretavan DW, Giger RJ, Kolodkin AL (2004) Semaphorin 5A is a bifunctional axon guidance cue regulated by heparan and chondroitin sulfate proteoglycans. Neuron 44:961–975.

Kazantsev V, Gordleeva S, Stasenko S, Dityatev A (2012) A homeostatic model of neuronal firing governed by feedback signals from the extracellular matrix. PloS one 7:e41646.

Khorkova O, Golowasch J (2007) Neuromodulators, not activity, control coordinated expression of ionic currents. J Neurosci 27:8709–8718.

Kiehn O (2006) Locomotor circuits in the mammalian spinal cord. Annual Review of Neuroscience 29:279–306.

Kim M, Baro DJ, Lanning CC, Doshi M, Farnham J, Moskowitz HS, Peck JH, Olivera BM, HarrisWarrick RM (1997) Alternative splicing in the pore-forming region of shaker potassium channels. Journal of Neuroscience 17:8213–8224.

Kim M, Baro DJ, Lanning CC, Doshi M, Moskowitz HS, Farnham J, Harris-Warrick RM (1998) Expression of Panulirus shaker potassium channel splice variants. Receptors & Channels 5:291–304.

King DG (1976a) Organization of crustacean neuropil. I. Patterns of synaptic connections in lobster stomatogastric ganglion. J Neurocytol 5:207–237.

King DG (1976b) Organization of crustacean neuropil. II. Distribution of synaptic contacts on identified motor neurons in lobster stomatogastric ganglion. J Neurocytol 5:239–266.

Kwok JCF, Dick G, Wang D, Fawcett JW (2011) Extracellular matrix and perineuronal nets in CNS repair. Developmental Neurobiology:n/a–n/a.

Kwok JCF, Warren P, Fawcett JW (2012) Chondroitin sulfate: A key molecule in the brain matrix. The International Journal of Biochemistry & Cell Biology 44:582–586.

Lander C, Kind P, Maleski M, Hockfield S (1997) A family of activity-dependent neuronal cell-surface chondroitin sulfate proteoglycans in cat visual cortex. J Neurosci 17:1928–1939.

Lee H, McKeon RJ, Bellamkonda R V (2010) Sustained delivery of thermostabilized chABC enhances axonal sprouting and functional recovery after spinal cord injury. Proceedings of the National Academy of Sciences of the United States of America 107:3340–3345.

Linsdell P, Moody WJ (1994) Na+ channel mis-expression accelerates K+ channel development in embryonic xenopus-laevis skeletal-muscle. Journal of Physiology-London 480:405–410.

Lovell P, Jezzini SH, Moroz LL (2006) Electroporation of neurons and growth cones in Aplysia californica. Journal of Neuroscience Methods 151:114–120.

Luo L, Callaway EM, Svoboda K (2008) Genetic dissection of neural circuits. Neuron 57:634–660.

Luther JA, Robie AA, Yarotsky J, Reina C, Marder E, Golowasch J (2003) Episodic bouts of activity accompany recovery of rhythmic output by a neuromodulator- and activity-deprived adult neural network. J Neurophysiol 90:2720–2730.

MacLean JN, Zhang Y, Goeritz ML, Casey R, Oliva R, Guckenheimer J, Harris-Warrick RM (2005a) Activity-independent coregulation of I-A and I-h in rhythmically active neurons. Journal of Neurophysiology 94:3601–3617.

MacLean JN, Zhang Y, Goeritz ML, Casey R, Oliva R, Guckenheimer J, Harris-Warrick RM (2005b) Activity-independent coregulation of I-A and I-h in rhythmically active neurons. Journal of Neurophysiology 94:3601–3617.

MacLean JN, Zhang Y, Johnson BR, Harris-Warrick RM (2003) Activity-independent homeostasis in rhythmically active neurons. Neuron 37:109–120.

Marder E (1974) Acetylcholine as an Excitatory Neuromuscular Transmitter in Stomatogastric System of Lobster. Nature 251:730–731.

Marder E (1976) Cholinergic Motor Neurons in Stomatogastric System of Lobster. Journal of Physiology-London 257:63–86.

Marder E, Bucher D (2007) Understanding circuit dynamics using the stomatogastric nervous system of lobsters and crabs. Annual Review of Physiology 69:291–316.

Marder E, Paupardintritsch D (1978) Pharmacological Properties of Some Crustacean Neuronal Acetylcholine, Gamma-Aminobutyric Acid, and L-Glutamate Responses. Journal of Physiology-London 280:213–236.

Marder E, Prinz AA (2002) Modeling stability in neuron and network function: the role of activity in homeostasis. Bioessays 24:1145–1154.

Marder E, Thirumalai V (2002) Cellular, synaptic and network effects of neuromodulation. Neural Networks 15:479–493.

Maroto M, Fernández-Morales J-C, Padín JF, González JC, Hernández-Guijo JM, Montell E, Vergés J, De Diego AMG, García AG (2013) Chondroitin sulfate, a major component of the perineuronal net, elicits inward currents, cell depolarization and calcium transients by acting on AMPA and kainate receptors of hippocampal neurons. Journal of neurochemistry.

Martin-de-Saavedra MD, Del Barrio L, Canas N, Egea J, Lorrio S, Montell E, Verges J, Garcia AG, Lopez MG (2011) Chondroitin sulfate reduces cell death of rat hippocampal slices subjected to oxygen and glucose deprivation by inhibiting p38, NF kappa B and iNOS. Neurochemistry International 58:676–683.

Maynard DM, Dando MR (1974) The structure of the stomatogastric neuromuscular system in Callinectes sapidus, Homarus americanus and Panulirus argus (Decapoda Crustacea). Philos Trans R Soc Lond B Biol Sci 268:161–220.

McAnelly ML, Zakon HH (2000) Coregulation of voltage-dependent kinetics of Na+ and K+ currents in electric organ. Journal of Neuroscience 20:3408–3414.

Medeiros GF, Mendes A, Castro RAB, Baú EC, Nader HB, Dietrich CP (2000) Distribution of sulfated glycosaminoglycans in the animal kingdom: widespread

occurrence of heparin-like compounds in invertebrates. Biochimica et Biophysica Acta (BBA) - General Subjects 1475:287–294.

Morris NP, Henderson Z (2000) Perineuronal nets ensheath fast spiking, parvalbumin-immunoreactive neurons in the medial septum/diagonal band complex. European Journal of Neuroscience 12:828–838.

Morriss-Kay G, Tuckett F (1989) Immunohistochemical localisation of chondroitin sulphate proteoglycans and the effects of chondroitinase ABC in 9- to 11-day rat embryos. Development (Cambridge, England) 106:787–798.

Mulloney B, Selverston AI (1974) Organization of Stomatogastric Ganglion of Spiny Lobster .1. Neurons Driving Lateral Teeth. Journal of Comparative Physiology 91:1–32.

Olypher A V, Calabrese RL (2007) Using constraints on neuronal activity to reveal compensatory changes in neuronal parameters. Journal of Neurophysiology 98:3749–3758.

Ouyang Q, Goeritz M, Harris-Warrick RM (2007) Panulirus interruptus I-h-channel gene PIIH: Modification of channel properties by alternative splicing and role in rhythmic activity. Journal of Neurophysiology 97:3880–3892.

Panchin Y V, Arshavsky YI, Selverston A, Cleland TA (1993) Lobster stomatogastric neurons in primary culture .1. Basic characteristics. Journal of Neurophysiology 69:1976–1992.

Peng IF, Wu CF (2007) Drosophila cacophony channels: A major mediator of neuronal Ca2+ currents and a trigger for K+ channel homeostatic regulation. Journal of Neuroscience 27:1072–1081.

Prinz AA, Billimoria CP, Marder E (2003) Alternative to hand-tuning conductance-based models: construction and analysis of databases of model neurons. J Neurophysiol 90:3998–4015.

Prinz AA, Bucher D, Marder E (2004) Similar network activity from disparate circuit parameters. Nat Neurosci 7:1345–1352.

Ross W (1989) Changes in intracellular calcium during neuron activity. Annual Review of Physiology:491–506.

Saito T, Nakatsuji N (2001) Efficient gene transfer into the embryonic mouse brain using in vivo electroporation. Developmental Biology 240:237–246.

Schulz DJ, Goaillard JM, Marder E (2006) Variable channel expression in identified single and electrically coupled neurons in different animals. Nat Neurosci 9:356–362.

Schulz DJ, Goaillard JM, Marder EE (2007) Quantitative expression profiling of identified neurons reveals cell-specific constraints on highly variable levels of gene expression. Proc Natl Acad Sci U S A 104:13187–13191.

Schulz DJ, Temporal S, Barry DM, Garcia ML (2008) Mechanisms of voltage-gated ion channel regulation: from gene expression to localization. Cellular and Molecular Life Sciences 65:2215–2231.

Selleck SB (2001) Genetic dissection of proteoglycan function in Drosophila and C. elegans. Seminars in Cell & Developmental Biology 12:127–134.

Selverston AI, Mulloney B (1974) Organization of Stomatogastric Ganglion of Spiny Lobster .2. Neurons Driving Medial Tooth. Journal of Comparative Physiology 91:33–51.

Selverston AI, Russell DF, Miller JP (1976) The stomatogastric nervous system: structure and function of a small neural network. Prog Neurobiol 7:215–290.

Shoemaker LD, Arlotta P (2010) Untangling the cortex: Advances in understanding specification and differentiation of corticospinal motor neurons. Bioessays 32:197–206.

Snow DM, Atkinson PB, Hassinger TD, Letourneau PC, Kater SB (1994) Chondroitin sulfate proteoglycan elevates cytoplasmic calcium in DRG neurons. Dev Biol 166:87–100.

Soofi W, Archila S, Prinz A a (2012) Co-variation of ionic conductances supports phase maintenance in stomatogastric neurons. Journal of computational neuroscience 33:77–95.

Stein W (2009) Modulation of stomatogastric rhythms. Journal of Comparative Physiology a-Neuroethology Sensory Neural and Behavioral Physiology 195:989–1009.

Sugahara K, Yamada S (2000) Structure and function of oversulfated chondroitin sulfate variants: Unique sulfation patterns and neuroregulatory activities. Trends in Glycoscience and Glycotechnology 12:321–349.

Sun Q, Dale N (1998) Developmental changes in expression of ion currents accompany maturation of locomotor pattern in frog tadpoles. The Journal of Physiology 507 (Pt 1):257–264.

Taylor AL, Goaillard JM, Marder E (2009) How multiple conductances determine electrophysiological properties in a multicompartment model. J Neurosci 29:5573–5586.

Taylor AL, Hickey TJ, Prinz AA, Marder E (2006) Structure and visualization of high-dimensional conductance spaces. J Neurophysiol 96:891–905.

Temporal S, Desai M, Khorkova O, Varghese G, Dai AH, Schulz DJ, Golowasch J (2012) Neuromodulation independently determines correlated channel expression and conductance levels in motor neurons of the stomatogastric ganglion. Journal of Neurophysiology 107:718–727.

Thoby-Brisson M, Simmers J (1998) Neuromodulatory inputs maintain expression of a lobster motor pattern-generating network in a modulation-dependent state: Evidence from long-term decentralization in vitro. Journal of Neuroscience 18:2212–2225.

Thoby-Brisson M, Simmers J (2002) Long-term neuromodulatory regulation of a motor pattern-generating network: maintenance of synaptic efficacy and oscillatory properties. J Neurophysiol 88:2942–2953.

Tierney AJ, Harris-Warrick RM (1992) Physiological role of the transient potassium current in the pyloric circuit of the lobster stomatogastric ganglion. J Neurophysiol 67:599–609.

Tobin AE, Cruz-Bermudez ND, Marder E, Schulz DJ (2009) Correlations in Ion Channel mRNA in Rhythmically Active Neurons. Plos One 4:8.

Toledo-Rodriguez M, Blumenfeld B, Wu C, Luo J, Attali B, Goodman P, Markram H (2004) Correlation Maps Allow Neuronal Electrical Properties to be Predicted from Single-cell Gene Expression Profiles in Rat Neocortex. Cerebral Cortex 14:1310–1327.

Turrigiano G, Abbott LF, Marder E (1994) Activity-dependent changes in the intrinsic properties of cultured neurons. Science 264:974–977.

Turrigiano G, LeMasson G, Marder E (1995) Selective regulation of current densities underlies spontaneous changes in the activity of cultured neurons. J Neurosci 15:3640–3652.

Vahasoyrinki M, Niven JE, Hardie RC, Weckstrom M, Juusola M (2006) Robustness of neural coding in Drosophila photoreceptors in the absence of slow delayed rectifier K+ channels. Journal of Neuroscience 26:2652–2660.

Vargas J, De-Miguel FF (2009) Growth-inhibiting extracellular matrix proteins also inhibit electrical activity by reducing calcium and increasing potassium conductances. Neuroscience 158:592–601.

Vigetti D, Andrini O, Clerici M, Negrini D, Passi A, Moriondo A (2008) Chondroitin Sulfates Act as Extracellular Gating Modifiers on Voltage-Dependent Ion Channels. Cellular Physiology and Biochemistry 22:137–146.

Von Holst A, Faissner A (2009) Pampered in the Nest - Structure and Functions of Neural Stem Cell Niches. Neuroforum 15:44+.

Wlodarczyk J, Mukhina I, Kaczmarek L, Dityatev A (2011) Extracellular matrix molecules, their receptors and secreted proteases in synaptic plasticity. Dev Neurobiol.

Zhang Y, Golowasch J (2011) Recovery of rhythmic activity in a central pattern generator: analysis of the role of neuromodulator and activity-dependent mechanisms. J Comput Neurosci.

Zhang Y, Khorkova O, Rodriguez R, Golowasch J (2009) Activity and neuromodulatory input contribute to the recovery of rhythmic output after decentralization in a central pattern generator. J Neurophysiol 101:372–386.

Zhang Y, Oliva R, Gisselmann G, Hatt H, Guckenheimer J, Harris-Warrick RM (2003) Overexpression of a hyperpolarization-activated cation current (Ih) channel gene modifies the firing activity of identified motor neurons in a small neural network. J Neurosci 23:9059–9067.

Zhao S, Golowasch J (2012) Ionic current correlations underlie the global tuning of large numbers of neuronal activity attributes. The Journal of neuroscience : the official journal of the Society for Neuroscience 32:13380–13388.